UNIVERSITY OF CATANIA

INTERNATIONAL PHD PROGRAM IN NEUROPHARMACOLOGY – XXVII CYCLE

UNIVERSITY OF BORDEAUX

DOCTORAL SCHOOL OF LIFE AND HEALTH SCIENCES – SPECIALTY

NEUROSCIENCE

Dynamics of hippocampal networks revealed by voltage sensitive dye imaging

---

PhD Thesis

Michelangelo Colavita

Coordinator: Pr. Salvatore Salomone

Thesis Director: Dr. Federico Massa

Co-Thesis Director: Pr. Filippo Drago

December 2015

This work was supported by a fellowship from the International PhD Program in Neuropharmacology of the University of Catania and by Fondation pour la Recherche Médicale (FRM).

The work in this thesis has been carried out as a joint-PhD program in the laboratories of:

Home Institute

Prof. Filippo Drago
BIOMETEC
Department of Biomedical and
Biotechnological Sciences
School of Medicine
University of Catania
Via S. Sofia 64
95125 Catania
Italy

Guest Institute

Drs. Giovanni Marsicano and
Federico Massa
Neurocentre Magendie – INSERM U862
University of Bordeaux
146 Rue Leo Saignat
33000 Bordeaux
France

TABLE OF CONTENTS

ABSTRACT

In order to better understand brain functioning we need to investigate all the structural domains present in it, from single cell to interconnected entire brain regions. However, while our knowledge in terms of single/few cells functioning is vast, very little is known about neuronal networks, which are interacting collections of neurons functionally related to the same task. Moreover, the balanced and concerted activity of excitatory and inhibitory networks plays a key role for proper cortical computations. However, while exist several tools to record excitatory networks activity, this is not the case for inhibitory networks. Voltage sensitive dye imaging (VSDI) is a technique that allows the recording of neuronal activity by mean of proportional emission of fluorescence according to changes in membrane potential. The advantage of using VSDI over other recording techniques using electrodes is that VSDI allows not invasive recording of neuronal activity from hundreds of sites at the same time.

During the last decades, VSDI has been widely used both *in vitro* and *in vivo* and to investigate both single cells and excitatory network activities. However, by using VSDI, investigations on excitatory networks activity have been mainly performed by quantifying fluorescence emission in defined regions of interest at time-fixed points, while inhibitory activity has been evaluated only at single cell level. The former approach misses several information of the dynamics of spreading of glutamatergic transmission because does not consider for example how fast a signal propagates and in which direction. The latter approach instead, does not allow the monitoring of network inhibitory events, which would be very important considering the extensive spatial spreading of interneurons within cortical areas.

During my doctoral course I aimed at studying in detail excitatory and inhibitory neuronal networks in the CA1 area of mouse hippocampus with VSDI.

To study excitatory networks more comprehensively, in collaboration with a team of mathematicians, we developed a mathematical algorithm that allowed measuring the velocity and the direction of spreading of the VSDI signal and it represents a new method to determine an optical flow. After successful validation of the algorithm with surrogate data to test its accuracy, we analysed two set of experiments in which network excitatory activity has been manipulated either by increasing Schaffer's collaterals stimulation intensity or by blocking GABAergic transmission with the $GABA_A$ receptor antagonist picrotoxin in order to increase the depolarization in the CA1 region of the hippocampus. The results of these manipulations significantly decreased signal velocity whereas picrotoxin application significantly modified the direction of spreading, making the depolarization-mediated VSDI signal less dispersed compared to control.

Using VSDI I was able to fully characterize $GABA_A$ receptor-mediated hyperpolarizing signals in all the CA1 sublayers (field IPSPs), thus providing a new way of monitoring inhibitory events at network level. Moreover, I found that the activation of mGluR5 receptors induced an increase in a long-lasting manner of the VSDI-recorded field IPSPs, with duration and magnitude that relied on the specific CA1 sublayer considered.

Overall, my work shows new methodologies and new findings that may represent a step forward in the quest for a better understanding of neuronal networks, both excitatory as well as inhibitory, which hopefully can contribute to reduce the gap of knowledge between single cell activity and behaviour.

Keywords: neuronal networks, voltage sensitive dye imaging, hippocampus

RÉSUMÉ

Dans le but de mieux comprendre le fonctionnement du cerveau nous devons examiner les domaines structuraux qui le composent, de la simple cellule à des régions entières du cerveau interconnectées. Cependant, bien que le fonctionnement d'une ou plusieurs cellules est relativement bien connu, il n'y a que peu d'informations concernant les groupements de neurones interagissant fonctionnellement dans une même tâche, les réseaux neuronaux. De plus, l'activité équilibrée et concertée des réseaux excitateurs et inhibiteurs joue un rôle clé pour les intégrations corticales appropriées. Par ailleurs, il existe plusieurs outils afin d'enregistrer l'activité des réseaux excitateurs, ce qui n'est pas le cas pour les réseaux inhibiteurs. L'imagerie du colorant sensible au voltage (VSDI) est une technique permettant l'enregistrement de l'activité neuronale en moyennant une émission de fluorescence proportionnelle au changement de potentiel de membrane. Par rapport aux autres techniques employant des électrodes, le VSDI permet l'enregistrement non évasif de l'activité de centaines de sites en même temps.

Au cours des dernières décennies, le VSDI a été largement utilisé tant *in vitro* qu'*in vivo* pour étudier l'activité d'unique cellule et des réseaux excitateurs. Néanmoins, en utilisant le VSDI, les recherches quant à l'activité des réseaux excitateurs ont été principalement réalisées par quantification d'émission de fluorescence en définissant des régions d'intérêts à des temps fixes, alors que l'activité inhibitrice n'a été évalué uniquement qu'à l'échelle cellulaire. La première approche ne permet pas l'obtention de toutes les informations de la dynamique de propagation de la transmission glutamatergique du fait qu'elle ne prenne pas en considération la vitesse à laquelle le signal se propage ni dans quelle direction. En revanche, la seconde approche n'offre pas la possibilité d'étudier l'activité du réseau inhibiteur ce qui serait toutefois important de

définir du fait de la propagation spatiale extensive des interneurones au sein des aires corticales.

Durant mon doctorat, le but de mon travail a été d'étudier en détail les réseaux neuronaux excitateurs et inhibiteurs de l'aire CA1 de l'hippocampe de souris à l'aide du VSDI.

Pour étudier les réseaux excitateurs de façon plus compréhensive, en collaboration avec une équipe de mathématicien, nous avons développé un algorithme mathématique permettant de mesurer la vitesse ainsi que la direction de propagation du signal VSDI, ce qui représente une nouvelle méthode pour analyser le flux optique. Après la validation réussie de l'algorithme avec des données de substitution pour tester sa précision, nous avons analysé deux séries d'expériences dans lesquelles l'activité des réseaux excitateurs a été manipulée soit par augmentation de l'intensité de stimulation passant de 10 à 30 Volts ou en bloquant la transmission GABAergique avec la picrotoxine, un antagoniste du récepeteur $GABA_A$. Les résultats de ces manipulations montrent une diminution significative de la vitesse alors que l'application de picrotoxine modifie de façon significative la direction de propagation, ce qui rend le signal de dépolarisation médié par le VSDI moins dispersées par rapport au contrôle.

L'utilisation du VSDI a permis l'entière caractérisation des signaux hyperpolarisants médiés par les récepteurs $GABA_A$ dans toutes les sous-couches de CA1 (champ IPSP), offrant ainsi une nouvelle façon d'étudier les évènements inhibiteurs à l'échelle d'un réseau. De plus, j'ai montré qu'en activant les récepteurs mGluR5, j'étais capable d'augmenter de façon durable le champ IPSP du VSDI, avec la durée et l'ampleur au niveau des sous-couches spécifiques de CA1.

Globalement, je présente dans cette thèse de nouvelles méthodes et nouveaux résultats qui peuvent représenter une avancée dans la quête d'une meilleure

compréhension des réseaux neuronaux, excitateurs et inhibiteurs, ce qui espérons, pourra contribuer à réduire l'écart de connaissance entre l'activité d'une seule cellule et celle du comportement.

Mots clés: réseaux neuronaux, imagerie du colorant sensible au voltage, hippocampe

LONG RESUME

Depuis l'antiquité, la compréhension du fonctionnement du cerveau a été un des objectifs majeurs de l'humanité. L'énorme progrès dans cette quête au cours des derniers siècles nous a permis de démontrer jusqu'à maintenant, que le cerveau fonctionne selon un niveau d'organisation multi-échelle, de l'activité de cellules individuelles à l'ensemble interconnecté de régions du cerveau, ce qui se traduit en fin de compte par des réponses comportementales. Cependant, entre activité de cellules individuelles et le comportement se trouvent les réseaux neuronaux, qui correspondent à un ensemble de cellules fonctionnellement liés à une même tâche et permettent la communication entre les différentes régions du cerveau. Néanmoins, alors que nous savons relativement beaucoup en termes de pathophysiologie à l'échelle de la cellule et que d'autre part, nous pouvons qualitativement et quantitativement étudier le comportement, il est plus difficile d'évaluer le fonctionnement des réseaux neuronaux. Par conséquent, si nous voulons mieux comprendre le comportement, nous devons améliorer la connaissance des réseaux neuronaux sous-jacents.

L'hippocampe, avec sa forme d'ampoule très conservée chez les mammifères, a été une zone du cerveau d'objet de recherches intensives au cours du temps. La principale raison à cela est sa structure en couches bien organisées, avec des entrées synaptiques bien définies au niveau des lamina dendritiques qui, avec le développement de la préparation de tranche d'hippocampe, à faciliter énormément les investigations électrophysiologiques et biochimiques. En fait, la plupart des informations connues concernant les mécanismes fonctionnels du cerveau ont été découvertes dans l'hippocampe, comme par exemple la plasticité synaptique activité-dépendante, les

mécanismes de les transmissions excitateurs et inhibiteurs et les processus d'absorption de neurotransmetteurs et d'excitotoxicité.

Dans l'hippocampe, comme dans d'autres régions du cerveau, les réseaux neuronaux utilisent principalement le glutamate et le GABA comme neurotransmetteur. Les réseaux glutamatergiques constitués de cellules principales sont le substrat structurel du flux d'information entre et à l'intérieur des régions du cerveau, tandis que les neurones GABAergiques limitent localement l'activité glutamatergique excessive et coordonnent la sortie de l'information de la cellule principale. En effet, alors que les cellules principales représentent un type cellulaire plutôt homogène, les interneurones GABAergiques diffèrent remarquablement en termes de morphologie, propriétés électrophysiologiques, d'expression de marqueur neurochimique et d'innervation fournis aux cellules principales. En effet, l'activité concertée et coordonnée des cellules glutamatergiques et GABAergiques assurent le bon fonctionnement du cerveau.

Bien que les techniques d'enregistrement des réseaux excitateurs soient déjà disponibles et populaires, la possibilité d'enregistrer l'activité GABAergique à grande échelle est très limitée à ce jour, du fait de l'utilisation d'une ou très peu électrodes ce qui ne permet pas de fournir des informations spatiales suffisantes. Les dernières décennies ont permis une grande amélioration de la technologie pour enregistrer l'activité neuronale, dans lequel les photons remplacent les électrons, avec le résultat d'un accès plus facile aux neurones en raison du manque d'électrodes d'enregistrement. Une des techniques les plus représentatives qui informe une activité neuronale au moyen de lumière est l'imagerie du colorant sensible au voltage (voltage sensitive dye imaging) (VSDI). A travers l'utilisation d'un colorant, le VSDI émet une fluorescence proportionnellement aux changements du potentiel de membrane. Le VSDI a été utilisé au cours des années pour évaluer l'activité neuronale *in vitro* et *in vivo*, tant au niveau de

cellules individuelles que de réseaux excitateurs. Avec les colorants, le VSDI a besoin d'un équipement supplémentaire afin d'être exécutées, comme l'optique avec une ouverture numérique élevée et un faible grossissement, une caméra très sensible pour l'acquisition de faibles variations de fluorescence émises par le colorant suivant l'activité neuronale et une source de lumière pour exciter le colorant lui-même.

Le travail présenté dans cette thèse vise à étudier en détail les réseaux excitateurs et inhibiteurs dans la région CA1 de l'hippocampe de souris en introduisant de nouvelles méthodes développées par le VSDI.

Une analyse détaillée des réseaux excitateurs a été réalisée par élaboration d'un algorithme avec la collaboration d'une équipe de mathématiciens, ce qui représente une nouvelle méthode pour estimer un flux optique à partir des données VSDI. Le flux optique dans le traitement de l'image est la mesure de la tendance du mouvement apparent des objets, des surfaces et des bords dans une scène visuelle causée par le mouvement relatif entre un observateur (un œil ou une caméra) et la scène. L'algorithme est basé sur un ancien problème mathématique conçu à l'origine par le mathématicien français Gaspard Monge à la fin du 18ème siècle et mis en œuvre plus tard par le mathématicien russe Leonid Kantorovich. Ce problème consiste à trouver une solution pour transporter une certaine quantité de masse à partir d'une configuration initiale à une configuration finale, en minimisant un coût donné fonctionnel. Dans notre cas, la sortie de cet algorithme est un champ vectoriel dans lequel chaque vecteur représente la distance minimale parcourue par la dépolarisation neuronale chaque 2,2 millisecondes, ce qui est la résolution temporelle des enregistrements VSDI utilisés dans cette étude. Particulièrement, ces vecteurs fournissent deux importantes informations quantitatives : la distance (quantifiée par le nombre de pixels couverts au cours de la propagation de la dépolarisation neuronale) et la direction générale de propagation à l'intérieur de chaque

région d'intérêt (représentée par la convergence / divergence). Après nous avons validé avec succès l'algorithme avec des données de substitution afin de tester sa précision, nous avons analysé deux séries d'expériences dans lesquelles nous avons manipulé l'activité du réseau excitateur dans CA1, soit en augmentant l'intensité de stimulation de 10 à 30 volts ou en bloquant la transmission GABAergique avec l'antagoniste du récepteur $GABA_A$, la Picrotoxine. Ce que nous avons constaté est le suivant :

- les deux manipulations ont augmenté significativement la dépolarisation neuronale (représenté par l'augmentation émission de fluorescence, $\Delta F*F^{-1}$) dans CA1 en général et en particulier dans ses sous-couches. Ce qui diffère entre ces deux expériences résulte du fait qu'en bloquant l'inhibition GABAergique, l'activité excitatrice est uniquement prolongée et n'est pas sensiblement affectée au cours des toutes premières étapes de propagation de signal (~ 10 millisecondes), ce qui suggère que les interneurones sont recrutés principalement pour empêcher excitation excessive et prolongée de l'activité excitatrice.
- les deux manipulations ont diminué de manière significative la vitesse du signal de dépolarisation (quantifié du rapport de la distance par le temps) uniquement lors de la phase intermédiaire/tardive de la propagation. Cette constatation peut être surprenante et paradoxale, mais peut être expliquée par la persistance du réseau dans un état plus dépolarisée par rapport aux conditions de contrôle, soit après augmentation de l'intensité de stimulation (30 Volts) ou après le blocage des récepteurs $GABA_A$.
- l'inhibition GABAergique bloquée influe considérablement la direction générale de propagation du signal de VSDI, ce qui le rend plus ciblée et moins divergent par rapport au contrôle. Cela démontre comment les interneurones participent activement à l'acheminement de signaux excitateurs le long du réseau de CA1.

En ce qui concerne les réseaux inhibiteurs, j'ai caractérisé pour la première fois avec le VSDI des champs de potentiels post-synaptiques inhibiteurs (fIPSP) évoqués, médiés par les récepteurs $GABA_A$, s'étendant dans l'ensemble CA1 et dans toutes ses sous-couches. Ceci démontre la possibilité d'utiliser le VSDI comme outil pour l'étude directe de l'activé inhibitrice au niveau du réseau et pas seulement à la résolution d'une seule cellule. En particulier, j'ai montré que le fIPSP se produit principalement dans la couche pyramidale et à une distance inférieure à ~ 500 µm par rapport à l'électrode de stimulation. Ces résultats sont compatibles avec le fait que la majorité des synapses GABAergiques sont dans la région périsomatique de cellules pyramidales dans CA1 et que la stimulation active des populations d'interneurones est locale. De façon intéressante, lors de l'application d'une brève période de temps (10 minutes) de l'agoniste des récepteurs du groupe I mGluR, le (S) -3,5-dihydroxyphénylglycine (DHPG), j'ai observé un phénomène de plasticité GABAergique caractérisé par une augmentation durable de la force synaptique, dont la durée et l'amplitude dépend des différentes couches de CA1, avec une plus longue durée (60 minutes) et plus élevé dans le *stratum radiatum* proximal par rapport à la couche pyramidale. Des expériences complémentaires ont montré que le récepteur mGluR5 est responsable de cette plasticité grâce à l'activation intracellulaire ultérieure du récepteur IP_3. Les phénomènes de plasticité à long terme des synapses GABAergiques sont déjà connues dans l'hippocampe, mais c'est la première fois qu'il est rapporté une potentialisation de longue durée des mGluR5 dépendant de l'inhibition GABAergique, et que celle-ci est couche spécifique concernant la durée et l'amplitude.

Globalement, ces données fournissent de nouveaux aperçus sur les mécanismes à travers lesquels les transmissions excitatrices et inhibitrices coopèrent étroitement dans la région de CA1. Les données de l'investigation mathématique des réseaux excitateurs

ont permis de mettre en évidence en particulier, la façon dont l'inhibition par les récepteurs $GABA_A$ est importante dans la propagation normale de l'activité glutamatergique, à un niveau neuroarchitectural supérieur comme au niveau du réseau, au lieu de quelques simples cellules. De plus, l'algorithme que nous avons développé pourrait potentiellement être utilisé pour analyser les données de diverses techniques d'imagerie optique, compte tenu leur large utilisation dans tous les domaines de recherche sur la santé et les maladies, ce qui pourrait accroitre considérablement les connaissances actuelles. Les données de l'inhibition du réseau en effet ont démontré la possibilité d'utiliser le VSDI avec une grande résolution spatiale sans précédente pour l'étude de la transmission et de la plasticité des phénomènes GABAergiques, contrairement aux enregistrements avec électrodes. En addition, ces données apportent de nouvelles connaissances quant au rôle neuromodulateur de la signalisation GABAergique sur la transmission glutamatergique.

LIST OF ABBREVIATIONS

AMPA = α-amino-3-hydroxy-5-methyl-isoxazole-propionic acid

CA = Cornu Ammonis

CCK = cholecystokinin

DG = Dentate Gyrus

DHPG = (S)-3,5-Dihydroxyphenylglycine

EPSC = excitatory post synaptic current

EPSP = excitatory post synaptic potential

GABA = γ-Aminobutyric acid

IP_3 = inositol 1,4,5-trisphosphate

IPSC = inhibitory post synaptic current

IPSP = inhibitory post synaptic potential

mGluR = metabotropic glutamate receptor

MKP = Monge – Kantorovich mass transport problem

ms = milliseconds

NMDA = N-methyl-D-aspartate

PDE = partial differential equations

PTX = picrotoxin

PV = parvalbumin

ROI = region of interest

VSD = voltage sensitive dye

VSDI = voltage sensitive dye imaging

CHAPTER I

GENERAL INTRODUCTION

"I have never had reason, up to now, to give up the concept which I have always stressed, that nerve cells, instead of working individually, act together, so that we must think that several groups of elements exercise a cumulative effect on the peripheral organs through whole bundles of fibres. It is understood that this concept implies another regarding the opposite action of sensory functions. However opposed it may seem to the popular tendency to individualize the elements, I cannot abandon the idea of a unitary action of the nervous system, without bothering if, by that, I approach old conceptions."

Camillo Golgi

Nobel Lecture, 11 December 1906

1.1 – Neuronal networks: definition and importance of their understanding

One of our greatest challenges nowadays is comprehend how brain works. To give a rough idea of its complexity, let's just consider the estimated amount of cells that compose the human brain: approximately 171 billion! (see Figure 1, from Azevedo et al., 2009).

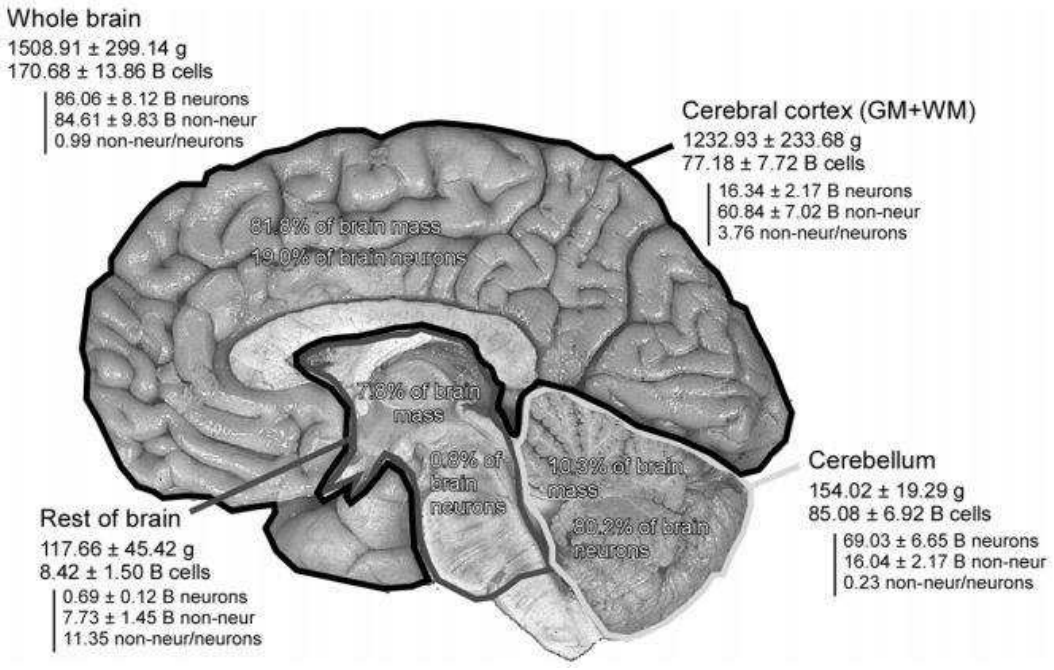

Figure 1 - Absolute mass, numbers of neurons, and numbers of nonneuronal cells in the entire adult human brain. Values are mean±SD and refer to the two hemispheres together. B, billion. *From Azevedo et al., 2009.*

Each neuron can connect to thousands of other neurons and these networks of neurons influence all behaviours, including perception, movement, memory and language (Parker, 2006). Moreover and actually surprising, some practical applications of ideas in neurobiology are not supported by strong scientific evidences. For example, lawyers

might propose brain scans as evidence of their clients' lack of responsibility and governments plan to scan the brains of employees, despite the lack of evidence that the scans predict behaviour. Another example is children to whom are given amphetamines to correct disruptive behaviour, despite the lack of evidence for disturbances in brain chemistry, while children with no obvious learning disabilities take cognitive 'enhancing' smart drugs ('Viagra for the brain'), with little evidence of any beneficial effects (Caplan, 2002; Parker, 2006; Rose, 2002). In addition, psychiatric and neurological treatments often lack insight into their mechanisms of action. For example, deep brain stimulation is used as a treatment for several disorders, including Parkinson's disease, but it is unclear how it alleviates symptoms (Greenberg, 2002; McIntyre et al., 2004; Parker, 2006), and the potential benefits and underlying mechanisms of electroshock therapy, psychosurgery and psychopharmacology are uncertain at best (Parker, 2006; Schloss and Henn, 2004).

The 1990s were declared the decade of the brain by the US congress (Parker, 2006). The Dana Alliance, an organization of neuroscientists, listed 10 objectives to be attained during the decade. These were: identifying the genes defective in Alzheimer's disease, Huntington's disease, hereditary blindness, deafness and manic depression; developing strategies for reducing nerve cell death and promoting regeneration after injury; developing drugs to alleviate chronic pain, multiple sclerosis, Alzheimers's disease, motor neuron disease, Parkinson's disease and epilepsy; developing treatments for manic depression, anxiety and schizophrenia; and understanding the mechanisms of addiction, learning and memory. In 2010 a Dana Alliance report from representative scientists of the organization highlights how our knowledge in basic neuroscience research improved significantly in all the domains thanks to the dramatic advance in available technology, which will certainly lead to the identification of treatments (2010).

This optimism, however, is not shared by people affected by the disorders listed

above, and is not shared by all neuroscientists (Parker, 2006). Torsten Wiesel, who won the Nobel prize for his work on visual cortex, claimed that 'we need a century, maybe a millennium' to comprehend the brain, and that beyond understanding a few simple mechanisms 'we are at a very early stage of brain science' (Horgan, 1999). Caution about our potential for understanding was earlier raised by the Nobel prize-winning neurophysiologist Charles Sherrington who said that 'physiology has not enough to offer about the brain in relation to mind to lend the psychiatrist much help' (Horgan, 1999).

We know a lot about the cellular properties of the nervous system and continuously increase our knowledge in order to identify molecular, developmental and functional properties of neurons and synapses. At the opposite end of the scale, we can characterize and quantify behaviours and correlate them with activity imaged with increasing sophistication in different regions of the brain (Parker, 2010). However, between these two levels there is an 'explanatory gap' that has prevented us from explaining behaviours directly in terms of their underlying cellular and synaptic mechanisms. We are thus data-rich but lack knowledge of how to integrate these data into a coherent picture of brain function (Parker, 2010).

Specific behaviours result from the activity in assemblies of interconnected nerve cells ('**neuronal networks'**). Neuronal networks process sensory inputs, perform cognitive functions, and programme specific outputs. These networks assemble interacting groups of neurons that act together to generate behaviours, making the network the interface between the physiological (cellular) and behavioural levels (Parker, 2006). Understanding these networks is thus an essential component to our understanding of normal and abnormal behaviour. There are obvious reasons for wanting to understand the brain: increasing knowledge of our thoughts and behaviours, to correct the effects of injury or disease and finally to have the opportunity to apply insight obtained

on the nervous system to technology, which may significantly improve our daily life (Parker, 2006).

1.2 – The Hippocampus as the brain structure to study neuronal networks

The hippocampal formation, comprised of the hippocampus itself (divided in dentate gyrus, CA3, CA2 and CA1), the subicular complex (subiculum, presubiculum, and parasubiculum) and the entorhinal cortex, has a bulb-like shape which protrudes into the lateral ventricles. The basic layout of cells and fiber pathways of the hippocampal formation is very similar in all mammals (Andersen P., 2007, Figure 2).

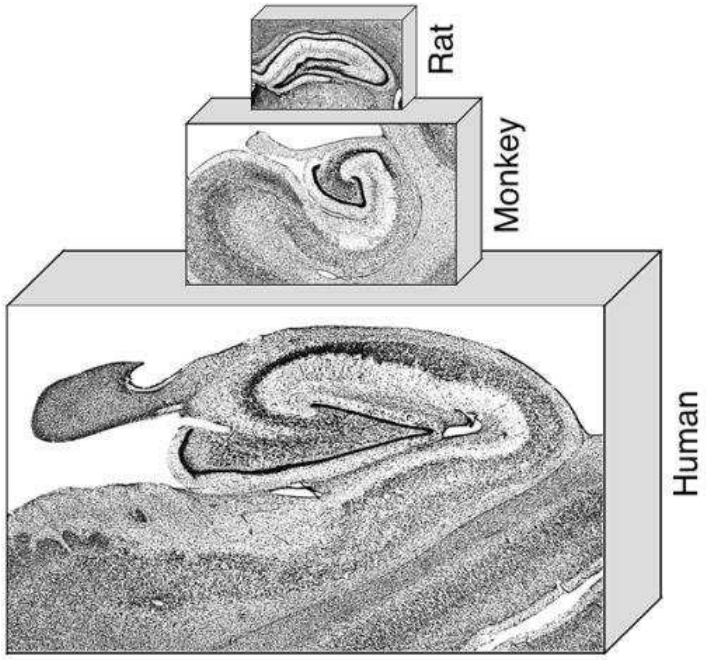

Figure 2 - Nissl-stained coronal sections through the rat, monkey, and human hippocampal formation. Note the general similarity of this brain region across species. *From Andersen P. et al., 2007.*

During the last decades the hippocampus has attracted the interest of scientists from many disciplines in neuroscience, from basic neurophysiology to cognitive and systems neuroscience. Thirty years ago, the most widely studied cell in the nervous system was the alpha motoneuron of the ventral horn of the spinal cord, today is the pyramidal cell of the hippocampus (Andersen P., 2007). One reason for the high amount of investigations carried out in hippocampus has been the peculiar anatomy of this brain area, with all principal cells oriented in a single layer and very organized synaptic inputs to well defined dendritic lamina. This simplified architecture facilitated electrophysiological and biochemical investigations, leading to ground-breaking discoveries about the mechanisms of excitatory and inhibitory transmissions, about the many neurotransmitter uptake mechanisms, about activity-dependent synaptic plasticity, and about the deleterious consequences of excitotoxicity for brain cells (Andersen P., 2007). These discoveries were dramatically facilitated by the development of the in vitro hippocampal slice preparation, which allowed the investigators to easily access and study cells on an unprecedented scale and to expand knowledge obtained in the hippocampus to other brain regions. An overview of some areas in neuroscience that have benefited from studies carried out on hippocampus is summarized in Table 1:

TABLE 1 (from Andersen P. et al., 2007)**:**
• First use of microelectrodes for extracellular neuronal studies
• Development of tetrodes for unit recording from behaving animals
• Interpretation of field synaptic potentials and population spikes as tools for analysis of extracellular signals
• Pioneering use of intracellular recording for central nervous system neurons
• Isolated slices of cortical tissue for neuroscience studies
• Development of histochemical methods for localization of neurotransmitters and receptor types
• Transplantation studies
• Pharmacological studies of central neurons and synapses
• Molecular biological analysis of synaptic function
• Formulation of computational models to explain ways in which neural networks can implement learning and memory

Another very interesting feature of the hippocampus is that the granule cells of the dentate gyrus are one of the rare types of neurons that regenerate throughout life, whose mechanistic findings offer potential benefits in neuronal repair research and for possible therapeutic interventions (Andersen P., 2007).

In addition, different studies in the hippocampus showed why and when pyramidal cells are activated in the living brain. Recordings from freely moving animals while they navigate in a familiar space have shown that individual hippocampal pyramidal cells fire in particular locations. These findings led to the development of new behavioural tools to study the neural mechanisms of memory in animals (Andersen P., 2007).

The hippocampal formation is involved in a plethora of neurological disorders such, as among others, epilepsy, Alzheimer's disease, and cerebrovascular disease (Andersen P., 2007). One of the hallmark features of epilepsy is the loss of neurons in several hippocampal fields and the pathological changes that occur in Alzheimer's disease manifest initially in the entorhinal cortex and then spread to the hippocampus proper and ultimately to the entire cerebral cortex (Andersen P., 2007). Such findings

have led to the development of model systems in which pathophysiological events like these may be studied and, hopefully, alleviated by treatment (Andersen P., 2007).

1.3 – Functional connectivity in the hippocampal formation

As defined in the previous paragraph, the hippocampus, the subicular complex and the entorhinal cortex compose the so-called hippocampal formation. The main reason for including the aforementioned areas under an unique hippocampal complex is that they are linked, one to the next, by largely unidirectional (functional) neuronal pathways (Amaral D., 2007).

The entorhinal cortex is considered the first step in the intrinsic hippocampal circuit because much of the neocortical input reaching the hippocampal formation does so through the entorhinal cortex. Cells in the layer II of the entorhinal cortex give rise to axons that project, among other destinations, to the dentate gyrus. The projections from the entorhinal cortex to the dentate gyrus form part of the major hippocampal input pathway called the perforant path. Although the entorhinal cortex provides the major input to the dentate gyrus, the dentate gyrus does not project back to the entorhinal cortex. This pathway is therefore nonreciprocated, or unidirectional (Amaral D., 2007; Neves et al., 2008).

Likewise, the principal cells of the dentate gyrus, the granule cells, give rise to axons called mossy fibers that connect with the proximal apical dendrites of pyramidal cells of the CA3 field of the hippocampus. The CA3 cells, however, do not project back to the granule cells, have substantial associative ipsilateral interconnections between them and can receive direct inputs from layer II of the entorhinal cortex. The pyramidal cells of CA3, in turn, are the source of the major input to the CA1 hippocampal field (the Schaffer

collateral axons). Following the pattern of its predecessors, CA1 does not project back to CA3 and distal apical dendrites of CA1 pyramidal neurons can receive a direct input from layer III cells of the entorhinal cortex. The CA1 field of the hippocampus then projects unidirectionally to the subiculum, providing its major excitatory input. Again, the subiculum does not project back to CA1 (Amaral D., 2007; Neves et al., 2008).

From the CA1 and the subiculum, other unidirectional projections close the hippocampal processing loop by making synapses with the deep layer of entorhinal cortex, the layer V. A schematic representation of the information flow throughout the hippocampal formation is in Figure 3.

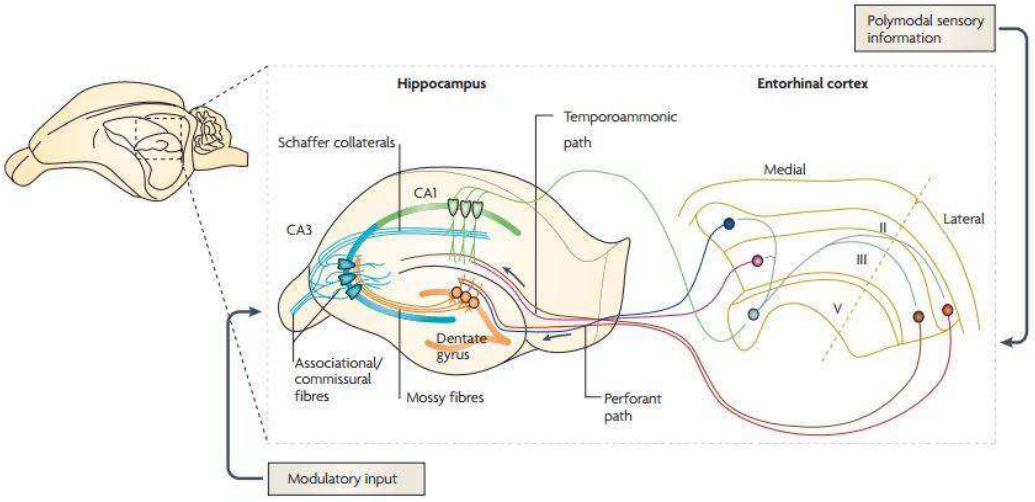

Figure 3 - Schematic representation of the information flow throughout the hippocampal formation. *From Neves G. et al., 2008.*

1.4 – The CA1 region of hippocampus

The vastness of the literature on CA1 and related cellular types, rather than other hippocampal areas, is largely attributable to a combination of structural considerations, cell viability, and historical accidents (Spruston N., 2007). Generally it is easier to keep cells in this region alive and healthy in slice preparations compared for example to the CA3, together with the fact that Schaffer collateral axons from CA3 form a homogeneous pathway that is easily activated to study synaptic transmission and plasticity (Spruston N., 2007).

The principal cellular layer is called the pyramidal cell layer, where the somata of pyramidal cells are tightly packed. Below the pyramidal cell layer is the *stratum oriens*, which is a narrow, relatively cell-free layer that contains the basal dendrites of the pyramidal cells, several classes of interneurons and is the sub-region in which some of the CA3 to CA3 associational connections and the CA3 to CA1 Schaffer collateral connections are located. Deep to the *stratum oriens* is the thin, fibre-containing alveus. The *stratum radiatum* is located immediately above the pyramidal cell layer and is the region in which the CA3 to CA1 Schaffer collateral connections are located. Above the *stratum radiatum* is the *stratum lacunosum-moleculare*, where the projections from the layer III of the entorhinal cortex terminate and where are present afferents from other regions, such as the nucleus reuniens of the midline thalamus (Spruston N., 2007, see Figure 4 for a schematic representation of the position and the connectivity of a pyramidal cell along the different CA1 layers).

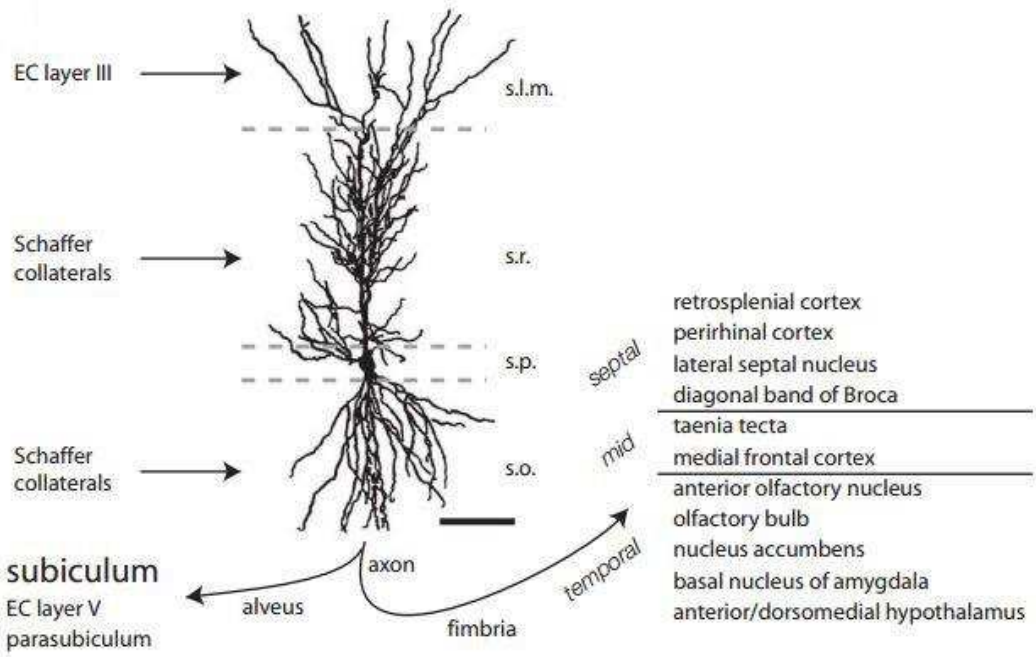

Figure 4 - CA1 dendritic morphology, spines, and synaptic inputs and outputs, respectively. Camera lucida drawing of a CA1 pyramidal neuron from an adult rat, showing the cell body in the stratum pyramidale (s.p.), basal dendrites in the *stratum oriens* (s.o.), and apical dendrites in the *stratum radiatum* (s.r.) and *stratum lacunosum-moleculare* (s.l.m.). The major excitatory inputs in each layer and the major outputs are also indicated. EC = entorhinal cortex. For the fimbrial projection, the septo-temporal positions noted indicate the source of CA1 cells projecting to different target regions. For the *alveus* projection, the subiculum is the major target. Bar = 100 μm. *Adapted from Spruston N. et al., 2007.*

Pyramidal cells of CA1: From the pyramid-shaped soma of rat CA1 neurons emerge two elaborately branching dendritic trees. The basal dendrites occupy the *stratum oriens*, and the apical dendrites occupy the *stratum radiatum* (proximal apical) and *stratum lacunosum-moleculare* (distal apical). Both the apical and basal dendritic trees occupy a roughly conical (sometimes ovoid) volume (Pyapali et al., 1998; Spruston N., 2007). The combined length of all CA1 dendritic branches is 12.0 to 13.5 mm: basal dendrites contribute about 36% of the total length, apical dendrites in the *stratum radiatum* contribute about 40%, and apical dendrites in the *stratum lacunosum-*

moleculare contribute the remaining 24% (Bannister and Larkman, 1995; Ishizuka et al., 1995; Megias et al., 2001; Spruston N., 2007; Trommald et al., 1995).

Along the length of the primary apical dendrite, several dendritic ramifications emerge obliquely in the *stratum radiatum*, which branch no more than a few times, with a typical branch bifurcating just once at a location close to its origin from the apical trunk (Spruston N., 2007). Despite their limited branching, however, oblique dendrites constitute most of the dendritic length in the *stratum radiatum* (Bannister and Larkman, 1995; Megias et al., 2001; Spruston N., 2007). After the primary apical trunk enters the *stratum lacunosum-moleculare* the apical dendrites continue to branch, forming a structure referred to as the apical tuft, which has an average of about 15 terminal branches (Bannister and Larkman, 1995; Spruston N., 2007; Trommald et al., 1995). Emerging from the base of the pyramidal soma are two to eight dendrites (a mean of five). Most of these dendrites branch several times (maximum 15 branch points), forming a basal dendritic tree with about 40 terminal segments (Bannister and Larkman, 1995; Pyapali et al., 1998; Spruston N., 2007).

Interneurons of CA1: Whereas pyramidal cells have their cell bodies organized into a highly structured layer (i.e., the pyramidal layer), the somata of GABAergic inhibitory interneurons show no such apparent organization. In fact, the somata of this highly diverse population of neurons are scattered throughout almost all subfields and strata of the hippocampus (Spruston N., 2007). Moreover, despite representing only ~11% of the total hippocampal neuronal population (Bezaire and Soltesz, 2013), each interneuron can connect with several hundreds of pyramidal cells (Freund and Buzsaki, 1996; Li et al., 1992; Sik et al., 1995) and other interneurons (Chamberland and Topolnik, 2012; Freund and Buzsaki, 1996) and represent perhaps one of the most diverse cell

populations. Because of this high heterogeneity, over the last decades numerous efforts have been made in trying to classify interneurons based on anatomical, neurochemical markers and connectivity patterns to pyramidal cells.

In classifying interneurons population based on their functional innervation to pyramidal cells, can be recognised two main classes: interneurons that innervate the soma and the axon initial segment and interneurons that innervate specifically dendrites of pyramidal cells (Freund and Buzsaki, 1996; Freund and Katona, 2007; Klausberger, 2009).

The class of interneurons which connect to the perisomatic region of pyramidal cells in the CA1 is represented by:

Basket cells = the predominant dendritic morphology of basket cells is pyramidal-shaped or bitufted. One to three dendrites originate from the apical pole of the triangular or fusiform soma, which then branch proximally, ascend through *stratum radiatum*, and often penetrate *stratum lacunosum-moleculare*. They also branch close to the soma and fan out toward the alveus, spanning the entire depth of *stratum oriens* (Freund and Buzsaki, 1996). All dendrites are spine-free, but occasionally a small number of short spine-like appendages can be observed. Basket cells in CA1 are likely to receive input from all major sources of excitatory afferents, such as Schaffer collaterals, commissural and entorhinal afferents, and recurrent collaterals of local principal cells in *stratum oriens* (Freund and Buzsaki, 1996). Basket cell axons instead fill the entire depth of *stratum pyramidale* and proximal *stratum oriens* (Freund and Buzsaki, 1996).

Basket cells do express several neurochemical markers such as the calcium-binding protein parvalbumin (PV) and the peptides cholecystokinin (CCK) and vasoactive intestinal polypeptide (VIP) (Freund and Buzsaki, 1996).

The main types of basket cells, the PV- and the CCK-expressing, have a functional dichotomy that is associated with characteristically different electrophysiological features and expression patterns for receptors, transmitters, and modulators (Freund and Katona, 2007). Several lines of research support the hypothesis that the PV-containing basket cells operate as clockworks for cortical network oscillations, whereas CCK-containing interneurons function as a plastic fine-tuning device (Freund and Katona, 2007). The latter cells modulate synchronous ensemble activities as a function of subcortical inputs that carry information about motivation, emotions, and the autonomic state of the animal, whereas the former have only a few receptor types for subcortical modulatory signals, but are efficiently and faithfully driven by local principal cells, as expected from an ‘‘oscillator’’ (Freund and Katona, 2007).

Chandelier cells = named also axo-axonic cells. The major distinguishing feature of chandelier cells is the characteristic termination of their axon, which run horizontally above the pyramidal cell layer and give rise to collaterals descending into the pyramidal layer, where they form characteristic bouton rows aligned parallel to the trajectory of axon initial segments of pyramidal cells (Freund and Buzsaki, 1996). The cell bodies are located within or immediately adjacent to the pyramidal cell layer and possess radially oriented dendrites spanning all layers. The dendrites are smooth, often varicose, and spines are only rarely present on a few branches. There is a rich arbor of basal dendrites in *stratum oriens*, which extends up to, or occasionally penetrates, the *alveus*. Thus, according to the distribution of the dendritic tree, chandelier cells are in a position to receive excitatory input from all major sources of afferents in the CA1 (Freund and Buzsaki, 1996). Chandelier cells contain mainly parvalbumin (Howard et al., 2005) and contribute to synchrony and oscillations in the hippocampus such as the theta rhythm (4–

8 Hz), which occurs during environmental exploration and REM sleep, and fast ripples (120–200 Hz), which occur during slow-wave sleep (Howard et al., 2005).

The class of interneurons which specifically contact the dendrites of pyramidal cells in the CA1 is represented by:

Oriens lacunosum-moleculare (O-LM) cells = they are the most studied interneurons that target dendrites of pyramidal cells. In the CA1 area, O-LM cells somata are located in *stratum oriens* and have horizontally extending dendrites with hairy spines on distal segments. The axons of O-LM cells give few collaterals in *stratum oriens* but project mainly through the *strata pyramidale* and *radiatum* to branch heavily in *stratum lacunosum-moleculare* (Klausberger, 2009), matching the glutamatergic input from the entorhinal cortex and thalamus. The axons give some collaterals also in the deep *stratum radiatum* but do not cross the fissure to the dentate gyrus. O-LM cells are often regarded as providing a classical example of GABAergic feedback inhibition. They express the neuropeptides somatostatin and parvalbumin (Klausberger, 2009).

Bistratified cells = the axonal arborization of bistratified cells overlaps with the glutamatergic input from CA3 pyramidal cells in *stratum radiatum* and *oriens*. This two-layered axonal arrangement gives the cell its name. Bistratified cells make GABAergic synapses with basal and oblique dendrites of CA1 pyramidal cells. Their somata are mainly located in *stratum pyramidale*, but have also been reported *oriens*-bistratified cells with somata and horizontally running dendrites in *stratum oriens*. The dendrites of bistratified cells in *stratum pyramidale* extend widely in the *strata oriens* and *radiatum* and form connexin36-containing gap junctions with other interneurons. Bistratified cells express parvalbumin to a similar extent to basket and axo-axonic cells and they also express somatostatin and neuropeptide Y (Klausberger, 2009).

Schaffer collateral-associated cells = the somata of Schaffer collateral-associated cells are located mainly in *stratum radiatum* with dendrites spanning all layers. The axons of these cells innervate the oblique and to a lesser extent basal dendrites of CA1 pyramidal cells and interneurons in *strata radiatum* and *oriens*, matching the excitatory input from CA3 pyramidal cells, giving the cell its name. In contrast to bistratified cells, the axons of Schaffer collateral-associated cells are concentrated more in *stratum radiatum* than in *stratum oriens*. Schaffer collateral-associated cells express CCK and the calcium-binding protein calbindin (Klausberger, 2009).

Perforant path-associated cells = the cell bodies of perforant path-associated cells are often located at the *stratum radiatum - lacunosum moleculare* border and their dendrites can either cover all layers or remain in *stratum lacunosum moleculare* and adjacent *stratum radiatum*. The axons of this cell type are concentrated in *stratum lacunosum moleculare*, overlapping with the excitatory perforant path input from the entorhinal cortex, giving the cell its name. Thus, they innervate the apical tuft of CA1 pyramidal cells. Interestingly, whereas the axons of O-LM cells always remain within the CA1 area, the axons of perforant path-associated cells often cross the fissure and also innervate the dendrites of granule cells in the dentate gyrus. Perforant path-associated cells express CCK and calbindin (Klausberger, 2009).

Neurogliaform cells = the cell bodies of neurogliaform cells are often located in *stratum lacunosum moleculare* and they have relatively short and numerous dendrites, giving the cell its name. The axons of neurogliaform cells are extremely dense, especially in *stratum lacunosum moleculare*. Similar to CCK-expressing perforant path-associated cells but in contrast to O-LM cells, the axons of neurogliaform cells often cross the fissure into the dentate gyrus. Many neurogliaform cells express neuropeptide Y and α-actinin-2 and are connected by gap junctions (Klausberger, 2009).

Ivy cells = in contrast to neurogliaform cells innervating the apical tuft of pyramidal cells, the very dense axons of ivy cells cover *strata oriens* and *radiatum*, making synapses onto the basal and oblique dendrites of pyramidal cells (Fuentealba et al., 2008; Klausberger, 2009). The cell bodies of ivy cells are located in *strata pyramidale* and *radiatum* and the usually short dendrites can cover all layers. Ivy cells express neuropeptide Y, neuronal nitric oxide synthase and a high level of $GABA_A$ receptor containing the α1 subunit (Klausberger, 2009).

In addition to the aforementioned interneuron types, other and less characterized interneurons exist in the CA1 region of hippocampus (Freund and Buzsaki, 1996; Klausberger, 2009). There are long-range projecting interneurons (i.e. trilaminar cells, backprojecting cells, *radiatum* retrohippocampal projection neurons, *oriens* retrohippocampal projection cells and double projection cells) which have their soma in the CA1 field and can send projections to the *subiculum*, to the CA3, the dentate gyrus and in areas outside the hippocampal formation as well (Freund and Buzsaki, 1996; Klausberger, 2009). There are also interneurons which are making synapses specifically with other interneurons (i.e. the interneuron-selective cells) and not with pyramidal cells, suggesting how an inhibitory control over other interneurons is essential.

In Figure 5 is schematically represented the overall interneuron population within the CA1 region.

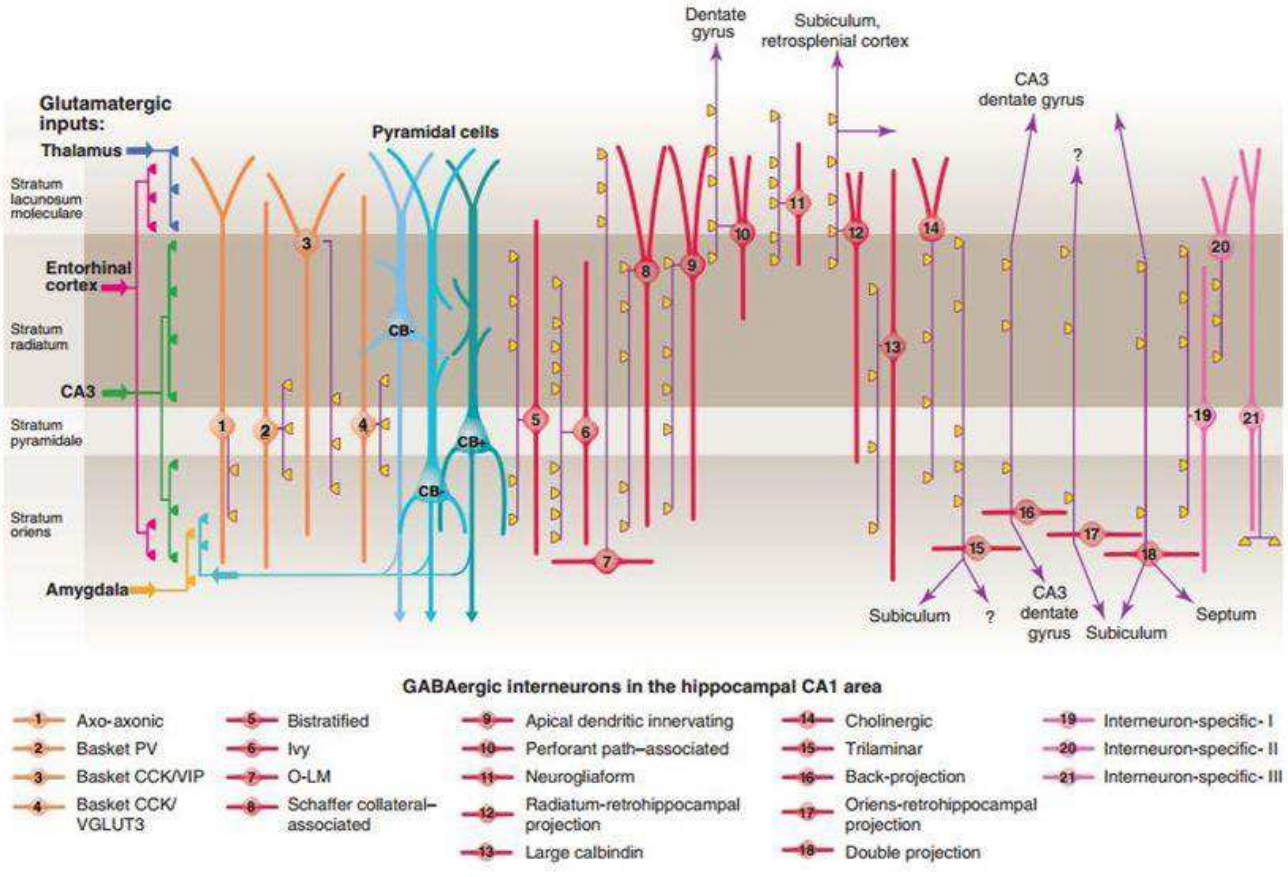

Figure 5 - Three types of pyramidal cell are accompanied by at least 21 classes of interneuron in the hippocampal CA1 area. The main termination of five glutamatergic inputs are indicated on the left. The somata and dendrites of interneurons innervating pyramidal cells (blue) are orange, and those innervating mainly other interneurons are pink. Axons are purple; the main synaptic terminations are yellow. Note the association of the output synapses of different interneuron types with the perisomatic region (left) and either the Schaffer collateral/commissural or the entorhinal pathway termination zones (right), respectively. VIP, vasoactive intestinal polypeptide; VGLUT, vesicular glutamate transporter; O-LM, oriens lacunosum moleculare. *From Klausberger and Somogyi, 2008.*

1.5 – Excitatory and inhibitory transmissions in the hippocampus

Excitatory transmission: The main excitatory transmitter in the hippocampus, as elsewhere in the mammalian central nervous system is glutamate (Kullmann, 2007). Although the earliest evidence for this was principally obtained in the spinal cord, many important insights came from work on hippocampal tissue: for example, glutamate depolarizes hippocampal neurons (Biscoe and Straughan, 1966; Kullmann, 2007), and electrical stimulation in the CA1 evokes glutamate release (Dolphin et al., 1982; Walker et al., 1995). Importantly, glutamate activates the three principal types of receptors that mediate ionotropic excitatory transmission: α-amino-3-hydroxy-5-methyl-isoxazole-propionic acid (AMPA), kainate, and N-methyl-D-aspartate (NMDA) (Kullmann, 2007), which take their names from the exogenous agonists that activate them in a relatively selective fashion (Watkins and Evans, 1981;Nakanishi et al., 1998; Ozawa et al., 1998). At most excitatory hippocampal synapses, EPSCs are mediated by AMPA and NMDA receptors, which have strikingly different biophysical and pharmacological properties. Instead, kainate receptors play a relatively poorly understood role in synaptic transmission (Kullmann, 2007).

In addition to ionotropic transmission, glutamate activates also metabotropic receptors (mGluRs), which are coupled to several G protein types, are typically outside of the pre- and postsynaptic domains and modulate glutamate release, GABA release, and neuronal excitability (Anwyl, 1999; De Blasi et al., 2001; Osten, 2007). The mGluR family subdivides into three groups based on their pharmacological and functional properties: group I (mGluR1, mGluR5), II (mGluR2, mGluR3), and III (mGluR4, mGluR6, mGluR7, mGluR8) (Osten, 2007; Shigemoto et al., 1997).

AMPA receptors = they are composed of different combinations of four subunits (GluR1-4, also known as GluRA-B) and are present at almost all excitatory synapses in the hippocampus, gating a cation-selective channel (Kullmann, 2007). At resting membrane potentials, Na^+ influx accounts for most of the current, but the channel is also permeant to other small monovalent cations, so K^+ efflux can also occur at depolarized potentials. Most AMPA receptors in pyramidal neurons of the adult hippocampus (at least in rodents) are thought to be GluR1-2 or GluR2-3 tetramers (Kullmann, 2007; Wenthold et al., 1996). When a membrane patch taken from the soma or proximal dendrite of a hippocampal neuron is exposed to a pulse of 1 mM glutamate (roughly corresponding to the synaptic glutamate transient) (Kullmann, 2007) a current is generated with a rapid rise time (100–600 μs at physiological temperature). Native AMPA receptors deactivate rapidly following clearance of synaptic glutamate (with a time constant of 2.3–3.0 ms) (Colquhoun et al., 1992), the latter being a faster phenomenon then the termination of AMPA receptor-mediated EPSCs (Kullmann, 2007). If glutamate is not cleared, however, AMPA receptors close rapidly and enter a desensitized state from which they recover relatively slowly, with a decay time constant of the order of 5–10 ms (Kullmann, 2007; Mosbacher et al., 1994). The time course of desensitization depends on the subunit composition of the receptors and is affected by alternative splicing of two exons encoding a 38-amino-acid segment of the GluR2 subunit, with the consequence of having each subunit as either a “flip” or a “flop” variant, depending on which exon is retained the subunit mRNA and with flip forms that desensitize with slower kinetics compared to flop forms (Osten, 2007).

AMPA receptors can even desensitize in the presence of glutamate concentrations that are insufficient to open them or if the glutamate concentration rises sufficiently slowly (Kullmann, 2007). This form of desensitization may be an adaptation that prevents

excessive receptor activation under pathological conditions where extracellular glutamate accumulates. Depending on their subunit composition, AMPA receptors can also show significant permeability to Ca^{2+} ions. This permeability is determined by the presence or absence of a critical aminoacid (arginine, R) in a pore-lining segment of the GluR2 subunit. This subunit undergoes post-transcriptional RNA editing resulting in a change of the aminoacid at this position from glutamine (Q) to arginine (R) (Kullmann, 2007; Sommer et al., 1991). The presence of the edited form of GluR2 ensures that the receptor is impermeable to Ca^{2+}, which is the case for most of the glutamate receptors in principal cells. If the GluR2 subunit is absent, the receptor has significant Ca^{2+} permeability and those receptors are present in some hippocampal interneurons (Geiger et al., 1995; Kullmann, 2007).

NMDA receptors = they consist of heteromultimers of subunits belonging to two relatively distinct subtypes, NR1 and NR2A-D (Kullmann, 2007; McBain and Mayer, 1994). The NR1 subunit is encoded by one gene but exists in several alternatively spliced isoforms. It does not bind glutamate but, instead, contains an important binding site for aminoacids such as glycine and D-serine, which act as co-agonists. The NR2A-D subunits, on the other hand, contain the glutamate-binding site (Kullmann, 2007; Laube et al., 1997). They are encoded by four genes and are variably expressed in different regions of the brain and at different stages of development. NMDA receptors have very slow kinetics and can continue to mediate an ion flux for several hundreds of milliseconds after the glutamate pulse has terminated (activation time constant is approximately 7 ms; deactivation time constants are approximately 200 ms and 1–3 s) (Kullmann, 2007). The slow kinetics are explained by an extremely slow receptor unbinding rate (Lester et al., 1990), that is, once glutamate binds to NMDA receptors, they remain bound for a long

time, during which time the ionophore can undergo repeated opening (Kullmann, 2007). In addition to their slow kinetics, NMDA receptors have three other important features. First, a second agonist-binding site (the “strychnine-insensitive glycine site”) must be occupied before glutamate is able to activate them (Johnson and Ascher, 1987; Kleckner and Dingledine, 1988; Kullmann, 2007), even though some estimates of the tonic extracellular glycine concentration in the brain suggest that the glycine-binding site is normally occupied (Kullmann, 2007). Alternatively, D-serine can substitute for glycine, and it has been proposed that this aminoacid plays a physiological role in regulating NMDA receptor function (Baranano et al., 2001; Schell et al., 1995). Second, NMDA receptors are highly permeable to Ca^{2+} ions and monovalent cations (Ascher and Nowak, 1988; Kullmann, 2007). Ca^{2+} influx via NMDA receptors plays a central role in several forms of long-term synaptic plasticity and NMDA receptor activation has been shown to trigger further release of Ca^{2+} from intracellular stores (Emptage et al., 1999; Kullmann, 2007). Third, Mg^{2+} ions block the ionophore in a voltage-dependent manner (Mayer et al., 1984; Nowak et al., 1984). Thus, at resting membrane potentials (more negative than approximately –50 mV), NMDA receptors are unable to mediate an EPSC even if glutamate and glycine (or D-serine) are present (Kullmann, 2007). They mediate an ion flux only when the membrane is depolarized. The Ca^{2+} permeability and Mg^{2+} blockade of NMDA receptors explain their role as synaptic coincidence detectors: Ca^{2+} influx occurs only if there is a conjunction of presynaptic glutamate release and postsynaptic depolarization, a situation that arises when pre- and postsynaptic activity occur together (Kullmann, 2007; Wigstrom and Gustafsson, 1986).

Kainate receptors = they share many features with AMPA receptors (Ben-Ari and Cossart, 2000; Kullmann, 2007; Kullmann, 2001; Lerma et al., 1997; Lerma et al., 2001)

because they are heteromultimeric as well, made up of different combinations of five subunits: GluR5-7 and KA1-2. However, not all of these subunits have the same status because receptors made up of KA1 or KA2 alone are non-functional (Kullmann, 2007). GluR5-6 undergoes Q/R editing with similar consequences as for the AMPA GluR2, although the proportion of edited subunits is much less spread. All this features of kainate receptors means that the Ca^{2+} permeability, single-channel conductance, and rectification of the receptor cannot be inferred easily from the subunit composition (Kullmann, 2007).

The biophysical properties of recombinant kainate receptors are similar to those of AMPA receptors because they open and desensitize rapidly, and they have single-channel conductances, rectification properties, and Ca^{2+} permeabilities that depend on Q/R editing (Bowie and Mayer, 1995; Kamboj et al., 1995; Kullmann, 2007). However, there are some unexplained discrepancies between the relatively low affinity and rapid kinetics of kainate receptors studied in isolated cells and the finding that synaptic kainate receptor-mediated signals exhibit very slow kinetics (Castillo et al., 1997; Kullmann, 2007; Lerma et al., 1997; Lerma et al., 2001). Some kainate receptor-mediated EPSCs can last more than 100 ms, at which time they would have been expected to have deactivated following clearance of glutamate or desensitized if glutamate persisted (Kullmann, 2007). Several explanations have been proposed for this discrepancy, including the possibility that synaptic kainate receptors differ from nonsynaptic receptors in their subunit composition because of the actions of accessory proteins or because of site-specific phosphorylation (Garcia et al., 1998; Kullmann, 2007). Among other possible explanations for the slow kinetics of kainate receptor-mediated EPSCs is that glutamate needs to diffuse a long distance to reach the receptors, perhaps because they are relatively remote from the site of exocytosis (Kullmann, 2007). In addition, synaptic co-release of a modulatory substance might alter the response of kainate receptors to

glutamate. Another puzzle is that, although kainate receptors are abundant in the hippocampus, synaptic responses mediated by them are very small and generally require trains of high frequency stimuli to be detected (Kullmann, 2007). Recently, however, relatively fast, apparently monoquantal kainate receptor-mediated EPSCs have been described in interneurons and CA3 pyramidal neurons (Cossart et al., 2002), further complicating the picture about the physiological role played by these receptor types.

Evidence has emerged for a major role of presynaptic kainate receptors in modulating transmitter release (Chittajallu et al., 1996; Cossart et al., 2001; Kullmann, 2007; Rodriguez-Moreno et al., 1997; Vignes et al., 1998), axon excitability (Semyanov and Kullmann, 2001) and synaptic plasticity (Contractor et al., 2001; Kullmann, 2007; Lauri et al., 2001). Surprisingly, kainate receptors at various synapses, activated by different concentrations of agonists, either enhance or depress transmitter release (Kullmann, 2007). The mechanisms underlying these phenomena are not completely understood (Kullmann, 2001) and may include depolarization, Ca^{2+} influx via permeable receptors, and coupling to a metabotropic cascade (Rodriguez-Moreno and Lerma, 1998). Although presynaptic kainate receptors exert a powerful influence on synaptic function, the adaptive significance of the enhancement and depression of transmitter release mediated by kainate receptors remains a subject of speculation (Kullmann, 2007).

Metabotropic glutamate receptors (mGluRs) = mGluRs are seven transmembrane receptors coupled to G proteins, which mediate most of their actions. Metabotropic glutamate receptors fall into three classes, although eight genes have been identified (Kullmann, 2007; Pin and Duvoisin, 1995; Schoepp, 2002). Group I receptors, which includes mGluR1 and 5, have a selective somatodendritic perisynaptic distribution

in principal neurons and are typically located at the outer edge of postsynaptic densities of dendritic spines (Baude et al., 1993; Lujan et al., 1996; Shigemoto et al., 1997).

mGluR1 mRNA is present in all principal cells, with the order of expression level DG>CA3>CA1, and in somatostatin-positive but not parvalbumin-positive interneurons in the CA1 *stratum oriens* and the *stratum oriens and radiatum* of CA3 (Kerner et al., 1997; Shigemoto et al., 1997). mGluR-5 mRNA is abundant in the hippocampus, expressed strongly in CA pyramidal cells, dentate granule cells, many types of GABAergic interneurons (somatostatin-positive and parvalbumin-positive) and in astrocytes (Ferraguti and Shigemoto, 2006; Fotuhi et al., 1994; Kerner et al., 1997).

Both mGluR1 and 5 are coupled to Gq heterotrimeric G proteins, thus leading to activation of phospholipase C and subsequent mobilization of inositol 1,4,5-trisphosphate (IP_3), which in turn increases cytosolic Ca^{2+} via activation of IP_3 receptors on the endoplasmic reticulum (Fagni et al., 2000).

Group II (mGluR 2, 3) and group III (mGluR4, 6, 7, 8) receptors tend to be located in presynaptic membranes (Kullmann, 2007). Several group III receptors, on the other hand, tend to be located in synapses, that is, very close to or even within active zones (Ferraguti and Shigemoto, 2006; Shigemoto et al., 1997). mGluR3 mRNA is abundant in dentate granule cells but absent from pyramidal cells (Kullmann, 2007) and is also expressed in hippocampal white matter tracts, the fimbria, and the fornix (Ohishi et al., 1993). mGluR4 and mGluR7 mRNAs are both expressed in CA1 and CA3 pyramidal cells, dentate granule cells, and scattered interneurons (Ohishi et al., 1995) with the mGluR4 markedly present in CA2 pyramidal cells (Osten, 2007). The mGluR2 and mGluR7a proteins are on axons and terminals of the medial perforant path, and at mossy fibers mGluR2 receptors are located relatively far from glutamate release sites (in axonal membranes) implying that they detect only glutamate molecules that have escaped from

the synaptic cleft (Kullmann, 2007; Yokoi et al., 1996). A prominent immunoreactivity for mGluR8 is present, instead, in the lateral perforant path in the dentate gyrus and the CA3 area (Osten, 2007). Both Group II and III mGluRs inhibit adenylate cyclase activity via Gi proteins.

The physiological roles of metabotropic receptors are not fully understood (Kullmann, 2007). The perisynaptic postsynaptic group I receptors may preferentially respond to trains of action potentials that result in the prolonged presence of glutamate in their vicinity and indeed, such stimulus patterns successfully evoke postsynaptic currents and Ca^{2+} signals mediated by group I receptors (Heuss et al., 1999; Kullmann, 2007; Yeckel et al., 1999). It is widely documented that activation of group I mGluRs does increase cells excitability in hippocampus (Anwyl, 1999). In particular, on pyramidal cells has been shown a direct depolarization mediated by mGluR1 as well as a decrease of the slow afterhyperpolarization and a potentiation of NMDA currents, both mediated by mGluR5 (Mannaioni et al., 2001). In addition to pyramidal cells, group I mGluRs excite interneurons as well (McBain and Mayer, 1994; van Hooft et al., 2000), leading to mGluR1-induced increased frequency but not amplitude of spontaneous IPSCs recorded on pyramidal cells (Mannaioni et al., 2001), suggesting a pre-synaptic mechanism.

However, in addition to the effects mentioned above which are short-lasting and ascribable to acute actions of the group I mGluRs agonists used, activation of those receptors in the adult hippocampus may in turn induce long-lasting forms of excitatory and inhibitory synaptic plasticity (Anwyl, 1999; Castillo et al., 2011). Regarding excitatory transmission, is well characterized a form of long-term depression following pharmacological activation of group I mGluRs (Gladding et al., 2009), while concerning inhibitory transmission is known a long-term depression mediated by retrograde endocannabinoids signaling (Chevaleyre and Castillo, 2003), and long-term potentiation

(Patenaude et al., 2003), the latter being expressed cooperatively with $GABA_B$ receptors and group II mGluRs activation.

Regarding group II receptors, their predominantly extrasynaptic presynaptic location implies that they detect the extracellular build-up of glutamate and that they therefore act as autoreceptors that regulate neurotransmitter release as a function of the volume-averaged excitatory traffic (Kullmann, 2007; Scanziani et al., 1997). The intrasynaptic presynaptic location of some group III receptors prompts the speculation that they act as autoreceptors on a smaller spatial scale (Kullmann, 2007). However, they are also present at some GABAergic terminals (Shigemoto et al., 1997), which are not known to release glutamate (Kullmann, 2007). Moreover, there is evidence that they detect glutamate released from neighboring synapses (Semyanov and Kullmann, 2000), so their role may be akin to that of group II receptors. Nevertheless, evidence has been put forward for an occlusion of presynaptic Ca^{2+} channels, an activation of presynaptic K^+ channels, and a direct inhibition of exocytosis in the group II/III mGluR- mediated decrease of neurotransmitters release (Anwyl, 1999).

Inhibitory transmission: The major inhibitory transmitter in the hippocampus as well as in the brain is γ-Aminobutyric acid (GABA), which acts on the ionotropic $GABA_A$ receptor and the metabotropic $GABA_B$ receptor (Fishell and Rudy, 2011).

$GABA_A$ receptor = they are heteropentameric, and consist of a combination of 7 different subunits: α_{1-6}, β_{1-3}, γ_{1-3}, δ, ε, π and θ (Fishell and Rudy, 2011; Mehta and Ticku, 1999). Of these, α_6, ε, π and θ, appear to be excluded from the rodent hippocampus or to occur at very low levels (Kullmann, 2007). Most hippocampal $GABA_A$ receptors contain

two α subunits and two β subunits, together with either a γ subunit or the δ subunit but not both (Chang et al., 1996; Farrar et al., 1999; Kullmann, 2007; Whiting et al., 1999). The α subunits play important roles in determining the affinity for GABA and the sensitivity to numerous modulatory agents such as Zn^{2+} ions, steroids, ethanol, and exogenous pharmacological agents such as benzodiazepines, barbiturates, and general anesthetics (Barnard et al., 1998; Kullmann, 2007). The γ subunits also affect several of these parameters and, in addition, mediate anchoring of $GABA_A$ receptors to synapses via an indirect interaction with gephyrin, a scaffolding protein that plays an important role in the formation and stabilization of both GABAergic and glycinergic synapses (Essrich et al., 1998; Kullmann, 2007). The δ-containing receptors, instead, tend not to be confined to synapses but have a high affinity for GABA and are relatively insensitive to benzodiazepines (Kullmann, 2007). There are evidences showing the involvement of δ subunits in mediating a $GABA_A$ receptor-dependent tonic inhibition in dentate granule cells (Nusser and Mody, 2002; Overstreet and Westbrook, 2001).

$GABA_A$ receptor-mediated IPSCs have a fast onset, although their decay is generally slower than that of AMPA receptor-mediated EPSCs. Their single-channel conductance is highly variable, ranging from < 1 to > 30 pS, depending on their subunit composition (Kullmann, 2007).

$GABA_A$ receptors are permeable only to anions, with the main being Cl^- ions, but is present also certain permeability to HCO_3^- ions (Kaila, 1994). In the mature brain, GABA, by acting on $GABA_A$ receptors, inhibits excitation via two main mechanisms: hyperpolarization and shunting inhibition (Fishell and Rudy, 2011). Hyperpolarization occurs when the resting membrane potential of the cell is more positive than the reversal potential for Cl^- (E_{Cl}), thus increasing the difference between the membrane potential and spike threshold, thereby decreasing the effectiveness of excitatory inputs. On the other

hand, when E_{Cl} is in between the resting membrane potential and threshold for spike generation the increase in anionic conductance after $GABA_A$ activation locally decreases the input resistance, thus reducing the impact of the currents generated by concurrent excitatory inputs, ultimately resulting in excitatory postsynaptic potentials of smaller amplitude. The situation is different in neurons at early stages of development (Ben-Ari et al., 1989). The intracellular Cl^- concentration is relatively high because the principal extrusion mechanism (the K^+/Cl^- co-transporter, KCC2) is not expressed abundantly (Kullmann, 2007; Rivera et al., 1999) and therefore the electrochemical gradient then induces Cl^- ions flow out of the cell, making the current depolarizing. Such depolarizing GABAergic signals can bring neurons to firing threshold and trigger Ca^{2+} influx, and they may play an important role in the early stages of neural circuit formation (Ben-Ari et al., 1997; Kullmann, 2007).

$GABA_B$ receptor = metabotropic $GABA_B$ receptors are heterodimers composed of GBR1 and GBR2 (Jones et al., 1998), both of which can undergo alternative splicing (Kullmann, 2007; Kuner et al., 1999). $GABA_B$ receptors are widely present at both pre- and postsynaptic elements of synapses and also in extrasynaptic domains (Fritschy et al., 1999). The $GABA_B$ receptor agonist baclofen powerfully depresses the synaptic release of both glutamate and GABA, suggesting a role as autoreceptor and not specifically restricted to inhibitory synapses (Kullmann, 2007). $GABA_B$ receptors in the presynaptic terminals downregulate N- and Q- type Ca^{2+} channels via a G-protein cascade (Anwyl, 1991; Kullmann, 2007; Mintz and Bean, 1993), although this may not account entirely for their effect on transmitter release (Capogna et al., 1996). On the postsynaptic side, $GABA_B$ activity leads to the opening of G protein-gated inward-rectifying K (GIRK) channels (Andrade et al., 1986; Misgeld et al., 1995). Activation of these channels causes

a slow IPSP, lasting several hundred milliseconds (Kullmann, 2007) which is easily distinguished from the $GABA_A$ receptor-mediated IPSP, not only because of its slow kinetics but also because it is independent of the Cl^- reversal potential. In contrast to $GABA_A$ receptor-mediated IPSCs, it has proved difficult to elicit $GABA_B$ receptor-mediated synaptic responses by activating individual presynaptic neurons, even though $GABA_B$ receptors have usually higher affinity for GABA than $GABA_A$ receptors (Kullmann, 2007). A possible explanation is that $GABA_B$ receptors are principally extrasynaptic and need accumulation of GABA in the synaptic cleft to activate them through spillover (Destexhe and Sejnowski, 1995; Scanziani, 2000).

.1.6 – The excitatory/inhibitory balance in hippocampal networks

Local circuits in the hippocampus are comprised of excitatory connections from principal cells to interneurons and mainly inhibitory interneuronal connections onto principal cells. Together with this, a smaller number of connections are made up of mutual inhibitory interneuronal interconnectivity and recurrent excitatory connectivity between principal cells (Buhl, 2007). This remarkable reciprocal wiring in hippocampal as well as in other cortical neuronal networks allows to the activity of individual cells to strongly influence the behaviour of the whole network (Buhl, 2007; Isaacson and Scanziani, 2011).

The mechanisms by which the mixed activity of pyramidal cells and interneurons (the "building blocks" of neuronal networks, Isaacson and Scanziani, 2011) do so can be recapitulated in two processes, feedback and feedforward inhibition, whose prevalence relies on the wiring diagram of interneurons onto principal cells. Feedback inhibition occurs when the firing of the pyramidal cell activates surrounding interneurons (e.g. basket cells, bistratified cells, and *oriens – lacunosum moleculare* cells) with the following inhibition of principal cell's output. On the other hand, feedforward inhibition happens when an interneuron (e.g. neurogliaform cells and Schaffer collateral-associated cells) receives an excitatory input with the consequent inhibition of the pyramidal cell's output (Buhl, 2007). The same scenario is enriched by the presence of interneurons that specifically target other interneurons (Freund and Buzsaki, 1996), making a network with the ones that have principal cells as targets, which massively amplifies the dynamics of local circuit responses to an afferent input.

The specific firing patterns of principal cells in a network will depend largely on the temporal and spatial distribution of inhibition, with the result that in response to the

same input, the same network can potentially produce several different output patterns at different times, depending on the state of inhibition (Isaacson and Scanziani, 2011; van Vreeswijk and Sompolinsky, 1996). Through the recruitment of interneurons via feedforward and/or feedback excitatory projections, inhibition generated in cortical networks is somehow proportional to local and/or incoming excitation (Isaacson and Scanziani, 2011). For example, acute experimental manipulations selectively decreasing either inhibition or excitation shift cortical activity to a hyperexcitable (epileptiform) or silent (comatose) state (Dudek and Sutula, 2007; Isaacson and Scanziani, 2011). Thus, not only excitation and inhibition increase and decrease together during physiological cortical activity (van Vreeswijk and Sompolinsky, 1996), but interfering with this relationship is highly disruptive (Isaacson and Scanziani, 2011). Highlighting the importance of a proper relationship between excitation and inhibition is the fact that changes in the weight of excitation or inhibition are accompanied by compensatory effects that preserve the excitability of cortical networks (Turrigiano, 2011). These observations have led to the concept that this two opposing synaptic conductances, balance each other out and that this balance is important for proper cortical function (Isaacson and Scanziani, 2011).

1.7 – Voltage sensitive dye imaging as a tool to record neuronal networks activity

In the previous paragraphs, we could appreciate the importance of studying neuronal networks and how do they assemble and function, being the result of the concerted activity of excitatory and inhibitory neurons. In this paragraph, I will describe the voltage sensitive dye imaging (VSDI) technique, which allows recording neuronal activity from single neurons as well as from entire brain regions, thus covering almost all the neuro-architectural organizations within the central nervous system.

Voltage sensitive dye imaging reports changes in membrane potential through proportional variations of fluorescence emitted by a molecule bound to the cellular membranes of excitable cells (Chemla and Chavane, 2010; Grinvald and Hildesheim, 2004; Peterka et al., 2011; Tominaga, 2013).

The pioneering work of the Nobel Prize laureate Edgar Douglas Adrian, which in the late '20s recorded neuronal activity from individual nerve cells using a combination of capillary electrometers and valve amplifiers (1932; Yuste, 2015), paved the way to the enormous progress of modern electrode-based electrophysiology. However, in recording neuronal network activity, information obtained from electrode-based recordings is intrinsically limited by the number of electrodes used. In addition, electrodes are invasive and cannot access thin structures such as dendritic spines, for example (Peterka et al., 2011). Therefore, during the last decades have been developed optical methods, in which neuronal activity is recorded through changes in adsorption or emission of light, rather than changes in electric currents.

The first optical signals detected during neuronal activity were variations in light scattering and birefringence that accompany action potentials in nerves and single axons following trains of stimuli (Cohen, 2010; Hill, 1950; Hill and Keynes, 1949). These signals were lasting several seconds and were very small, thus required averaging of tens of trials to improve the signal/noise ratio (Cohen et al., 1968). Nevertheless, the use of dyes allowing to measure changes in the optical properties of stained preparations started in the late '50s (Nasonov, 1957) and was further developed in the following years, up to recently ago (Cohen, 2010; Fluhler et al., 1985; Fromherz et al., 2008; Ross et al., 1977; Tasaki et al., 1968; Vereninov, 1962). During the years, numerous evidences accumulated demonstrating the membrane voltage-dependence of those dyes, with some of them following membrane potential with a time constant of <1 μs (Cohen et al., 1974; Davila et al., 1974; Loew et al., 1992; Loew et al., 1985; Salzberg and Bezanilla, 1983).

The proposed mechanisms for the voltage-dependence of voltage sensitive dyes include (Loew, 2010; Peterka et al., 2011):

- Redistribution, that is the dye move partly into or out of cell's membrane following the change in the electric field caused by action potentials. This alters the concentration and the spectroscopic properties of the fluorophore, due to the changes in the chemical environment between membrane and cytosol following currents flow. These types of chromophores are sometimes referred to ''slow'' dyes, because their insertion or detachment from the membrane is a relatively slow (lasting seconds) equilibrium process when compared with other mechanisms and are useful for applications where high time resolution is not crucial.

- Reorientation, in which the chromophore lies in or on the membrane with a particular orientation, determined by the sum of the interaction forces on the

chromophore. Changes in the electric field modify the orientation angle, thus leading to variations of the spectral properties of the molecule. Reorientation can be fast since it does not involve a significant movement of the chromophore.

- Electrochromism, in which the change of potential across the membrane as the result of neuronal activity directly influences the electronic structure, and thus the spectra, of a chromophore. The best characterized electrochromic dye is di-4-ANEPPS, whose chromophore changes its electron configuration upon excitation such that the charge shifts from the pyridinium nitrogen in the ground state to the amino nitrogen in the excited state (Figure 6).

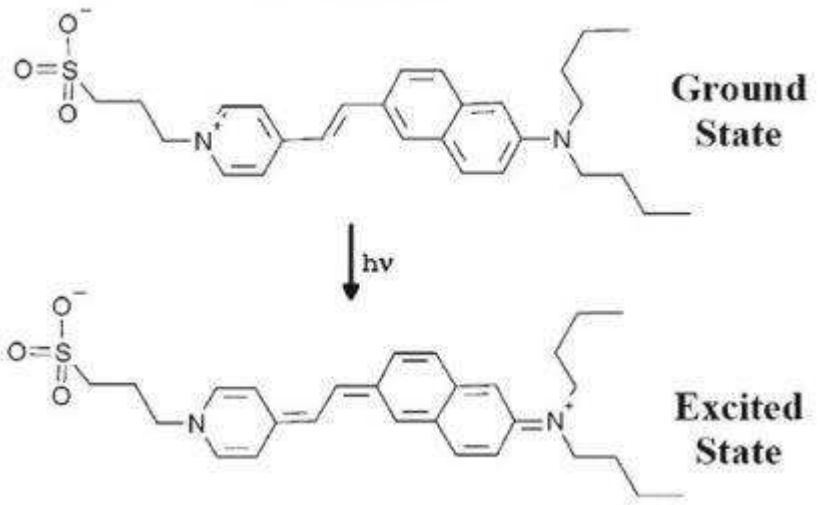

Figure 6 – Resonance structures for the ground and excited states of the most widely used voltage sensitive dyes, di-4-ANEPPS. In this chromophore, the donor moiety is an aminonaphthyl group, the linker is a simple double bond and the acceptor is a pyridinium moiety. *Adapted from Loew, 2010.*

Electrochromic dyes are usually amphiphilic molecules which use their hydrophobic tail to anchor to the membrane in a position approximately perpendicular to the surface. This orients the direction of the excitation-induced

charge motion parallel to the electric field vector within the membrane, with the consequence that the ground and excited states are differentially stabilized by the intramembrane electric field, causing a shift in the spectrum when the membrane potential changes. The electrochromic effect, also known as Stark effect, is fast since it only involves intramolecular charge redistribution, without chromophore movement.

Voltage sensitive dyes (VSD) stain cellular membranes of all cell types, both neurons and glial cells. However, they report mainly neuronal signals because glial cells do not generate action potentials and do not participate on the fast millisecond time scales of neuronal transmission (Chemla and Chavane, 2010). Has been proven, in fact, that a glial component in neuronal transmission can be detected after several seconds from stimulus onset (Chemla and Chavane, 2010; Schummers et al., 2008). In addition, VSD report signals mainly from dendrites because they represent approximately 90% of the total neuronal cell surface (Eberwine, 2001), therefore the VSD signal can be considered as dendritic post-synaptic activity (Chemla and Chavane, 2010).

Together with the dyes, voltage sensitive dye imaging of large scale recordings of neuronal activity needs additional equipment in order to be performed (Tominaga, 2013), such as optics (low magnification lenses with high numerical aperture), imaging cameras (modern charge-coupled devices [CCDs] and complementary metal-oxide-semiconductor [CMOS] image sensors rather than older photo-diodes arrays) and a light source to excite the dye (halogen lamps with appropriate excitation filters or LED lights).

AIM OF THE THESIS

Cellular entities that share the same functionality assemble in neuronal networks, which are the structural interface between single cells and behavior (Parker, 2006, 2010). However, while we know a lot in terms of pathophysiology of single cells and we can directly assess behavioral responses, information on neuronal networks functioning are quite lacking.

The balanced action of excitatory and inhibitory networks is instrumental for proper cortical computations (Buhl, 2007; Isaacson and Scanziani, 2011; Kullmann, 2011), which are responsible for many behavioral responses. Nevertheless, while tools to record large scale excitatory activity are available and widely used (Buzsaki, 2004; Buzsaki et al., 2012), there is not the same technical capacity to monitor network inhibition.

During my doctoral course I used voltage sensitive dye imaging (VSDI) to study excitatory and inhibitory networks in the mouse hippocampus because VSDI allows the monitoring of membrane potential changes with very good temporal resolution (milliseconds) as well as, in the configuration I used, wide spatial resolution, which has been fit to record neuronal activity from all the CA1 region and specifically in its layers.

Regarding the study of excitatory networks, with the collaboration of a team of mathematicians of the University of Bordeaux led by Prof. Angelo Iollo, I developed an algorithm for a more detailed analysis of the VSDI data obtained in the CA1 network. The need of a more comprehensive analysis of VSDI recordings is justified by the fact that in most of the studies so far using VSDI are quantified only time-fixed changes in fluorescence emission in determined regions of interest (ROIs). In this way, however, are missed other features of the dynamics of excitatory signals such as, among others, the

velocity and the direction of spreading and how these parameters may change during the fast time-scales of neuronal transmission. With our algorithm, we quantify all of these parameters. This algorithm represents a new method to determine an optical flow, that in image processing is the measure of the pattern of apparent motion of objects, surfaces, and edges in a visual scene caused by the relative motion between an observer (an eye or a camera) and the scene (Warren, 1985). It is based on the application of a mathematical problem called “optimal mass transfer problem” (also known as “Monge-Kantorovich” problem, MKP; Iollo, 2011; Kantorovich, 1942; Monge, 1781; Villani, 2009), which consists in finding a way to transport a certain quantity of mass from a starting point to a final one, minimizing a given functional cost. In our case, the quantity of mass to be displaced is neuronal depolarization and the functional cost to be minimized is the distance. The output of the algorithm is a vectorial field in which each vector represents the least distance travelled by neuronal depolarization across the CA1 network in each pixel of the image and at every time-step (2.2 milliseconds).

Regarding the study of inhibitory networks, I aimed at testing if was possible to record network GABAergic inhibition with VSDI in hippocampus, since a previous study reported the possibility to record inhibitory events on a single hippocampal pyramidal cell (Canepari et al., 2010) using the same technique. Because I was able to record network inhibition with VSDI in the whole CA1 region and specifically in its layers, I tested if group I mGluRs activity could have an impact on it, because metabotropic glutamatergic transmission strongly influences neuronal excitability (Anwyl, 1999).

The results reported in this thesis might enlarge knowledge of neuronal networks functioning in hippocampus because provide additional tools for the study of both excitatory and inhibitory circuits.

CHAPTER II

In submission

Quantitative assessment of CA1 network dynamics by combining voltage sensitive dye imaging and optical flow methods

Michelangelo Colavita[1,2,3], Afaf Bouharguane[4], Geoffrey Terral[1,2], Andrea Valenti[4], Clement E. Lemercier[1,2], Filippo Drago[3], Angelo Iollo[4], Giovanni Marsicano[1,2,♯], Federico Massa[1,2,♯,*]

1:INSERM U862, NeuroCentre Magendie, AVENIR Group "Endocannabinoids and Neuroadaptation", 33077 Bordeaux, France

2:Université de Bordeaux, 33077 Bordeaux, France

3:University of Catania, Biometec – Department of Biomedical and Biotechnological Sciences, 95125 Catania, Italy

4:Institut de Mathématiques de Bordeaux UMR 5251 Université Bordeaux 1 and INRIA Bordeaux-Sud Ouest, 33405 Talence, France

♯ = Share last authorship

* = Corresponding author

Abstract

Understanding neuronal networks functioning is fundamental because represent the fundamental link between the activity of single cells and the resulting behaviour. To accomplish the study of neuronal networks within the mouse hippocampus we employed voltage sensitive dye imaging (VSDI) and we developed a novel algorithm for the analysis of the VSDI data, which is based on the application of the optimal mass transportation theory. With this algorithm we quantified the velocity and the overall orientation of the VSDI signal spreading. We found that increasing stimulation intensity of Schaffer's collaterals and blocking $GABA_A$ receptors activity with picrotoxin (PTX) led to decrease of the velocity of VSDI-recorded depolarization signals within the CA1 hippocampal region. In addition, the application of PTX restrained the VSDI signals specifically in *strata oriens* and *radiatum* proximal to pyramidal layer, making them more convergent within the above sublayers. Overall, in this study we highlight new features of hippocampal neuronal networks dynamics by introducing a novel analytical approach of data from the optical monitoring of neuronal activity.

Introduction

Neuronal networks (NN) consist of interacting collections of individual neurons, which are functionally related to the same task[1, 2]. Much is known about the cellular properties of the nervous system and on the other hand, we can characterize and quantify behaviours and correlate them with the activity of different regions of the brain. However, it is often difficult to explain behaviours with mechanisms mediated by single cell or synapses. Closing the explanatory gap between the cellular and behavioural levels requires a deep understanding of the neuronal networks that pool the cellular components underlying behaviour.

Voltage sensitive dye imaging (VSDI) is a strong candidate technique to probe neuronal networks functioning because it allows not invasive optical monitoring of neuronal activity from very small compartments such as dendrites to areas several mm^2 wide, with milliseconds time resolution[3-5]. The readout of such technique is values of fluorescence emitted proportionally to changes in membrane potential in each pixel, which are organized in two-dimensional spatial arrays spaced out by milliseconds time steps.

However, considering the amount of experimental data obtained with VSDI applied to the investigation of NN dynamics up to now, most of these studies rely on time-fixed evaluations of neuronal activity, represented by quantification of membrane potential-dependent variations of fluorescence emissions inside a given region of interest (ROI). This approach nevertheless misses key information of neuronal computation: (i) how does neuronal activity change at time resolution relevant for neuronal processes? (ii) Are there other parameters that could better explain NN behavior?

Some VSDI studies already answered to these questions[6-9], but these methods mainly rely on the analysis of integral quantities and in some cases on *ad hoc* approaches to determine how the signal is propagated through the NN. For example, in a recent work

Takagaki and collaborators[8] employed a flow-detection algorithm to study the propagation of neuronal activity with VSDI. This algorithm exploits a maximum correlation principle classical in fluid mechanics to determine spatial flow patterns. For simple propagation patterns this approach can lead to reasonable results. However, when signal spreads in complex threads, a statistical approach is unable to deliver valuable information due to the lack of an underlying model.

Here we propose a model-based objective way to quantitatively analyze the distributed information obtained via VSDI, with the advantage that no additional parameter is tuned to determine the model. It represents a novel method to estimate an optical flow[10-12] and derives from the resolution of an optimal mass transfer problem[13] in order to analyze the propagation patterns from successive frames of images reporting VSDI-recorded depolarization changes. Its underlying principle is to find a way to transport a certain amount of mass from a starting configuration to a final one, by minimizing a given functional cost. The dynamic vector fields provided by this technique can be analyzed by conventional point-wise statistical methods, but taking into account the spatial nature of the time-resolved VSDI data, we have the possibility to provide a deeper understanding of the distributed neuronal activity.

Results

VSDI-recorded depolarization changes after CA1 network manipulations

VSDI has been extensively used since many years for the investigation of glutamatergic transmission across neuronal networks in hippocampus as well as in other brain regions[3, 4, 6-8, 14-19]. The usual practice in such technique is quantifying variations of fluorescence respect to background ($\Delta F*F^{-1}$ values), which occur proportionally to changes in membrane potential.

In order to record with VSDI hippocampal network activity in CA1, we stimulated the Schaffer's collaterals and we used two different approaches to manipulate CA1 glutamatergic network activity: increasing stimulation intensity from 10 to 30 Volts and blocking $GABA_A$ receptor-mediated inhibitory activity with picrotoxin (PTX, 100 μM). As shown in Figure 1a and b, both manipulations dramatically increased depolarization-mediated fluorescence emission, represented by a higher $\Delta F*F^{-1}$ value, which is color-coded onto the representative frames of VSDI activity at the indicated time points on the right bottom (red is the highest value of $\Delta F*F^{-1}$). We next aimed at quantify $\Delta F*F^{-1}$ values inside the whole CA1 region, by drawing a region of interest (ROI; see Fig.1c for a representative drawing of the ROI) covering the entire CA1. As shown in Figure 1d and e, by increasing Schaffer's collaterals stimulation intensity to 30 Volts, significantly boosts $\Delta F*F^{-1}$ values during all the time window containing the VSDI-recorded depolarization (45.2 milliseconds; 7 slices from 4 mice; two-tailed paired t test in e), consistent with the notion of higher recruitment of glutamatergic fibers. In addition, blockade of GABAergic transmission by application of PTX remarkably prolongs neuronal depolarization (Fig. 1f and g, 7 slices from 5 mice; two-tailed paired t test in g) and does not affect the early phase of VSDI signal propagation spreading (Fig. 1g, "until 12.2 ms"). These results are in agreement with the ones obtained analyzing the different CA1 subregions (Supplementary Figure 1 and 2), demonstrating how VSDI is a powerful tool to dissect neuronal transmission across several ROIs at the same time.

Validation of the algorithm

In order to obtain more parameters that could deeper describe the spreading of depolarization recorded with VSDI in the CA1 network, we developed an algorithm based on the application of the optimal mass transport problem. Before the analysis of the VSDI

data mentioned above, we tested the accuracy of the method by analyzing a set of surrogate data (see Methods). As shown in Figure 2a, when we shifted each value inside the square of 1 pixel along the x axis [initial coordinates for each value are (x,y); final coordinates after the movement are (x+1,y)], the resulting vectorial field coherently reports the movement, as all the vectors have 1 pixel length, pointing to the right of the field. Correct results come also from the movement of each value in the square by 1 pixel along the x axis and 1 pixel along the y axis [Figure 2b, final coordinates (x+1, y+1)], which results in each vector having a length of 1 pixel on the x and y axis, respectively. Altogether, these data demonstrate that our algorithm coherently reports changes in position, showing accurate spatial resolution.

Increased depolarization state decreases VSDI signal velocity in CA1 network

After validation, we analysed using the algorithm the data resulting from the VSDI recordings of CA1 network depolarization after increased stimulation intensity and application of PTX. As shown in Figure 3b, augmenting stimulation intensity from 10 to 30 Volts leads to a significant overall decrease of VSDI signal velocity in the whole CA1 (7 slices from 4 mice; two-tailed paired t test). This effect is widespread, since is preserved across all CA1 sublayers (Fig.3d, f, h, j; 7 slices from 4 mice; two-tailed paired t test). Notably, the overtime reduction of signal velocity is mainly due to the effect in the middle-end of the time course of signal propagation, since in the first phase the two stimulation intensities show similar velocities. A closer evaluation of the time courses of velocity changes (Fig.3a, c, e, g, I; 7 slices from 4 mice) shows how 30 Volts stimulation-induced speed changes reach their highest value 2.2 milliseconds before control condition (10 Volts) and then gradually decrease until a steady level of approximately 0.02 m/s.

Regarding the analysis of velocity changes after inhibition of $GABA_A$ receptors (Fig.4b, d, f, h, j; 7 slices from 5 mice; two-tailed paired t test) we can appreciate an overtime reduction of signal speed respect to baseline level in the whole CA1 and in its subfields, similarly to what obtained by changing stimulation intensities. However, there are some differences between the two manipulations. The evaluation of the time course curves (Fig. 4a, c, e, g, l; 7 slices from 5 mice) highlights how there are no differences in latency between baseline and PTX application and can be observed a slight but significant decrease of signal velocity in the first seven time steps in the whole CA1 (Fig.4b, "until 12.2 ms"), which is likely due to the significant reduction obtained in *radiatum proximal* (Fig.4h). Another difference between experiments with PTX and diverse stimulation intensities is that on average the reduction in signal velocity after $GABA_A$ receptors blockade is much more pronounced in the middle-end part of signal propagation (Fig.4b, d, f, h, j, between 14.4 and 45.2 ms), having a value of approximately 0.01 m/s.

Altogether, these data show how an increased and persistent depolarized state as it is after 30 Volts stimulation and blockade of GABAergic inhibition strongly reduces signal velocity, consistent with the notion of a decreased displacement of neuronal depolarization during time.

$GABA_A$ receptors blockade restrains neuronal depolarization

A useful feature that can be quantified from a vectorial field is the expansion and the compression of the vectors in the spatial domain, namely positive divergence and negative divergence, respectively. Here we refer to negative divergence as convergence, in order to give a more immediate and familiar meaning of its significance.

In our case, we quantified changes in divergence and convergence in the vectorial fields reporting the optimal displacement of neuronal depolarization in the whole CA1 and in its

sublayers following the previously mentioned network manipulations. These measures would give an index of the overall direction of spreading of the neuronal depolarization signals recorded with VSDI inside a given ROI.

As shown in Figure 5, increasing stimulation intensity to 30 Volts does not change signal direction compared to 10 Volts stimulation, neither in the whole CA1 (Fig.5a,b; 7 slices from 4 mice; two-tailed unpaired t test in b), nor in its subfields (Fig.5c-j; 7 slices from 4 mice; two-tailed unpaired t test in d, f, h and j). Interestingly, blocking $GABA_A$ receptor conductances significantly impacts on the overall signal spreading, making it more convergent and less divergent compared to baseline specifically in *strata oriens* and *radiatum proximal* both at the early and middle-late phase of the propagation (Fig.6d and h; 7 slices from 5 mice; two-tailed unpaired t test).

These data therefore suggest how inhibition played by $GABA_A$ receptors is instrumental for a proper routing of glutamatergic activity across the CA1 region of hippocampus.

Discussion

In this study we provide a new method to determine an optical flow[10-12], which is based on the application of the optimal mass transfer problem[13, 20], that is finding a plan to transfer a quantity of mass from a starting configuration to a final one minimizing a functional cost. Optimal transport theory has been applied for the analysis of disparate phenomena such as crowd motion[21], geophysical flows[22], collapsing sand piles[23], nonlinear electrodynamics[24] and magnetic resonance imaging (MRI) data[20].

In our case, the mass to be transported is VSDI-recorded depolarization and the functional cost to be minimized is distance. The analysis of the two sets of experiments presented here, the increasing of stimulation intensity and the blockade of $GABA_A$ receptors-mediated inhibition within the CA1 excitatory network, showed how optimal

transfer theory can be successfully applied for the analysis of VSDI data. Indeed, by combining the advantage of VSDI in recording neuronal activity from different region of interests with millisecond time-resolution and the mathematical analysis of the VSDI data, we could more deeply investigate the dynamics within neuronal networks. For instance, the main findings obtained by using this approach are that keeping the network in a depolarized state by increasing stimulation intensity from 10 to 30 Volts or by blocking GABAergic inhibition (Fig.1 and Supplementary Figures 1 and 2), induce an overall decrease of VSDI signal velocity (Fig.3 and 4), together with a layer-specific modulation of signal propagation patterns only after blockade of $GABA_A$ receptors conductances (Fig.6c, d and Fig.6g, h). The fact that either increasing stimulation intensity or blocking inhibitory activity lead to reduction of signal velocity may seem countersense, as one would expect an increase of signal velocity instead. This apparent discrepancy may be explained by the fact that the more the signal is kept constant in amplitude during time, the less distance it covers frame by frame due to its persistence, hence decreasing the resulting velocity. In addition, the finding that the blockade of $GABA_A$ receptors activity makes the signal more convergent specifically in *strata oriens* and *radiatum* proximal may be explained by the loss of feedback/feedforward inhibition onto basal and apical dendrites of pyramidal cells in CA1, which then facilitates the routing of excitatory signals along Schaffer's collaterals present in these *strata*[25].

Altogether, in this study we provide a novel and innovative method for the analysis of VSDI data which potentially can be used for the extraction of further information from all the techniques of optical imaging of neuronal activity, from voltage to calcium imaging and from single cell to neuronal networks spatial domains in different brain regions.

Online Methods

Slice preparation and staining with Voltage sensitive dye

Experiments were approved by the Committee on Animal Health and Care of INSERM and the French Ministry of Agriculture and Forestry.

8 to 11 weeks-old C57BL/6-N male mice (Janvier, France) were kept with *ad libitum* access to food and water, with 12 hours dark/light cycle (8h00 pm/am).

After isoflurane anesthesia mice were decapitated and 350 µm-thick sagittal slices containing dorsal hippocampus were cutted with a vibratome (VT1200S, Leica, Germany). During this procedure, the brain was immerged in ice-cold sucrose-based cutting solution bubbled with carbogen gas (95% O_2/ 5% CO_2) containing (in millimolar): 180 sucrose, 2.5 KCl, 26 $NaHCO_3$, 1.25 NaH_2PO_4, 11 Glucose, 0.2 $CaCl_2$, 12 $MgCl_2$. After preparation, slices were transferred and incubated 30 minutes at 34°C in oxygenated artificial cerebrospinal fluid (ACSF) containing (in millimolar): 123 NaCl, 2.5 KCl, 26 $NaHCO_3$, 1.25 NaH_2PO_4, 11 Glucose, 2,5 $CaCl_2$, 1,3 $MgCl_2$ and then allowed to recover at room temperature in the same solution for at least 30 minutes before the staining procedure with the dye. Each slice was stained for 15 minutes in ACSF under continuous carbogen flow with the voltage sensitive fluorescent dye Di-4-ANEPPS (Sigma-Aldrich, France) at a concentration of 16,4 µM in DMSO (DMSO<0.1%). The stained slice was then left to recover for at least 45 minutes in dye-free ACSF at room temperature before recordings.

Optical recording method

Slices were placed in a recording chamber (Membrane Chamber, Scientific Systems Design Inc., Canada,[26]) under constant oxygenated ACSF flow (~2 mL/min) at room temperature.

To record neuronal signals with VSDI we used an epifluorescence microscope (Brainvision, Japan) equipped with the MiCAM02 optical imaging system (MiCAM02 – HR; Brainvision, Japan) with a spatial resolution of 33.3 x 37.5 μm (horizontal and vertical, respectively) for each pixel.

A stereoscopic microscope (Leica, Germany) was used to visually guide the stimulating concentric bipolar electrode (FHC Inc., USA) into the proximal (respect to CA3) part of *stratum radiatum* to activate the Schaffer's collateral pathway. Duration of stimulation was 200 μseconds each stimulus, using an isolated voltage stimulator (DS2A, Digitimer Ltd., United Kingdom) and intensity of stimulation in the experiment with Picrotoxin was set at 20 Volts.

One acquisition consisted of 256 frames sampled every 2.2 milliseconds averaged 15 times at a time interval of 5 seconds (acquisition duration is ~70 seconds). Each experimental point was the mean of four acquisitions interleaved of 20 seconds, averaged by using the utility of the imaging analysis software (Brainvision, Japan), which ultimately gives a unique data file.

VSDI data and ROI extractions

For each averaged data file we calculated the fractional change in fluorescence ($\Delta F*F^{-1}$) and we extracted 22 frames containing the signal of interest, starting from one frame before stimulus, thus covering all the time-lapse of neuronal depolarization (~46 milliseconds). Exclusively for Figure 1a and b, we used a spatial filter of 5x5 pixels after $\Delta F*F^{-1}$ calculation and we isolated the CA1 region with a region of interest (ROI) by zeroing smoothed $\Delta F*F^{-1}$ values outside the ROI.

A depolarization produces a reduction in fluorescence emitted by Di-4-ANEPPS, while a hyperpolarization an increase; therefore, for clarity, $\Delta F*F^{-1}$ values representing

depolarization (Fig. 1 and Supplementary Figure 1 and 2) were considered positive. ROIs were *post-hoc* visually drawn onto the slice according to the representative spatial arrangement as shown in Fig. 1c and Supplementary Figure 1, using the image analysis-acquisition software (Brainvision, Japan). All the possible has been done to exactly match the ROI boundaries with anatomical landmarks. However, the large spatial resolution of our VSDI recordings together with the relatively large size of each pixel, make difficult an exact anatomical sub-division inside the CA1 region and therefore, the ROI named "Radt. Distal" (*radiatum* distal) contain *stratum lacunosum-moleculare* as well, while the ROI named "Pyr. Layer" (Pyramidal Layer) may include very limited parts of *stratum oriens* and *stratum radiatum*.

To extract signal of interest inside each ROI over the 22 frames of neuronal activity we used the image analysis software by zeroing $\Delta F*F^{-1}$ values outside ROI boundaries.

Data analysis

The 22 frames containing the signal extracted from each ROI were used to calculate the optimal displacement of neuronal depolarization between successive frames, according to the optimal mass transfer problem[13]. The code used for the estimation of the optimal displacement is compiled using Matlab (MathWorks®, R2012a) and is freely available as Supplementary Information. A previous description and application of this approach to the analysis of magnetic resonance imaging (MRI) data has been already reported[20].

In this algorithm we consider the numerical solution of the L^2 optimal mass transfer problem in $\mathbb{R}^d$, where d is the number of space dimensions. Let $\rho_0(\xi)$ and $\rho_1(x)$ be two non-negative scalar (density) functions with compact support Ω_0 and Ω_1, respectively. In the present case, these densities represent two arrays of depolarization values corresponding to two subsequent frames.

We assume that:

$$\int_{\Omega 0} \rho 0(\xi) d\,\xi = \int_{\Omega 1} \rho 1(x) dx = 1 \qquad (1)$$

Let $x = X(\xi)$ be a smooth one-to-one map taking Ω_0 onto Ω_1 that verifies the jacobian equation:

$$det(\nabla_{\xi} X)\rho_1(X(\xi)) = \rho_0(\xi) \qquad (2)$$

As a consequence, we have that $\forall \Omega \subseteq \Omega 0$:

$$\int_{\Omega} \rho 0(\xi) d\,\xi = \int_{X(\Omega)} \rho 1(x) dx \qquad (3)$$

The jacobian equation (2) has many admissible solutions. Among all these mappings, we consider a lagrangian method to find $X^*(\xi)$ such that:

$$\int_{\Omega 0} \rho 0(\xi) \parallel X*(\xi) - \xi \parallel^2 d\xi \leq \int_{\Omega 0} \rho 0(\xi) \parallel X(\xi) - \xi \parallel^2 d\xi \qquad (4)$$

for all smooth one-to-one mappings $X(\xi)$.

This functional measures the cost of the mass transport by a distance called Wasserstein distance (when the infimum is achieved).

Other classes of optimal transport problems can be defined by introducing different norms instead of the L^2 norm above. However, we concentrate on this approach because it has been proved that it admits a unique solution and we have numerically efficient ways to solve it[20].

In order to test the model accuracy, we analyzed a set of surrogate data consisting of a square of 26 equal numbers shifted in two subsequent frames by user-defined two-dimentional spatial coordinates (see Results). Signal velocity (Figure 3 and 4) has been calculated as follows: each value of Wasserstein distance gives a measure of the

displacement in pixels; this distance is then converted in μm by considering a pixel as a square of 35.4 μm, resulting from the mean of actual pixel size; each distance expressed in μm is then divided by 2.2 milliseconds, which is the time step between each frame containing the signal: this calculation gives velocity in μm/ms; final velocity values have been then converted in m/s.

Data regarding divergence/convergence (Fig. 5 and 6, a, c, e, g and i) were obtained by subtracting values of negative divergence (here referred as “convergence”) to values of positive divergence.

Pharmacology

Picrotoxin (PTX) was purchased from Sigma-Aldrich (France), dissolved in 100% ethanol and bath-applied for 30 minutes.

Statistics

Data are expressed as mean±s.e.m. All graphs and statistical analyses were performed with GraphPad Prism software (version 6.0). Two-tailed paired or unpaired t-test were used as appropriate. Differences were considered significant if $p<0.05$.

References:

1. Parker, D. Complexities and uncertainties of neuronal network function. *Philos Trans R Soc Lond B Biol Sci* **361**, 81-99 (2006).

2. Sporns, O. Networks of the brain (The MIT press, 2011).

3. Grinvald, A. & Hildesheim, R. VSDI: a new era in functional imaging of cortical dynamics. *Nat Rev Neurosci* **5**, 874-85 (2004).

4. Hill, E.S., Bruno, A.M. & Frost, W.N. Recent developments in VSD imaging of small neuronal networks. *Learn Mem* **21**, 499-505 (2014).

5. Peterka, D.S., Takahashi, H. & Yuste, R. Imaging voltage in neurons. *Neuron* **69**, 9-21 (2011).

6. Xu, W., Huang, X., Takagaki, K. & Wu, J.Y. Compression and reflection of visually evoked cortical waves. *Neuron* **55**, 119-29 (2007).

7. Roland, P.E. et al. Cortical feedback depolarization waves: a mechanism of top-down influence on early visual areas. *Proc Natl Acad Sci U S A* **103**, 12586-91 (2006).

8. Takagaki, K., Zhang, C., Wu, J.Y. & Lippert, M.T. Crossmodal propagation of sensory-evoked and spontaneous activity in the rat neocortex. *Neurosci Lett* **431**, 191-6 (2008).

9. Peyré, G. Manifold Models for Signals and Images. *Computer Vision and Image Understanding* **113**, 249-260 (2009).

10. Burton, A. & Radford, J. Thinking in Perspective: Critical Essays in the Study of Thought Processes (Methuen, 1978).

11. Warren, D.H. & Strelow, E.R. Electronic Spatial Sensing for the Blind: Contributions from Perception, Rehabilitation, and Computer Vision (Springer Netherlands, 1985).

12. Horn, B.K.P.S., B.G. . Determining Optical Flow. *Artificial Intelligence* **17**, 185-203 (1981).

13. Villani, C. Optimal Transport, Old and New (Springer Verlag, 2009).

14. Grinvald, A., Lieke, E.E., Frostig, R.D. & Hildesheim, R. Cortical point-spread function and long-range lateral interactions revealed by real-time optical imaging of macaque monkey primary visual cortex. *J Neurosci* **14**, 2545-68 (1994).

15. Grinvald, A., Manker, A. & Segal, M. Visualization of the spread of electrical activity in rat hippocampal slices by voltage-sensitive optical probes. *J Physiol* **333**, 269-91 (1982).

16. Mann, E.O., Suckling, J.M., Hajos, N., Greenfield, S.A. & Paulsen, O. Perisomatic feedback inhibition underlies cholinergically induced fast network oscillations in the rat hippocampus in vitro. *Neuron* **45**, 105-17 (2005).

17. Tominaga, T., Tominaga, Y., Yamada, H., Matsumoto, G. & Ichikawa, M. Quantification of optical signals with electrophysiological signals in neural activities of Di-4-ANEPPS stained rat hippocampal slices. *J Neurosci Methods* **102**, 11-23 (2000).

18. Tsau, Y., Guan, L. & Wu, J.Y. Initiation of spontaneous epileptiform activity in the neocortical slice. *J Neurophysiol* **80**, 978-82 (1998).

19. von Wolff, G. et al. Voltage-sensitive dye imaging demonstrates an enhancing effect of corticotropin-releasing hormone on neuronal activity propagation through the hippocampal formation. *J Psychiatr Res* **45**, 256-61 (2011).

20. Iollo, A.a.L., D. A lagrangian scheme for the solution of the optimal mass transfer problem. *Journal of Computational Physics* **230**, 3430–3442 (2011).

21. Maury, B.V., J. A mathematical framework for a crowd motion model. *Comptes Rendu Mathematiques* **346**, 1245–1250 (2008).

22. Brenier, Y. Optimal transport, convection, magnetic relaxation and generalized Boussinesq equations. *Journal of Nonlinear Science* **19**, 547–570 (2009).

23. Evans, L.C.a.F., M. Fast/slow diffusion and collapsing sandpiles. *Journal of Differential Equations* **137**, 166–209 (1997).

24. Crasta, G.a.M., A. A variational approach to the macroscopic electrodynamics of anisotropic hard superconductors. *Archive for Rational Mechanics and Analysis* **192**, 87–115 (2009).

25. Amaral, D.a.L., P. in The Hippocampus book 37 - 114 (Oxford University Press, 2007).

26. Hill, M.R. & Greenfield, S.A. The membrane chamber: a new type of in vitro recording chamber. *J Neurosci Methods* **195**, 15-23 (2011).

Acknowledgements

We thank all the members of Marsicano's lab for useful discussions. M.C. is part of the international PhD program in Neuropharmacology (University of Catania, Italy).

This work was supported by INSERM (G.M., F.M.), EU–Fp7 (REPROBESITY, HEALTH–F2–2008–223713 and PAINCAGE, HEALTH-603191, G.M.), European Research Council (ENDOFOOD, ERC–2010–StG–260515, G.M.), Fondation pour la Recherche Medicale (FDT20140930853, M.C. and DRM20101220445, G.M.), Human Frontiers Science Program (G.M.), Region Aquitaine (G.M.), Agence Nationale de la Recherche (ANR Blanc NeuroNutriSens ANR-13-BSV4-0006, G.M. BRAIN ANR-10-LABX-0043, G.M., F.M.).

Author contributions

M.C., A.B., G.T., A.V. and C.E.L. contributed to experimental design, performed experiments, analyzed data, interpreted the results and wrote the manuscript. F.D., A.I., G.M. and F.M. supervised the project, interpreted the results and wrote the manuscript.

Competing financial interests

The authors declare no competing financial interests

Figure 1:

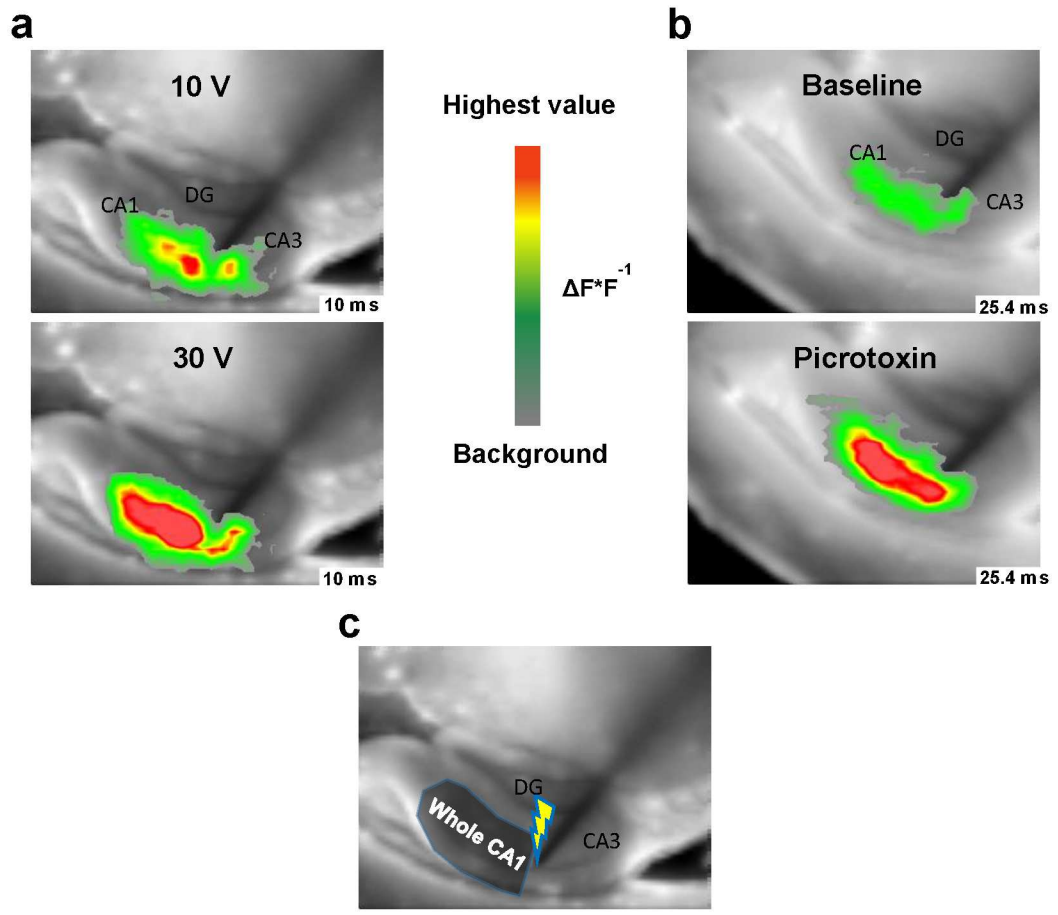
a
10 V
CA1
DG
CA3
10 ms
30 V
10 ms
Highest value
ΔF*F-1
Background
b
Baseline
CA1
DG
CA3
25.4 ms
Picrotoxin
25.4 ms
c
DG
Whole CA1
CA3
d
10V
30V
ΔF*F-1
Time after stimulation onset (ms)
e
over time
until 12.2 ms
14.4 - 27.6 ms
29.8 - 45.2 ms
****
f
Baseline
100 µM PTX
ΔF*F-1
Time after stimulation onset (ms)
g
over time
until 12.2 ms
14.4 - 27.6 ms
29.8 - 45.2 ms
*
ns
**

Figure 1. Increased stimulation intensity and blockade of $GABA_A$ receptors activity boost neuronal depolarization throughout CA1. (a) Representative frames containing VSDI-recorded depolarization ($\Delta F*F^{-1}$, color-coded with red representing highest values) at 10 and 30 Volts (V) stimulation of Schaffer's collaterals at the indicated right-bottom time point after stimulus onset. **(b)** Representative frames containing VSDI-recorded depolarization ($\Delta F*F^{-1}$, color-coded with red representing highest values) before ("Baseline") and after application of the $GABA_A$ receptor antagonist picrotoxin (PTX, 100 µM) at the indicated right-bottom time point after stimulus onset. **(c)** Representative arrangement of the region of interest (ROI) covering the whole CA1 used for the quantification of the VSDI-recorded depolarization. **(d)** Time course of VSDI-recorded depolarization ($\Delta F*F^{-1}$) in a ROI covering the whole CA1 after increasing stimulation intensity from 10 to 30 Volts (V). **(e)** Average values of VSDI-recorded depolarization ($\Delta F*F^{-1}$) at the respective top indicated time points of the time course in (d). **(f)** Time course of VSDI-recorded depolarization ($\Delta F*F^{-1}$) in a ROI covering the whole CA1 before and after application of PTX. **(g)** Average values of VSDI-recorded depolarization ($\Delta F*F^{-1}$) at the respective top indicated time points of the time course in (f). ms = milliseconds. N in experiments in d and e is 7 slices from 4 mice while in experiments in f and g is 7 slices from 5 mice. Statistical analysis in e and g is two-tailed paired t test. Data in d, e, f and g are mean±s.e.m. **** = $p<0.0001$; ** = $p<0.01$; * = $p<0.05$; ns = not significant.

Figure 2:

a

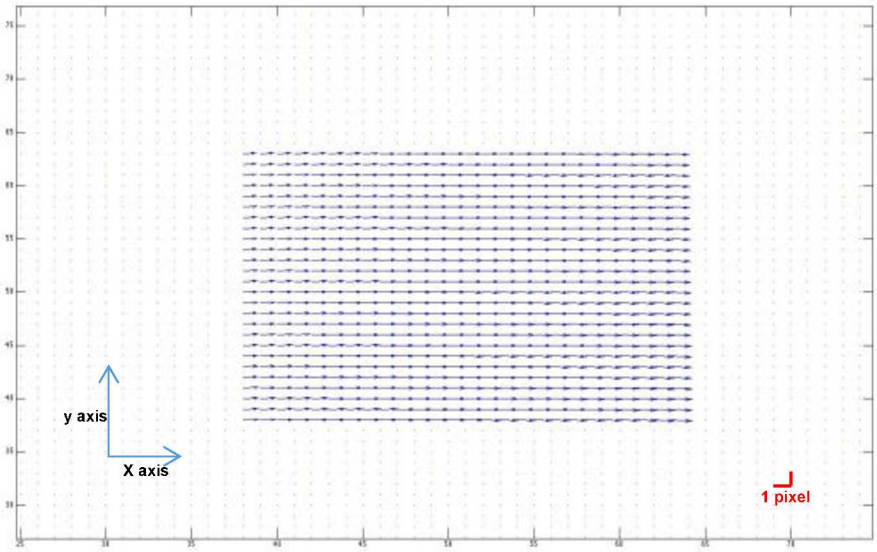

b

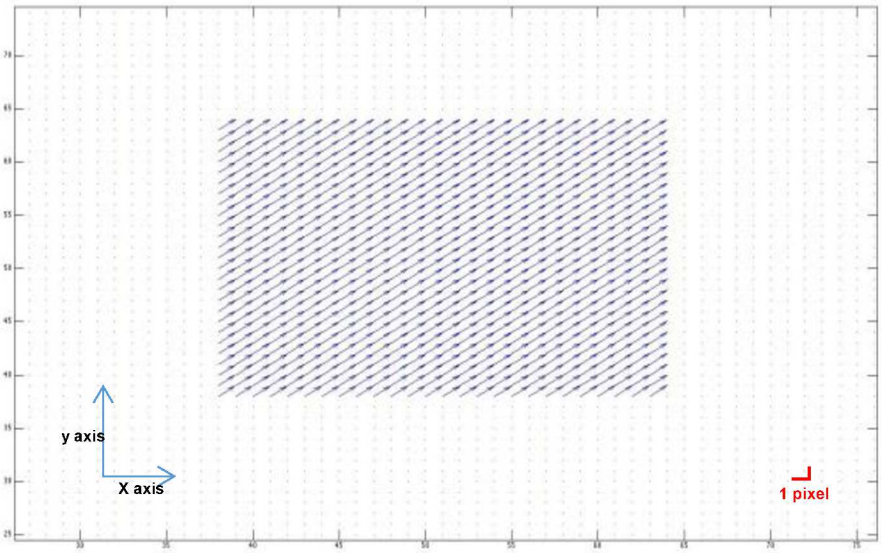

Figure 2. Validation of the algorithm with surrogate data. Vectorial fields showing the result of the movements of a squared array of values of one pixel on the right **(a)** and one pixel on the right and one on the top **(b)** respectively, demonstrating the accuracy of the algorithm as the represented vectors in the field coherently reports the user-defined movements.

Figure 3:

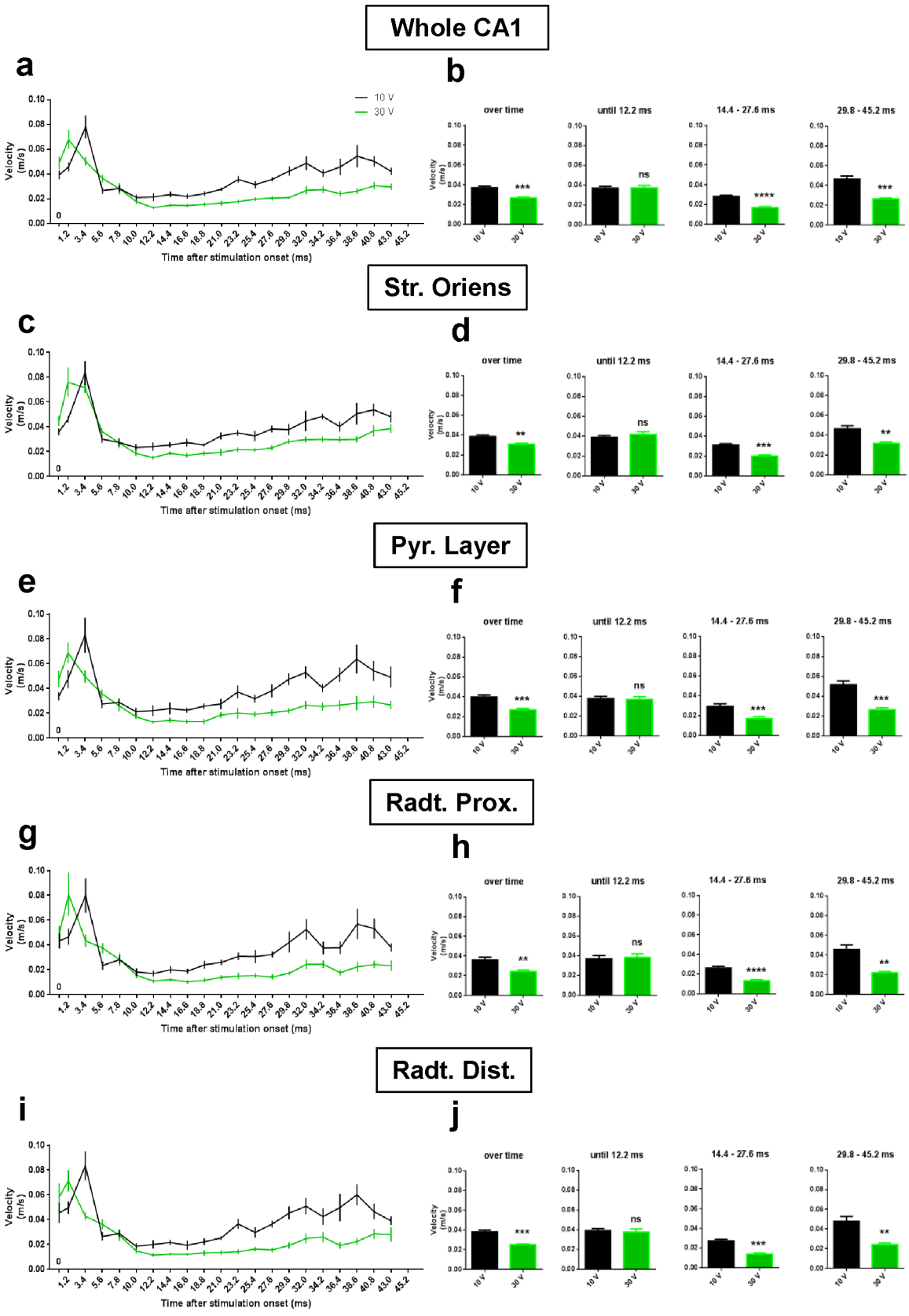
Whole CA1
a
b
10 V
30 V
Velocity (m/s)
Time after stimulation onset (ms)
over time
until 12.2 ms
14.4 - 27.6 ms
29.8 - 45.2 ms
***
ns
****
***
Str. Oriens
c
d
**
ns
***
**
Pyr. Layer
e
f
***
ns
***
***
Radt. Prox.
g
h
**
ns
****
**
Radt. Dist.
i
j
***
ns
***
**

Figure 3. Increased stimulation intensity slows-down the VSDI signals. Changing Schaffer's collaterals stimulation intensity from 10 to 30 Volts (V) decreases signal velocity specifically at the top indicated region of interests (ROIs). Whole CA1 = **(a)** and (**b)**; *stratum oriens* = **(c)** and **(d)**; pyramidal layer = **(e)** and **(f)**; *radiatum* proximal = **(g)** and **(h)**; *radiatum* distal = **(i)** and **(j)**. Graphs in a, c, e, g and i represent time course of VSDI-recorded depolarization velocity changes, while graphs in b, d, f, h and j represent average values of signal velocity changes at the top indicated time points of the respective ROIs time courses. N is 7 slices from 4 mice. Statistical analysis used in b, d, f, h and j is two-tailed paired t test. Data are represented as mean±s.e.m. **** = $p<0.0001$; *** = $p<0.001$; ** = $p<0.01$; ns = not significant.

Figure 4:

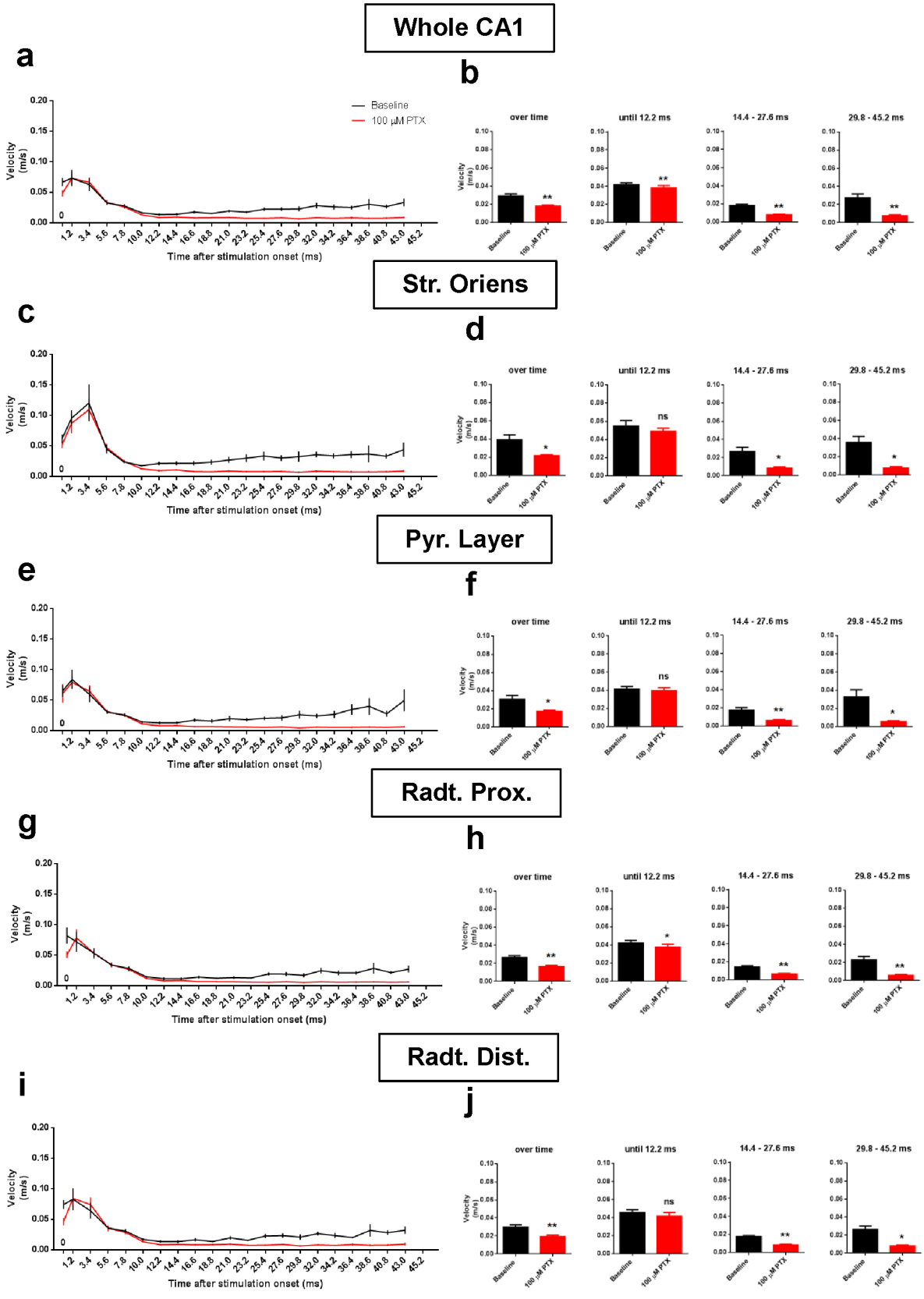
Whole CA1
a
b
Baseline
100 µM PTX
Velocity (m/s)
Time after stimulation onset (ms)
over time
until 12.2 ms
14.4 - 27.6 ms
29.8 - 45.2 ms
Str. Oriens
c
d
Pyr. Layer
e
f
Radt. Prox.
g
h
Radt. Dist.
i
j
ns

Figure 4. Blockade of GABAergic inhibition decreases the velocity of VSDI signals. Application of the $GABA_A$ receptor antagonist picrotoxin (PTX, 100 µM) decreases signal velocity specifically at the top indicated region of interests (ROIs). Whole CA1 = **(a)** and **(b)**; *stratum oriens* = **(c)** and **(d)**; pyramidal layer = **(e)** and **(f)**; *radiatum* proximal = **(g)** and **(h)**; *radiatum* distal = **(i)** and **(j)**. Graphs in a, c, e, g and i represent time course of VSDI-recorded depolarization velocity changes, while graphs in b, d, f, h and j represent average values of signal velocity changes at the top indicated time points of the respective ROIs time courses. N is 7 slices from 5 mice. Statistical analysis in b, d, f, h and j is two-tailed paired t test. Data are mean±s.e.m. ** = $p<0.01$; * = $p< 0.05$; ns = not significant.

Figure 5:

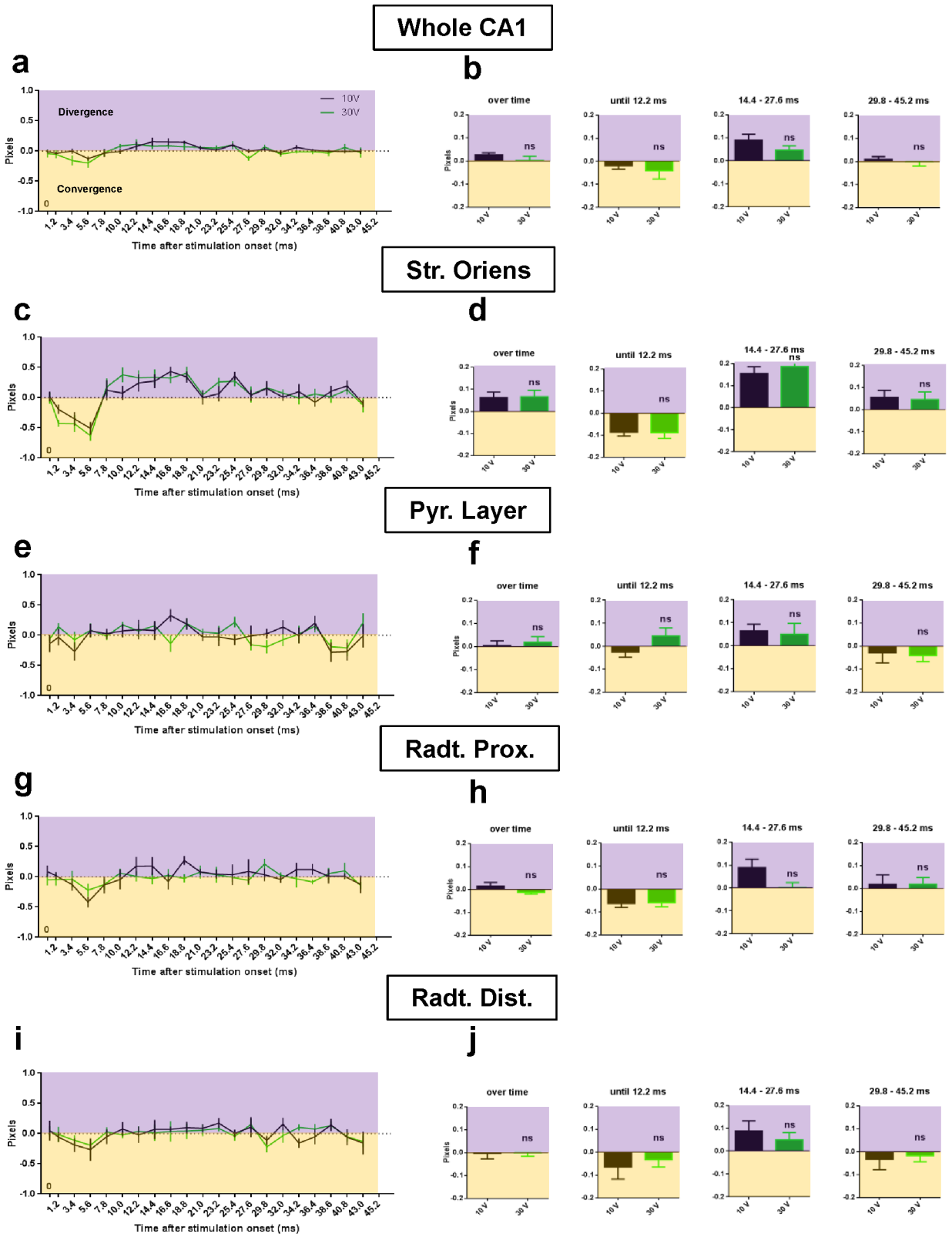
Whole CA1
a
b
Divergence
Convergence
10V
30V
Pixels
Time after stimulation onset (ms)
over time
until 12.2 ms
14.4 - 27.6 ms
29.8 - 45.2 ms
ns
Str. Oriens
c
d
Pyr. Layer
e
f
Radt. Prox.
g
h
Radt. Dist.
i
j

Figure 5. Increasing stimulation intensity does not change the orientation of VSDI-recorded depolarization signals. Changing Schaffer's collaterals stimulation intensity from 10 to 30 Volts (V) does not change the divergence/convergence of the vectorial field specifically at the top indicated region of interests (ROIs). Whole CA1 = **(a)** and **(b)**; *stratum oriens* = **(c)** and **(d)**; pyramidal layer = **(e)** and **(f)**; *radiatum* proximal = **(g)** and **(h)**; *radiatum* distal = **(i)** and **(j)**. Graphs in a, c, e, g and i represent time course of the changes in divergence/convergence of the VSDI-recorded depolarization, while graphs in b, d, f, h and j represent average values of signal divergence/convergence changes at the top indicated time points of the respective ROIs time courses. N is 7 slices from 4 mice. Statistical analysis in b, d, f, h and j is two-tailed unpaired t test. Data are mean±s.e.m. ns = not significant.

Figure 6:

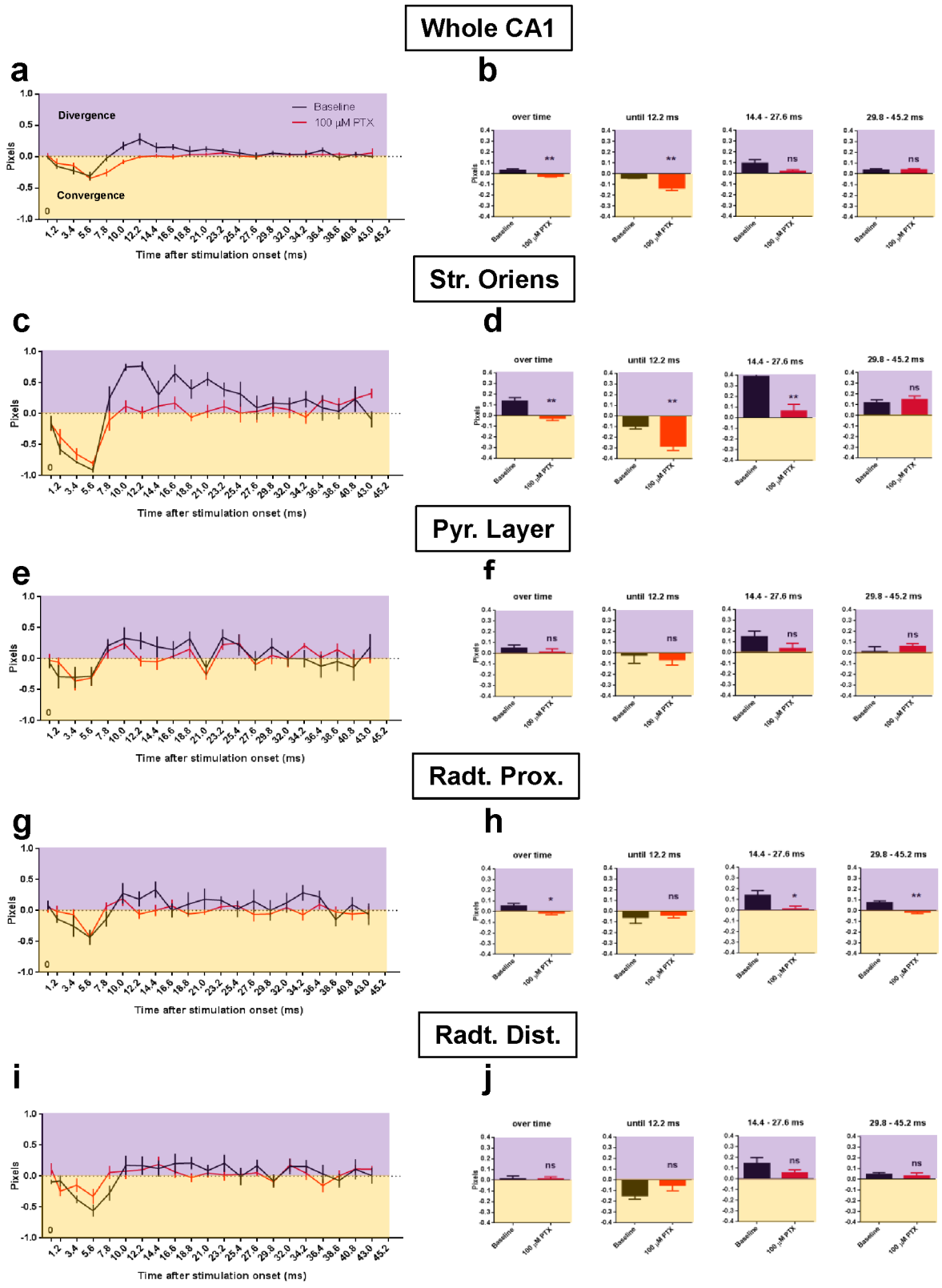
Whole CA1
a
b
Divergence
Convergence
Baseline
100 µM PTX
Pixels
Time after stimulation onset (ms)
over time
until 12.2 ms
14.4 - 27.6 ms
29.8 - 45.2 ms
Str. Oriens
c
d
Pyr. Layer
e
f
Radt. Prox.
g
h
Radt. Dist.
i
j

Figure 6. Blocking GABAergic inhibition renders depolarization signals more convergent and less divergent specifically in *strata oriens* and *radiatum* proximal. Application of the $GABA_A$ receptor antagonist picrotoxin (PTX, 100 μM) changes the divergence/convergence of the vectorial field specifically at the top indicated region of interests (ROIs). Whole CA1 = **(a)** and **(b)**; *stratum oriens* = **(c)** and **(d)**; pyramidal layer = **(e)** and **(f)**; *radiatum* proximal = **(g)** and **(h)**; *radiatum* distal = **(i)** and **(j)**. Graphs in a, c, e, g and i represent time course of the changes in divergence/convergence of the VSDI-recorded depolarization, while graphs in b, d, f, h and j represent average values of signal divergence/convergence changes at the top indicated time points of the respective ROIs time courses. N is 7 slices from 5 mice. Statistical analysis in b, d, f, h and j is two-tailed unpaired t test. Data are mean±s.e.m. ** = $p<0.01$; * = $p< 0.05$; ns = not significant.

Supplementary Figure 1:

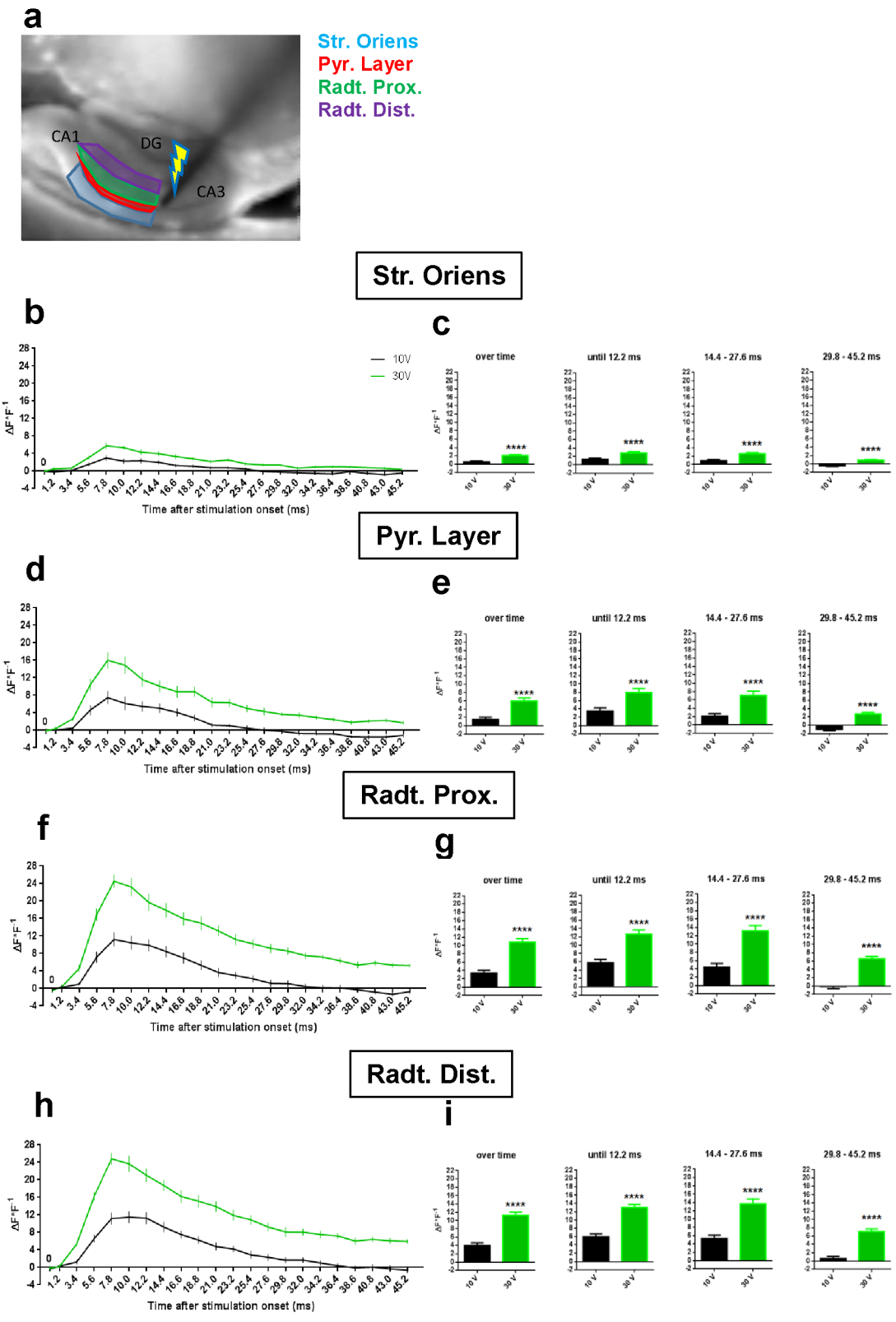

Supplementary Figure 1. Increasing stimulation intensity boosts neuronal depolarization in the CA1 subfields. (a) Representative arrangement of the regions of interest (ROIs) covering the CA1 subfields used for the quantification of the VSDI-recorded depolarization ($\Delta F*F^{-1}$); Str. Oriens = *stratum oriens*; Pyr. Layer = pyramidal layer; Radt. Prox. = *radiatum* proximal; Radt. Dist. = *radiatum* distal. Graphs in b, d, f and h represent time course of the changes in VSDI-recorded depolarization after modulation of stimulus intensity, while graphs in c, e, g and i represent average values of depolarization changes at the top indicated time points of the respective ROIs time courses. N is 7 slices from 4 mice. Statistical analysis in c, e, g and i is two-tailed paired t test. Data are mean±s.e.m. **** = $p<0.0001$.

Supplementary Figure 2:

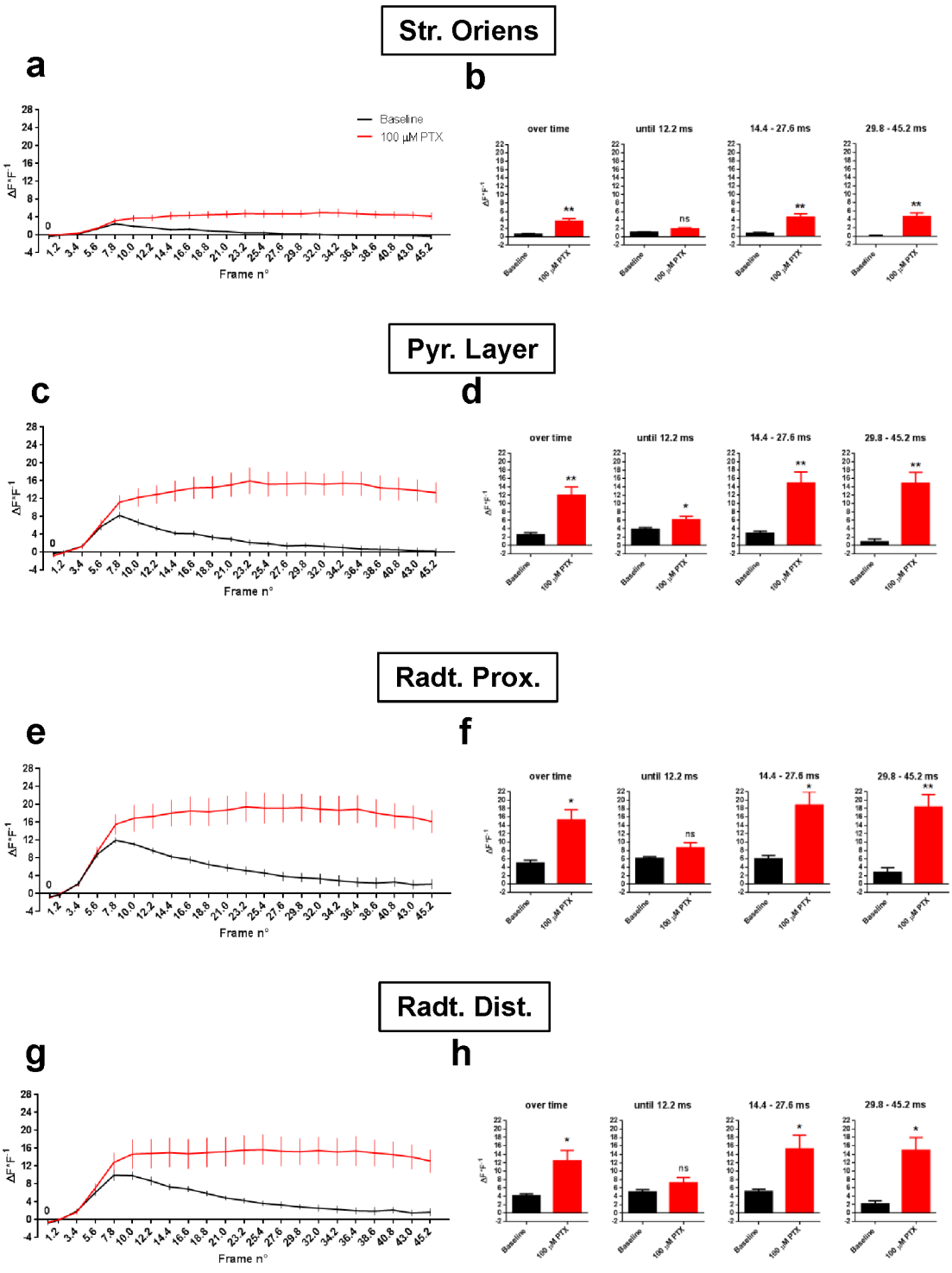

Supplementary Figure 2. Blocking GABAergic inhibition increases neuronal depolarization in the CA1 subfields. Str. Oriens = *stratum oriens*; Pyr. Layer = pyramidal layer; Radt. Prox. = *radiatum* proximal; Radt. Dist. = *radiatum* distal. Graphs in a, c, e and g represent time course of the changes in VSDI-recorded depolarization ($\Delta F*F^{-1}$) before and after application of the $GABA_A$ receptor antagonist picrotoxin (PTX, 100 μM), while graphs in b, d, f and h represent average values of depolarization changes at the top indicated time points of the respective ROIs time courses. N is 7 slices from 5 mice. Statistical analysis in b, d, f and h is two-tailed paired t test. Data are mean±s.e.m. ** = $p<0.01$; * = $p<0.05$; ns = not significant.

CHAPTER III

Submitted to *Scientific Reports*

Layer-specific potentiation of network GABAergic inhibition in the hippocampus

Michelangelo Colavita[1,2,3], Geoffrey Terral[1,2], Clement E. Lemercier[1,2], Filippo Drago[3], Giovanni Marsicano[1,2,♯], Federico Massa[1,2,♯,*]

1:INSERM U862, NeuroCentre Magendie, AVENIR Group "Endocannabinoids and Neuroadaptation", 33077 Bordeaux, France

2:Université de Bordeaux, 33077 Bordeaux, France

3:University of Catania, Biometec – Department of Biomedical and Biotechnological Sciences, 95125 Catania, Italy

♯ = Share last authorship

* = Corresponding author

Abstract

One of the most important functions of GABAergic inhibition in cortical regions is the tight control of spatiotemporal activity of principal neurons ensembles. However, electrophysiological recordings do not provide sufficient spatial information and therefore the spatiotemporal properties of inhibitory plasticity are currently unknown.

Using Voltage Sensitive Dye Imaging (VSDI) in mouse hippocampal slices, we demonstrate that field GABAA-mediated inhibitory postsynaptic potentials undergo layer-specific potentiation upon activation of metabotropic glutamate receptors (mGluRs). VSDI recordings allowed detecting pharmacologically isolated GABAA dependent hyperpolarization signals. Brief bath-application of the selective group I mGluR agonist (S)-3,5-Dihydroxyphenylglycine (DHPG) induces an enhancement of the GABAergic VSDI-recorded signal, which is more or less pronounced in different hippocampal layers. This potentiation is mediated by mGluR5 and downstream activation of IP_3 receptors. Our results depict network GABAergic activity in the hippocampal CA1 region and its sub-layers showing also a novel form of inhibitory synaptic plasticity tightly coupled to glutamatergic activity.

Introduction

In the mammalian brain, the main source of inhibition is provided by the neurotransmitter gamma-aminobutyric acid (GABA), which acts on two classes of receptors: the ionotropic GABAA and the metabotropic GABAB (1).

In cortical areas, GABA is released by locally projecting cells, the interneurons, which are estimated to account for approximately 11% of total cells population in the hippocampal CA1 region (2, 3). However, despite the relative paucity of these cells at this region, each interneuron can make synapses with several hundreds of pyramidal cells (4-6) and other interneurons (4, 7), providing an extremely complex and powerful spatiotemporal control of network activity.

At least 21 different classes of interneurons have been described In the CA1, classified on the basis of firing patterns, molecular expression profiles, and innervation properties (4, 8, 9). This high morpho-physiological heterogeneity together with the high degree of synaptic connectivity between pyramidal cells and other interneurons suggest the existence of a “network of interneurons” with a key role in controlling hippocampal computations (7, 10-12). For instance, GABAergic cells through the release of GABA and subsequent activation of GABAA receptors hyperpolarize pyramidal cells (13). Thus, depending on the wiring scheme of interneurons onto principal cells, feedback and/or feed forward inhibition may occur, which are fundamental processes in shaping the spatial and temporal profile of principal cell firing and global network activity (14-17).

Moreover, the existence of GABAergic synapses between different types of interneurons (6, 18, 19), including specialized interneuron-specific cells(20-22), suggests that the inhibitory control of other interneurons is crucial in providing a higher level of coordination of hippocampal network activity (7).

Due to technical limitations, such as the difficulty to obtain reliable electrophysiological recordings of local “inhibitory fields” by standard electrophysiological approaches (23-25), very little is known concerning the global network activity and dynamics of interneurons. Indeed, powerful single-cell recordings techniques are widely used to study the roles of inhibitory activity in specific brain regions. Although this approach represents the best standard technique to identify the properties of single interneurons and of inhibitory transmission on single pyramidal neurons, it is not fit to observe the global spatiotemporal patterns of activity of inhibitory networks. Such a “mesoscopic” level of analysis of local inhibitory systems is, therefore, a lacking element in the quest for understanding dynamics and properties of principal networks.

Voltage sensitive dye imaging (VSDI) allows coincident optical monitoring of neuronal activity within a wide range of spatial resolution (from very small cell compartments such as dendrites to areas of several mm2), at a millisecond-range time scale (26-28). After binding cell membranes, voltage-sensitive dye molecules emit fluorescence proportionally to changes in membrane potential (29, 30). VSDI have been widely used to study excitatory network activity and single cell properties of neurons (31-34). Notably, at local regional (mesoscopic) level, VSDI allows the dissection of depolarization signals within different anatomical compartments (e.g. hippocampal sublayers). However, these properties of VSDI have not been used yet to study inhibitory network activity.

Group I metabotropic glutamate receptors (group I mGluRs) include mGluR1 and mGluR5(35). They constitute a subclass of metabotropic glutamate receptors that are coupled to Gq heterotrimeric G proteins, thus leading to activation of phospholipase C and subsequent mobilization of inositol 1,4,5-trisphosphate (IP_3), which in turn increases cytosolic Ca^{2+} via activation of IP_3 receptors on the endoplasmic reticulum(36). Activation

of Group I mGluRs is known to strongly impact on synaptic properties and plasticity of hippocampal circuits (37, 38).

In this study, we took advantage of the VSDI technique to visualize and quantify evoked field inhibitory post-synaptic potentials (fIPSPs) in the CA1 hippocampal region, and to analyze their temporal and spatial features within its different sub-layers. In addition, we found that a brief activation of mGluR5 leads to an IP_3-dependent potentiation of fIPSPs in a sub-region specific manner. These findings demonstrate the spatial and temporal distribution of GABAergic activity in the CA1 region of hippocampus and, most importantly, they show that metabotropic glutamatergic signaling bears a strong impact on the global and local activity of inhibitory networks in specific brain regions.

Results

GABAA – mediated network activity in the hippocampal CA1

Stimulation of Schaffer's collateral pathway in hippocampal slices stained with Di-4-ANEPPS in drug-free ACSF produces a depolarization spanning along the horizontal axis of CA1 (Fig. 1a; green to red color-scale; Supplementary Movie 1). To quantify depolarization-mediated VSDI signal, we drew a region of interest (ROI) covering the whole CA1 (Fig. 1b) and the resulting mean $\Delta F*F^{-1}$ values over time are shown as an upward deflection of the signal lasting approximately 30 milliseconds (Fig. 1b, trace). Furthermore, a more detailed analysis of VSDI-recorded depolarization shows detectable signal specifically in the different layers of CA1, due to action potentials spreading along pyramidal cells (Fig. 1c, representatives ROIs arrangement and corresponding traces). Consistent with previous reports in similar conditions (33, 39), these images represent the spreading of depolarization signals in the CA1 region. Next, we asked whether a GABAergic component could be identified in these VSDI recordings. The application of

the GABAA receptor antagonist Picrotoxin (100 µM) induced an increase of the intensity of evoked depolarization signals both in the whole CA1 (Fig. 1d-f, Supplementary Movie 2; AUC: baseline, 3±0.2; PTX, 7.5±2.4; p=0.0068 baseline vs PTX, paired t test) and in the different subfields (Supplementary Fig. 1). Thus, VSDI depolarization signals result from the simultaneous activation of excitatory and inhibitory networks. To study in detail this GABAergic component of network activity, we isolated inhibitory neurotransmission by applying a cocktail of AMPA/Kainate and NMDA receptors antagonists (NBQX 10 µM and APV 50 µM, respectively). This treatment fully abolished the depolarization signals in the whole CA1 and each CA1 subregion (Fig.1g-i; Supplementary Movie 3), confirming their glutamatergic ionotropic origins. Importantly, however, blockade of ionotropic glutamatergic receptors also revealed a clear downward deflection of the traces below background fluorescence levels, which lasted approximately 200-250 milliseconds and was compatible with a hyperpolarizing event (Fig.1g-i; blue color scale; Supplementary Movie 3). Thus, stimulation of Schaffer's collaterals induces reliable and quantifiable hyperpolarizing field signals (hereafter called fIPSPs, i.e. field inhibitory postsynaptic potentials) in the CA1 region of the hippocampus.

Next, we set to characterize the nature of these hyperpolarization signals. First, input/output experiments revealed that evoked fIPSPs depend on the intensity of the stimulation, reaching a plateau level at 15-20 Volts (Fig. 2a), suggesting that they rely onto neuronal activity. The application of the voltage-gated Na+ channel blocker Tetrodotoxin (TTX, 1 µM) fully abolished fIPSPs in the whole CA1 (Fig. 2b, AUC: baseline, 7.8±0.9; TTX, 2.3±0.3; background, 2.6±0.3; p=0.0002 baseline vs TTX, paired t test; p=0.5177 TTX vs background, unpaired t test) and in all hippocampal sub-regions (Supplementary Fig. 2) reducing them to basal background levels (see Methods for

background definition). Thus, VSDI-recorded fIPSPs are not due to artifacts and depend on neuronal activity.

Acting at ionotropic GABAA or metabotropic GABAB receptors, GABA is the main neurotransmitter mediating hyperpolarization in the brain (1). The application of the GABAA receptor antagonist Picrotoxin (PTX, 100 μM) abolished fIPSPs signal in the whole CA1 region (Fig. 2c; AUC: baseline, 8.0±0.7; PTX, 1.4±0.4; background, 1.8±0.7; p=0.0014 baseline vs PTX, paired t test; p=0.6610 PTX vs background, unpaired t test). Conversely, the GABAB receptor antagonist CGP55845 (5 μM) did not significantly alter CA1 fIPSPs (Fig. 2d; AUC: baseline, 9.3±1.3; CGP55845, 8.1±1.9; background, 1.1± 0.1; p= 0.3545 baseline vs CGP55845, paired t test; p=0.01 CGP55845 vs background, unpaired t test), suggesting a specific involvement of GABAA receptors in the observed network hyperpolarization. This was further confirmed by the application of the positive allosteric modulator of GABAA receptor Chlordiazepoxide (CDP, 5 μM), which significantly increased recorded fIPSPs amplitude (Fig. 2e; AUC: baseline, 5.7±0.9; CDP, 7.3±0.9; background, 1.3±0.3; p=0.0320 Baseline vs CDP, paired t test; p<0.0001 CDP vs Background, unpaired t test). Importantly, similar results were obtained when specific CA1 sub-regions were analyzed (Supplementary Fig. 2), further confirming the reliable nature of the observed VSDI signals as GABAA receptor-dependent synaptic hyperpolarization events.

Thus, VSDI allows detecting and quantifying activity-dependent hyperpolarization events in the CA1 hippocampal region after stimulation of a large network of GABAergic interneurons.

Spatial distribution of network GABAA - mediated optical signals

As compared to classical electrophysiological recordings, the VSDI technique allows simultaneously observing synaptic events in different sub-regions of the observed area. Thus, we next quantified the distribution amongst different CA1 sub-regions of the hyperpolarization signals induced by electrode stimulation. Quantification of activity in equal ROIs distributed along the dorso-ventral axis of the CA1 region (Fig. 3a, b, see Methods) revealed that the strongest hyperpolarization is present in the CA1 pyramidal layer, whereas the *strata oriens* and *radiatum* (proximal and distal) display signals of lower amplitude (Fig. 3c, d). This observation is consistent with the fact that the majority of GABAergic synapses are located in the perisomatic area of CA1 pyramidal cells (2, 40).

Conversely, the intensity of the hyperpolarization signals decreases along the proximo-distal axis of CA1 (Fig. 3a, e-g), becoming undistinguishable from background levels at the most distal observed area (Fig. 3f, g), which were thereby excluded from further evaluations. These data indicate that the stimulation induces significant activation of the CA1 inhibitory network up to a distance of approximately 300-400 µm relative to the stimulation electrode, consistent with previous data obtained by single cell recordings (41). Thus, electrical stimulation in the Schaffer's collaterals region can activate a large population of CA1 interneurons, of which a relative majority appears to form perisomatic innervation of pyramidal cells.

Group I mGluR activation potentiates network hyperpolarization

Group I mGluRs have profound impact on neuronal activity, both on glutamatergic and GABAergic transmission (37). In particular, field electrophysiological recordings of excitatory postsynaptic potentials (fEPSPs) showed that activation of group I mGluRs

decreases network excitatory transmission in the hippocampus and several other brain regions (37, 42). The study of metabotropic glutamatergic signaling on GABAergic activity, however, has been limited to date to single-cell recording settings (43-46), with no studies focusing on network inhibition.

A brief application of the selective group I mGluRs agonist (S)-3,5-Dihydroxyphenylglycine (DHPG, 50 µM, 10 minutes) led to a persistent enhancement of VSDI-recorded evoked fIPSPs in the whole CA1 region compared to control condition in which no DHPG has been added, which lasted beyond washout of the drug (Fig. 4a).

A closer dissection of the subregional fIPSPs distribution revealed that this effect of DHPG is present in different layers and in proximal and medial regions relative to stimulation electrode (Fig. 4b). Interestingly, however, the DHPG effect differed in amplitude and duration in the different sub-regions analyzed. The magnitude was the highest in the proximal *stratum radiatum*, and minimal in the *stratum oriens* and pyramidal layer (Fig. 4b-h). Time-course analyses showed that the effect of DHPG was lasting up to 60 minutes in the whole CA1 region (Fig. 4a), likely due to the impact of proximal *stratum radiatum* (Fig.4e). Conversely, the DHPG-induced potentiation of fIPSPs was shorter lasting in the pyramidal layer and distal *stratum radiatum* (Fig. 4d and f, 20 min). In the *stratum oriens*, two-way ANOVA analysis revealed a significant treatment effect ($F(1, 60) = 6.934$, $p = 0.0107$), without “time x treatment” interaction, impeding the post-hoc determination of the time-dependent impact of DHPG (Fig. 4c). On the longitudinal axis, the amplitude of DHPG effect was not significantly different between areas located closer or farer from the stimulation electrode (fig. 4b). However, the DHPG-induced potentiation of fIPSPs was longer lasting in the CA1 portion closer to the electrode (Fig. 4g).

mGluR5 mediates DHPG-induced potentiation of fIPSPs

As DHPG activates both mGluR1 and 5, we asked if either or both of these receptors are involved in the fIPSPs potentiation. Pretreatment of the slices with the specific mGluR1 antagonist LY367385 (100 μM) was not able to alter the effect of DHPG in the CA1 region (Fig. 5a). Conversely, the application of the specific mGluR5 antagonist MPEP (25 μM) fully blocked the DHPG-induced potentiation of fIPSPs (Fig. 5a). At subregional level, similar results were obtained, with the exception of the *stratum oriens*, where, due to the weak effect of DHPG (see Fig. 4c), the data displayed only non-significant trends (Fig. 5b). Thus, LY367385 did not alter the DHPG effect in any subregion analyzed (Fig. 5c-g), whereas MPEP blocked this effect in all areas (Fig. 5c-g). These data show that DHPG-induced potentiation of fIPSPs in different CA1 hippocampal sub-regions share the same mechanisms, which relies on activation of mGluR5 receptors.

Role of IP_3 intracellular receptors

Activation of mGluR5 triggers Gq protein signaling, which, via the inositol 1,4,5-trisphosphate cascade, ultimately leads to the recruitment of the ligand-gated Ca^{2+} release channel IP_3 receptors in the endoplasmic reticulum (ER) and the increase of cytosolic Ca^{2+}(36, 47). Therefore, we asked whether IP_3 receptors are involved in the DHPG-induced potentiation of fIPSPs in the CA1 hippocampal region. Application of DHPG in continuous presence of the membrane permeable IP_3 receptor antagonist 2-APB failed to increase VSDI-recorded hyperpolarization in the whole CA1 and in all sub-regions analyzed (Fig. 6a-g), clearly pointing to the involvement of intracellular IP_3 receptors in this effect.

Discussion

This study shows that VDSI is a suitable technology to address network inhibitory activity in hippocampal slices, providing an equivalent of “field inhibitory postsynaptic potentials”, which depend on neuronal activity and are inhibited or potentiated by antagonism or allosteric enhancement of GABAA receptors, respectively. As compared to classical electrophysiological techniques, a clear advantage of this approach is the opportunity of dissecting intensity and distribution of fIPSPs amongst different sub-regions of a given brain area. We took advantage of these properties to highlight a novel form of inhibitory synaptic plasticity, characterized by a long-lasting increase of GABAergic strength following mGluR5 and IP_3 receptors activation.

The remarkable heterogeneity of CA1 hippocampal interneurons in terms of morphology and electrophysiological properties together with the extensive functional coupling to pyramidal cells (4, 9), underline the importance of monitoring GABAergic inhibitory activity at different neuro-architectural levels, from single cells to local circuits. Single cell recordings are valuable tools because of their ability to uncover subcellular input-output relationships and plasticity processes, but these approaches intrinsically lack the possibility to detect inhibitory transmission at larger network level, which can only be extrapolated, but not directly observed, from the data obtained. Very few attempts have been made to record network GABAergic activity (23-25). In all these studies, single or few recording electrodes were used, thereby limiting the spatial information obtained about the GABAergic activity at network level.

In this context, our data reveal the possibility to study network GABAergic activity in large brain regions.

The presence of blockers of ionotropic glutamatergic transmission excludes synaptic activation of interneurons by glutamate released after Schaffer collaterals stimulation and

suggests that the observed phenomenon is likely mediated by direct recruitment of interneurons, leading to synchronous release of GABA in an action potential-dependent manner. Indeed, this is strengthen by the fact that minimal stimulation intensity is sufficient to engage significant interneuronal population.

In the mature brain, GABA, by acting on ionotropic GABAA receptors, inhibits excitation via two main mechanisms: hyperpolarization and shunting inhibition (1). In our VSDI experiments, only hyperpolarization can be observed. Recent data, however, suggest that in the CA1 hippocampal region the hyperpolarizing component of GABAA receptor activity might be preponderant (13). Nevertheless, we cannot exclude the presence of GABAA receptor shunting inhibition, which depends on the membrane potential state. These undetected events, however, would determine an underestimation of the GABAergic activity observed by VSDI recordings, further underlying the reliability of the approach.

Our data reveal a novel form of mGluR5-dependent plasticity of fIPSPs. In the hippocampal CA1 region, mGluR1 and mGluR5 are predominantly post-synaptic (48). Whereas mGluR1 is mainly expressed in interneurons, primarily in those present in *alveus* and *stratum oriens*, mGluR5 is more widely present throughout CA1, comprising the somatodendritic field of pyramidal cells, in several classes of interneurons and in astrocytes(35, 48). Group I mGluRs have strong impact on neuronal activity by modulating cationic conductances, synaptic transmission and plasticity (37). It is widely documented that activation of group I mGluRs does increase cells excitability in hippocampus (37). In particular, a direct depolarization of pyramidal cells by mGluR1 activation has been shown, as well as a decrease of the slow afterhyperpolarization and a potentiation of NMDA currents, both mediated by mGluR5(44). Our data provide an additional effect to mGluR5 activation (potentiation of fIPSPs), which will have to be

considered in further study on group I-mediated synaptic and plasticity effects. The study of specific group I mGluRs signaling on GABAergic activity in hippocampal CA1 has been restricted to date at single cell resolution (43, 44, 46), with currently no data about network inhibitory activity. Interestingly, however, Gereau et al. (43), showed that activation of group I mGluRs by DHPG increases the frequency and not the amplitude of spontaneous IPSC recorded from pyramidal cells, suggesting an increase of GABA release by interneurons excited by the agonist. In addition, van Hooft and colleagues(46) showed that group I mGluRs activation in several classes of *oriens-alveus* interneurons induces a dramatic increase of spike frequency and appearance of an inward current, consistent with group I mGluRs-induced increase of interneuron excitability. Furthermore, increased excitability of interneurons and/or increased release of GABA by group I mGluRs is not exclusive of hippocampal CA1 region, but it has been reported also in thalamocortical neurons of dorsal lateral geniculate nucleus (49), in the ventral pallidum (50), in the periaqueductal grey (51), in retinal amacrine cells (52) and in entorhinal cortex (53). These studies, however, showed only a transient effect of DHPG on the electrophysiological activity of interneurons, which rapidly recovered to pre-drug conditions after washout of the compound. When we applied DHPG to network GABAA receptor-mediated activity recorded with VSDI in the CA1 we found a persistent enhancement of the signal that lasted for approximately 40-60 minutes after washout of the drug. Therefore, our present data are in agreement with previous studies performed at single cell level and, in addition, show that the potentiating effect of mGluR5 activation on inhibitory currents induces long-lasting plasticity effects when examined at inhibitory network level.

The degree of the enhancement is region-specific inside the CA1, being generally more accentuated in the proximal part of *stratum Radiatum* and in the region closer to the

stimulation electrode, and weaker in the *stratum oriens* and in the pyramidal layer. The reasons of these differences are currently unknown. They could be related to the coincidence of interneuron activity in areas close to the stimulation, but they could also depend on intrinsic differences between GABAergic network activity in different CA1 subfields. For instance, despite that fIPSPs amplitude in the *stratum oriens* is comparable to other CA1 sublayers and that mGluR5 receptors are abundantly expressed in this subregion (54), this layer seems to be less sensitive to DHPG-induced potentiation of fIPSPs. Importantly, our data also show that the activation of IP_3 receptors is a necessary step for mGluR5-induced potentiation of fIPSPs. Anatomical data (55, 56) indicate that IP_3 receptors are less abundant in the *stratum oriens* than in other CA1 hippocampal layers (e.g. pyramidal layer and *stratum radiatum*), suggesting that the lower effect of DHPG in this subregion might be due to the lower expression of key elements of the mGluR5 downstream intracellular cascade machinery. The use of VSDI to study fIPSPs will allow future studies aimed at the precise anatomical, cellular and molecular dissection of the plastic regulation of inhibitory transmission at network level. For instance, given the growing body of literature suggesting that astrocytes are active regulators of GABAergic transmission (57-61), it will be very interesting to address the role of these cell types in the regulation of fIPSPs.

Both mGluR5 and inhibitory transmission are involved in important central pathologies, such as, among others, epilepsy and Fragile X Syndrome (62-65). The possibility to study GABAergic transmission at network level provides an additional tool for a better understanding of brain functioning in physiological and pathological conditions. For instance, Deng and co-workers (53), showed that high glutamate levels, such as in epilepsy, increases frequency and amplitude of spontaneous IPSC recorded on principal neurons in entorhinal cortex, an effect that is mediated by mGluR5. In line of these

results, we could speculate that in case of intense glutamatergic activity as during seizures, high ambient glutamate may activate through spillover peri-synaptic mGluR5 receptors leading to compensatory increase of network GABAergic activity.

Collectively, our data show that VSDI allows the detection and the quantification of bona fide inhibitory network activity and highlight the tight neuromodulatory coupling of excitation and inhibition at mesoscale level.

Methods

Slice preparation and staining with Voltage sensitive dye

Experiments were approved by the Committee on Animal Health and Care of INSERM and the French Ministry of Agriculture and Forestry.

8 to 11 weeks-old male C57BL/6-N mice (Janvier, France) were kept with ad libitum access to food and water, with 12 hours dark/light cycle (8h00 pm/am).

Mice were decapitated after isoflurane anesthesia and 350 µm-thick sagittal slices containing dorsal hippocampus were cutted with a vibratome (VT1200S, Leica, Germany).

During this procedure, the brain was immerged in ice-cold sucrose-based cutting solution bubbled with carbogen gas (95% O2/ 5% CO2) containing (in millimolar): 180 sucrose, 2.5 KCl, 26 NaHCO3, 1.25 NaH2PO4, 11 Glucose, 0.2 CaCl2, 12 MgCl2. After preparation, slices were transferred and incubated 30 minutes at 34°C in oxygenated artificial cerebrospinal fluid (ACSF) containing (in millimolar): 123 NaCl, 2.5 KCl, 26 NaHCO3, 1.25 NaH2PO4, 11 Glucose, 2,5 CaCl2, 1,3 MgCl2 and then allowed to recover at room temperature in the same solution for at least 30 minutes before the staining procedure with the dye. Each slice was stained for 15 minutes in ACSF under continuous

carbogen flow with the voltage sensitive fluorescent dye Di-4-ANEPPS (Sigma-Aldrich, France) at a concentration of 16,4 µM in DMSO (DMSO<0.1%).

The stained slice was then left to recover for at least 45 minutes in dye-free ACSF at room temperature before recordings. Mennerick et al (66). found that Di-4-ANEPPS increases GABAA receptor conductance which is associated to a decreased network spontaneous spiking activity in dissociated cultures of hippocampal neurons (Fig. 6 and 8). However, the effects reported are completely reversible to baseline level after washout of the cultures with dye-free solution and therefore exclude the impact of Di-4-ANEPPS-induced modulation of GABAergic activity on our VSDI recordings.

Optical recording method

Slices were placed in a recording chamber (Membrane Chamber(67), Scientific Systems Design Inc., Canada,) under constant oxygenated ACSF flow (~2 mL/min) at room temperature.

To record neuronal signals with VSDI we used an epifluorescence macroscope (Brainvision, Japan) equipped with the MiCAM02 optical imaging system (MiCAM02 – HR; Brainvision, Japan) with a spatial resolution of 33.3 x 37.5 µm (horizontal and vertical, respectively) for each pixel.

A stereoscopic microscope (Leica, Germany) was used to visually guide the stimulating concentric bipolar electrode (FHC Inc., USA, catalog number CBARC75) into the proximal (respect to CA3) part of *stratum radiatum* to activate the Schaffer's collateral pathway. To improve the signal-to-noise ratio of the GABAA receptor-mediated hyperpolarization we set stimulation intensity at the maximum of the Input-Output curve (20 Volts, Fig. 2a) with duration of 200 µseconds each stimulus, using an isolated voltage stimulator (DS2A, Digitimer Ltd., United Kingdom).

One acquisition consisted of 256 frames sampled every 2.2 milliseconds averaged 15 times at a time interval of 5 seconds (acquisition duration is ~70 seconds).

In experiments with DHPG, we performed six acquisitions for the baseline, we then applied DHPG for ten minutes and finally we performed thirteen acquisitions during wash out of DHPG. Each acquisition was interleaved of 4 minutes.

In all experiments, before application of blockers of ionotropic glutamatergic transmission, one acquisition was taken in drug-free ACSF to check for slice health.

Data analysis

To quantify VSDI signals we calculated the fractional change in fluorescence ($\Delta F*F^{-1}$) and we spatially smoothed the $\Delta F*F^{-1}$ values with a 3x3 spatial filter using the image analysis-acquisition software (Brainvision, Japan). Exclusively for Supplementary Movie 1, 2 and 3, we used a spatial filter of 5x5 pixels, after $\Delta F*F^{-1}$ signal normalization. In Fig.1a, d and g and Supplementary Movie 1, 2 and 3 we isolated the CA1 region with a region of interest (ROI) by zeroing smoothed $\Delta F*F^{-1}$ values outside the ROI.

A depolarization produces a reduction in fluorescence emitted by Di-4-ANEPPS, while a hyperpolarization an increase; therefore, for clarity, $\Delta F*F^{-1}$ values representing depolarization (Fig. 1b and e) were considered positive.

ROIs were post-hoc visually drawn onto the slice according to the representative spatial arrangement as shown in Fig. 1b and c, and Fig. 3b and e, using the image analysis-acquisition software (Brainvision, Japan). All the possible has been done to exactly match the ROI boundaries with anatomical landmarks. However, the large spatial resolution of our VSDI recordings together with the relatively large size of each pixel, make difficult an exact anatomical sub-division inside the CA1 region and therefore, the ROI named “Radt. Distal” (*radiatum* distal) contain *stratum lacunosum-moleculare* as well, while the ROI

named “Pyr. Layer” (Pyramidal Layer) may include very limited parts of *stratum oriens* and *stratum radiatum*.

To draw ROIs in *stratum radiatum*, we first defined the ROI “Radt. Prox” and then we moved it ventrally at a position adjacent of the previous one to obtain the ROI “Radt. Dist”. To design ROIs along the proximo-distal axis of the CA1 relative to the stimulation electrode (named “P = proximal”, “M = medial” and “D = distal), we drawn first the ROI “P” and then the same one was then moved distally at adjacent points to obtain the ROIs “M” and then “D”. For the quantification of hyperpolarization signal across the sub-regions of CA1 (Fig. 3; schematic representation in b and e), we did as follows: at the middle of each dorso-ventral ROI (“str. Oriens”, “Pyr. Layer”, “Radt. Prox” and “Radt. Dist”) we drew a line (1 pixel wide, 8 pixels long) starting from the initial boundary relative to the stimulation electrode position. The same eight pixels long line has been then positioned in the middle of each proximo-distal ROI (“P”, “M”, and “D”). To measure lengths along the proximo-distal axis of CA1 (Fig. 3f, g) we considered a pixel as a square of 35.4 μm side, resulting from the mean of actual pixel size. A summary of all ROI sizes for experiments in Fig.1f, Fig.2, Fig.4-6 and Supplementary Figure 1 and 2 is available in the Supplementary Table 1.

To quantify GABAA receptor-mediated hyperpolarization recorded with VSDI we calculated the Area under Curve (AUC) of traces representing mean $\Delta F*F^{-1}$ values over time of each ROI, using a time interval of 200 milliseconds, starting from the time of hyperpolarization appearance (approximately 5 milliseconds after stimulus onset). To quantify depolarization signals in presence of Picrotoxin (Fig.1f and Supplementary Figure 1) we calculated AUC values considering a time window of 30 milliseconds starting from the time point before stimulation. AUCs quantifications were performed with Axograph X (version 1.5, Axograph, USA).

Background AUC values (Fig. 2b-e; Fig. 3c,d and f,g; Supplementary Fig. 2) were calculated by measuring AUC of traces from the same ROIs used for evaluation of signal of interest, which have been moved outside the hippocampus (in either cortex or thalamus). Final AUC values of background are the mean from three ROIs (except in Fig. 2b-e and Supplementary Fig. 2 where they are the mean of three ROIs for baseline and drug application, respectively).

In experiments with DHPG, "Baseline" is the mean of AUC values calculated for each ROI from the last four acquisitions before DHPG application. Except time "zero", all others time points after DHPG are the mean of AUC from subsequent four acquisitions. Data are then represented as percentage variation of mean AUC values respect to mean baseline.

Pharmacology

2,3-Dioxo-6-nitro-1,2,3,4-tetrahydrobenzo[f]quinoxaline-7-sulfonamide disodium salt (NBQX), D-(-)-2-Amino-5-phosphonopentanoic acid (APV), (S)-3,5-Dihydroxyphenylglycine (DHPG), (S)-(+)-α-Amino-4-carboxy-2-methylbenzeneacetic acid (LY367385), 2-Methyl-6-(phenylethynyl)pyridine hydrochloride (MPEP) were purchased from Abcam (France). Stock solutions of NBQX, D-APV, DHPG and MPEP were made in water, while LY367385 was dissolved in 100 mM of NaOH (final NaOH was ~0.1%). Once aliquoted, DHPG was used within one week. Slices were incubated with mGluR antagonists during the recovery post-staining with the dye and kept until the end of DHPG application.

Octahydro-12-(hydroxymethyl)-2-imino-5,9:7,10a-dimethano-10aH-1,3]dioxocino[6,5-d]pyrimidine-4,7,10,11,12-pentol citrate (TTX), (2S)-3-[[(1S)-1-(3,4-Dichlorophenyl)ethyl]amino-2-hydroxypropyl](phenylmethyl)phosphinic acid hydrochloride (CGP55845) and 2-Aminoethoxydiphenylborane (2-APB) were purchased from Tocris

(United Kingdom). TTX was dissolved in water, while CGP55845 and 2-APB in DMSO (DMSO<0.1%).

Picrotoxin (PTX) and 7-Chloro-2-(methylamino)-5-phenyl-3H-1,4-benzodiazepine 4-oxide hydrochloride (Chlordiazepoxide, CDP) were from Sigma-Aldrich (France). CDP was dissolved in water, while PTX in 100% ethanol. Drugs were bath-applied.

NBQX, APV and TTX were applied during 15 minutes whereas PTX, CDP and CGP55845 during 30 minutes.

Statistics

Data are expressed as mean±s.e.m. All graphs and statistical analyses were performed with GraphPad Prism software (version 6.0). Two-tailed paired or unpaired t-test, one-way ANOVA, one-way repeated measures ANOVA or two-way ANOVA followed by Tukey, Bonferroni or Dunnett post-hoc tests were used as appropriate. Differences were considered significant if $p<0.05$.

References

1. Fishell G & Rudy B (2011) Mechanisms of inhibition within the telencephalon: "where the wild things are". Annual review of neuroscience 34:535-567.

2. Bezaire MJ & Soltesz I (2013) Quantitative assessment of CA1 local circuits: knowledge base for interneuron-pyramidal cell connectivity. Hippocampus 23(9):751-785.

3. Aika Y, Ren JQ, Kosaka K, & Kosaka T (1994) Quantitative analysis of GABA-like-immunoreactive and parvalbumin-containing neurons in the CA1 region of the rat hippocampus using a stereological method, the disector. Experimental brain research 99(2):267-276.

4. Freund TF & Buzsaki G (1996) Interneurons of the hippocampus. Hippocampus 6(4):347-470.

5. Li XG, Somogyi P, Tepper JM, & Buzsaki G (1992) Axonal and dendritic arborization of an intracellularly labeled chandelier cell in the CA1 region of rat hippocampus. Experimental brain research 90(3):519-525.

6. Sik A, Penttonen M, Ylinen A, & Buzsaki G (1995) Hippocampal CA1 interneurons: an in vivo intracellular labeling study. The Journal of neuroscience : the official journal of the Society for Neuroscience 15(10):6651-6665.

7. Chamberland S & Topolnik L (2012) Inhibitory control of hippocampal inhibitory neurons. Frontiers in neuroscience 6:165.

8. Klausberger T & Somogyi P (2008) Neuronal diversity and temporal dynamics: the unity of hippocampal circuit operations. Science 321(5885):53-57.

9. Petilla Interneuron Nomenclature G, et al. (2008) Petilla terminology: nomenclature of features of GABAergic interneurons of the cerebral cortex. Nature reviews. Neuroscience 9(7):557-568.

10. Bartos M, Vida I, & Jonas P (2007) Synaptic mechanisms of synchronized gamma oscillations in inhibitory interneuron networks. Nature reviews. Neuroscience 8(1):45-56.

11. Isaacson JS & Scanziani M (2011) How inhibition shapes cortical activity. Neuron 72(2):231-243.

12. Kullmann DM (2011) Interneuron networks in the hippocampus. Current opinion in neurobiology 21(5):709-716.

13. Glickfeld LL, Roberts JD, Somogyi P, & Scanziani M (2009) Interneurons hyperpolarize pyramidal cells along their entire somatodendritic axis. Nature neuroscience 12(1):21-23.

14. Buzsaki G (1984) Feed-forward inhibition in the hippocampal formation. Progress in neurobiology 22(2):131-153.

15. Freund TF & Katona I (2007) Perisomatic inhibition. Neuron 56(1):33-42.

16. Pouille F & Scanziani M (2001) Enforcement of temporal fidelity in pyramidal cells by somatic feed-forward inhibition. Science 293(5532):1159-1163.

17. Pouille F & Scanziani M (2004) Routing of spike series by dynamic circuits in the hippocampus. Nature 429(6993):717-723.

18. Cobb SR, et al. (1997) Synaptic effects of identified interneurons innervating both interneurons and pyramidal cells in the rat hippocampus. Neuroscience 79(3):629-648.

19. Vida I, Halasy K, Szinyei C, Somogyi P, & Buhl EH (1998) Unitary IPSPs evoked by interneurons at the stratum radiatum-stratum lacunosum-moleculare border in the CA1 area of the rat hippocampus in vitro. The Journal of physiology 506 (Pt 3):755-773.

20. Acsady L, Arabadzisz D, & Freund TF (1996) Correlated morphological and neurochemical features identify different subsets of vasoactive intestinal polypeptide-immunoreactive interneurons in rat hippocampus. Neuroscience 73(2):299-315.

21. Acsady L, Gorcs TJ, & Freund TF (1996) Different populations of vasoactive intestinal polypeptide-immunoreactive interneurons are specialized to control pyramidal cells or interneurons in the hippocampus. Neuroscience 73(2):317-334.

22. Gulyas AI, Hajos N, & Freund TF (1996) Interneurons containing calretinin are specialized to control other interneurons in the rat hippocampus. The Journal of neuroscience : the official journal of the Society for Neuroscience 16(10):3397-3411.

23. Arai A, Silberg J, & Lynch G (1995) Differences in the refractory properties of two distinct inhibitory circuitries in field CA1 of the hippocampus. Brain research 704(2):298-306.

24. Bazelot M, Dinocourt C, Cohen I, & Miles R (2010) Unitary inhibitory field potentials in the CA3 region of rat hippocampus. The Journal of physiology 588(Pt 12):2077-2090.

25. Lambert NA, Borroni AM, Grover LM, & Teyler TJ (1991) Hyperpolarizing and depolarizing GABAA receptor-mediated dendritic inhibition in area CA1 of the rat hippocampus. Journal of neurophysiology 66(5):1538-1548.

26. Chemla S & Chavane F (2010) Voltage-sensitive dye imaging: Technique review and models. Journal of physiology, Paris 104(1-2):40-50.

27. Grinvald A & Hildesheim R (2004) VSDI: a new era in functional imaging of cortical dynamics. Nature reviews. Neuroscience 5(11):874-885.

28. Peterka DS, Takahashi H, & Yuste R (2011) Imaging voltage in neurons. Neuron 69(1):9-21.

29. Loew LM, et al. (1992) A naphthyl analog of the aminostyryl pyridinium class of potentiometric membrane dyes shows consistent sensitivity in a variety of tissue, cell, and model membrane preparations. The Journal of membrane biology 130(1):1-10.

30. Loew LM, Cohen LB, Salzberg BM, Obaid AL, & Bezanilla F (1985) Charge-shift probes of membrane potential. Characterization of aminostyrylpyridinium dyes on the squid giant axon. Biophysical journal 47(1):71-77.

31. Airan RD, et al. (2007) High-speed imaging reveals neurophysiological links to behavior in an animal model of depression. Science 317(5839):819-823.

32. Grinvald A, Manker A, & Segal M (1982) Visualization of the spread of electrical activity in rat hippocampal slices by voltage-sensitive optical probes. The Journal of physiology 333:269-291.

33. Tominaga T, Tominaga Y, Yamada H, Matsumoto G, & Ichikawa M (2000) Quantification of optical signals with electrophysiological signals in neural activities of Di-4-ANEPPS stained rat hippocampal slices. Journal of neuroscience methods 102(1):11-23.

34. Canepari M, Willadt S, Zecevic D, & Vogt KE (2010) Imaging inhibitory synaptic potentials using voltage sensitive dyes. Biophysical journal 98(9):2032-2040.

35. Ferraguti F, Crepaldi L, & Nicoletti F (2008) Metabotropic glutamate 1 receptor: current concepts and perspectives. Pharmacological reviews 60(4):536-581.

36. Fagni L, Chavis P, Ango F, & Bockaert J (2000) Complex interactions between mGluRs, intracellular Ca2+ stores and ion channels in neurons. Trends in neurosciences 23(2):80-88.

37. Anwyl R (1999) Metabotropic glutamate receptors: electrophysiological properties and role in plasticity. Brain research. Brain research reviews 29(1):83-120.

38. Castillo PE, Chiu CQ, & Carroll RC (2011) Long-term plasticity at inhibitory synapses. Current opinion in neurobiology 21(2):328-338.

39. Mann EO, Tominaga T, Ichikawa M, & Greenfield SA (2005) Cholinergic modulation of the spatiotemporal pattern of hippocampal activity in vitro. Neuropharmacology 48(1):118-133.

40. Megias M, Emri Z, Freund TF, & Gulyas AI (2001) Total number and distribution of inhibitory and excitatory synapses on hippocampal CA1 pyramidal cells. Neuroscience 102(3):527-540.

41. Davies CH, Davies SN, & Collingridge GL (1990) Paired-pulse depression of monosynaptic GABA-mediated inhibitory postsynaptic responses in rat hippocampus. The Journal of physiology 424:513-531.

42. Luscher C & Huber KM (2010) Group 1 mGluR-dependent synaptic long-term depression: mechanisms and implications for circuitry and disease. Neuron 65(4):445-459.

43. Gereau RWt & Conn PJ (1995) Multiple presynaptic metabotropic glutamate receptors modulate excitatory and inhibitory synaptic transmission in hippocampal area CA1. J Neurosci 15(10):6879-6889.

44. Mannaioni G, Marino MJ, Valenti O, Traynelis SF, & Conn PJ (2001) Metabotropic glutamate receptors 1 and 5 differentially regulate CA1 pyramidal cell function. J Neurosci 21(16):5925-5934.

45. McBain CJ, DiChiara TJ, & Kauer JA (1994) Activation of metabotropic glutamate receptors differentially affects two classes of hippocampal interneurons and potentiates excitatory synaptic transmission. The Journal of neuroscience : the official journal of the Society for Neuroscience 14(7):4433-4445.

46. van Hooft JA, Giuffrida R, Blatow M, & Monyer H (2000) Differential expression of group I metabotropic glutamate receptors in functionally distinct hippocampal interneurons. The Journal of neuroscience : the official journal of the Society for Neuroscience 20(10):3544-3551.

47. Foskett JK, White C, Cheung KH, & Mak DO (2007) Inositol trisphosphate receptor Ca2+ release channels. Physiological reviews 87(2):593-658.

48. Ferraguti F & Shigemoto R (2006) Metabotropic glutamate receptors. Cell and tissue research 326(2):483-504.

49. Errington AC, Di Giovanni G, Crunelli V, & Cope DW (2011) mGluR control of interneuron output regulates feedforward tonic GABAA inhibition in the visual thalamus. The Journal of neuroscience : the official journal of the Society for Neuroscience 31(23):8669-8680.

50. Diaz-Cabiale Z, et al. (2002) Metabotropic glutamate mGlu5 receptor-mediated modulation of the ventral striopallidal GABA pathway in rats. Interactions with adenosine A(2A) and dopamine D(2) receptors. Neuroscience letters 324(2):154-158.

51. de Novellis V, et al. (2003) Group I metabotropic glutamate receptors modulate glutamate and gamma-aminobutyric acid release in the periaqueductal grey of rats. European journal of pharmacology 462(1-3):73-81.

52. Hoffpauir BK & Gleason EL (2002) Activation of mGluR5 modulates GABA(A) receptor function in retinal amacrine cells. Journal of neurophysiology 88(4):1766-1776.

53. Deng PY, Xiao Z, & Lei S (2010) Distinct modes of modulation of GABAergic transmission by Group I metabotropic glutamate receptors in rat entorhinal cortex. Hippocampus 20(8):980-993.

54. Smialowska M, et al. (2002) Effect of chronic imipramine or electroconvulsive shock on the expression of mGluR1a and mGluR5a immunoreactivity in rat brain hippocampus. Neuropharmacology 42(8):1016-1023.

55. Hertle DN & Yeckel MF (2007) Distribution of inositol-1,4,5-trisphosphate receptor isotypes and ryanodine receptor isotypes during maturation of the rat hippocampus. Neuroscience 150(3):625-638.

56. Pieper AA, et al. (2001) Differential neuronal localizations and dynamics of phosphorylated and unphosphorylated type 1 inositol 1,4,5-trisphosphate receptors. Neuroscience 102(2):433-444.

57. Christian CA & Huguenard JR (2013) Astrocytes potentiate GABAergic transmission in the thalamic reticular nucleus via endozepine signaling. Proceedings of the National Academy of Sciences of the United States of America 110(50):20278-20283.

58. Egawa K, Yamada J, Furukawa T, Yanagawa Y, & Fukuda A (2013) Cl(-) homeodynamics in gap junction-coupled astrocytic networks on activation of GABAergic synapses. The Journal of physiology 591(Pt 16):3901-3917.

59. Jo S, et al. (2014) GABA from reactive astrocytes impairs memory in mouse models of Alzheimer's disease. Nature medicine 20(8):886-896.

60. Kaczor P, Rakus D, & Mozrzymas JW (2015) Neuron-astrocyte interaction enhance GABAergic synaptic transmission in a manner dependent on key metabolic enzymes. Frontiers in cellular neuroscience 9:120.

61. Yoon BE, et al. (2014) Glial GABA, synthesized by monoamine oxidase B, mediates tonic inhibition. The Journal of physiology 592(Pt 22):4951-4968.

62. Piers TM, et al. (2012) Translational Concepts of mGluR5 in Synaptic Diseases of the Brain. Frontiers in pharmacology 3:199.

63. Bear MF, Huber KM, & Warren ST (2004) The mGluR theory of fragile X mental retardation. Trends in neurosciences 27(7):370-377.

64. D'Hulst C & Kooy RF (2007) The GABAA receptor: a novel target for treatment of fragile X? Trends in neurosciences 30(8):425-431.

65. Treiman DM (2001) GABAergic mechanisms in epilepsy. Epilepsia 42 Suppl 3:8-12.

66. Mennerick S, et al. (2010) Diverse voltage-sensitive dyes modulate GABAA receptor function. The Journal of neuroscience : the official journal of the Society for Neuroscience 30(8):2871-2879.

67. Hill MR & Greenfield SA (2011) The membrane chamber: a new type of in vitro recording chamber. Journal of neuroscience methods 195(1):15-23.

Acknowledgements

We thank Dr. A. Bacci for critical reading of the manuscript, Dr. Ilaria Belluomo and all the members of Marsicano's lab for useful discussions. M.C. is part of the international PhD program in Neuropharmacology (University of Catania, Italy).

This work was supported by INSERM (G.M., F.M.), EU–Fp7 (REPROBESITY, HEALTH–F2–2008–223713 and PAINCAGE, HEALTH-603191, G.M.), European Research Council (ENDOFOOD, ERC–2010–StG–260515, G.M.), Fondation pour la Recherche Medicale (FDT20140930853, M.C. and DRM20101220445, G.M.), Human Frontiers Science Program (G.M.), Region Aquitaine (G.M.), Agence Nationale de la Recherche (ANR Blanc NeuroNutriSens ANR-13-BSV4-0006, G.M. BRAIN ANR-10-LABX-0043, G.M., F.M.).

Author contributions

M.C. contributed to experimental design, performed experiments, interpreted the results and wrote the manuscript. G.T. and C.L. contributed to experimental design and performed experiments. F.D., G.M. and F.M. supervised the project, interpreted the results and wrote the manuscript.

Competing financial interests

The authors declare no competing financial interests

Figure 1:

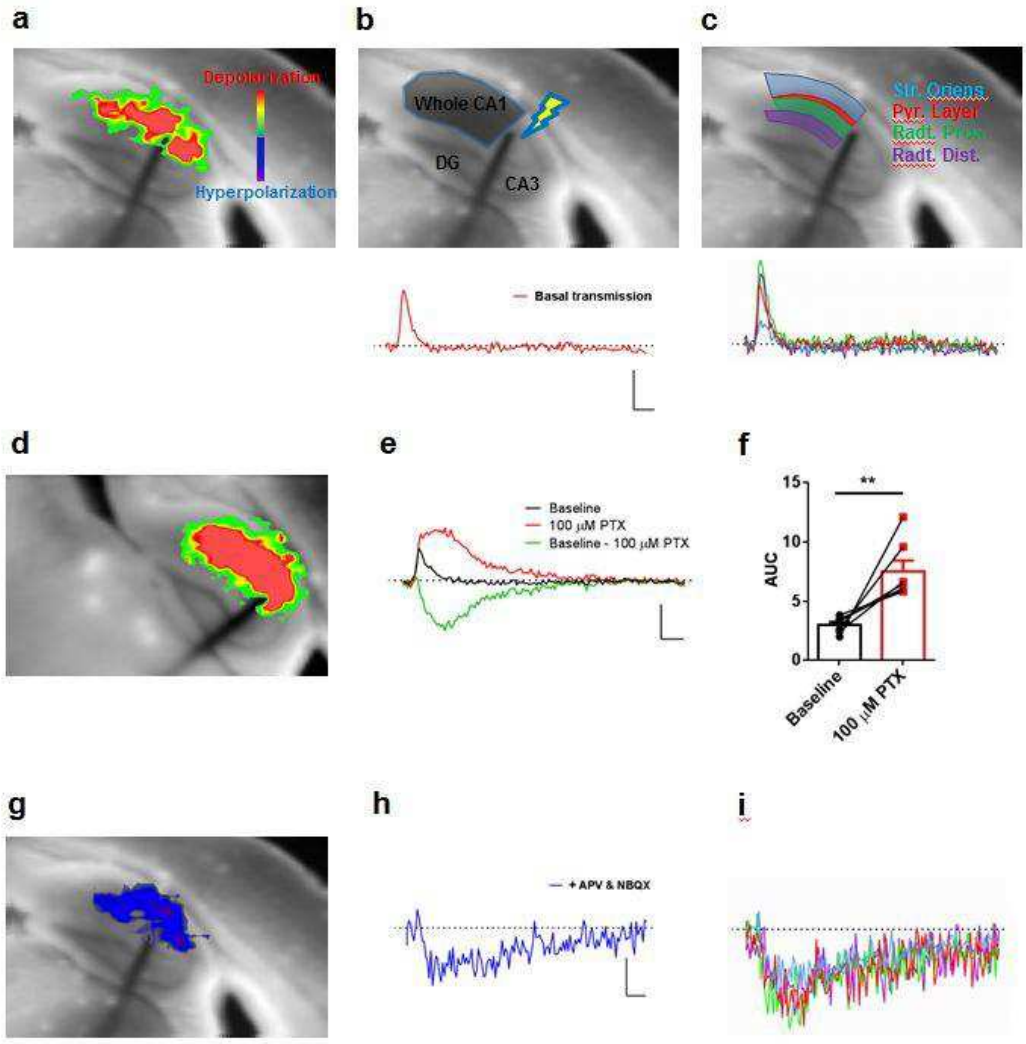

Figure 1. Blockade of ionotropic glutamatergic transmission reveals network hyperpolarization throughout CA1. (a) Representative frame showing VSDI-recorded depolarization activity after stimulation of Schaffer's collateral in drug-free ACSF. Inset color scale indicates depolarization (green to red) and hyperpolarization (blue to purple). **(b)** and **(c)** Representative regions of interest (ROIs) arrangement (upper panels) and

corresponding traces (lower panels) showing resulting average VSDI-recorded depolarization in drug-free ACSF from a ROI covering the whole CA1 (b) and in its different sub-regions (c). Str. Oriens = *stratum oriens*, Pyr. Layer = Pyramidal Layer, Radt. Prox. = *radiatum* proximal, Radt. Dist. = *radiatum* distal. **(d)** Representative frame showing VSDI-recorded depolarization activity after stimulation of Schaffer's collateral following application of Picrotoxin (PTX, 100 µM). **(e)** Representative traces showing the impact of GABAergic transmission on VSDI-recorded depolarization from a ROI covering the whole CA1 before (Baseline) and after application of PTX. The GABAergic component (Baseline – 100 µM Picrotoxin) is obtained from the difference between Baseline and PTX conditions, respectively. **(f)** Quantification through area under curve (AUC) calculation of VSDI-recorded depolarization in the whole CA1 before (Baseline) and after application of PTX. n = 7 slices from 5 mice. Bars represent mean ± s.e.m. whereas over imposed lines are single values. ** = $p<0.01$, two-tailed paired t-test. **(g)** Representative frame showing VSDI-recorded hyperpolarization activity after stimulation of Schaffer's collateral in presence of blockers of ionotropic glutamatergic transmission (APV & NBQX). **(h)** and **(i)** Representative traces showing VSDI-recorded hyperpolarization activity following APV & NBQX application from a ROI covering the whole CA1 (h) and in its different sub-regions (i). Scale bars are 25 milliseconds on X-axis and 0.2% $\Delta F*F^{-1}$ on y-axis for traces in (b), (c) and (e) whereas 0.05% $\Delta F*F^{-1}$ on y-axis for traces in (h) and (i).

Figure 2:

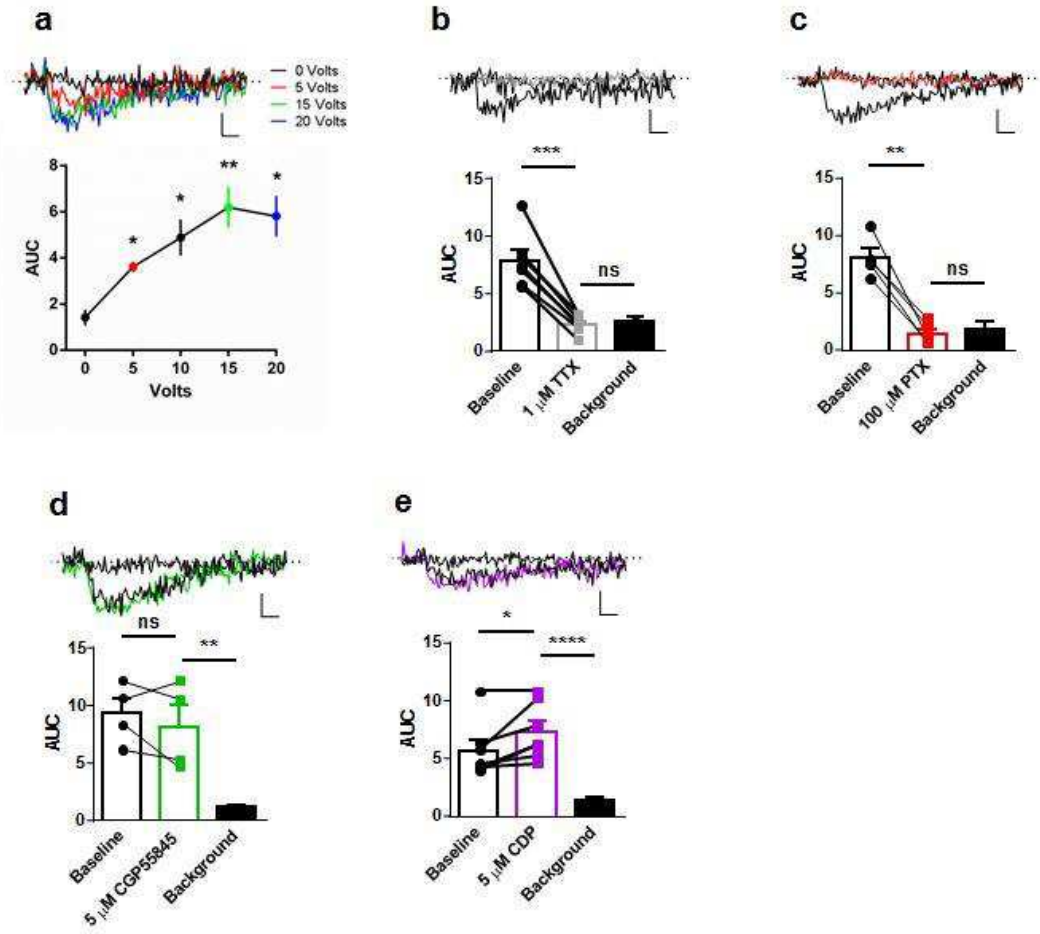

Figure 2. Characterization of the VSDI-recorded fIPSPs.

(a) Increasing stimulation intensity every 5 minutes time steps significantly enhances the signal compared to 0 Volts [lower panel, one-way ANOVA with repeated measures over stimulation intensities (F (2,605, 13,02) = 12,95, p = 0.0005) followed by Tukey post-hoc test. n = 6 slices from 5 mice]. Representative traces (upper panel) at indicated voltage steps. **(b)** 1 µM Tetrodotoxin (TTX) significantly abolishes the signal, which is statistically not different from the background, lower panel, n = 7 slices from 5 mice. Upper panel, representative traces before (thin black) and after (gray) TTX application, with

background (thick black). **(c)** 100 µM Picrotoxin (PTX) significantly abolishes the signal, which is then not different from background, lower panel, n = 5 slices from 3 mice. Upper panel, representative traces before (thin black) and after (red) PTX application, with background (thick black). **(d)** 5 µM CGP55845 does not affect the hyperpolarization signal, lower panel, n = 4 slices from 2 mice. Upper panel, representative traces before (thin black) and after (green) drug application, with background (thick black). **(e)** 5 µM Chlordiazepoxide (CDP) significantly increases the signal, lower panel, n = 7 slices from 4 mice. Upper panel, representative traces before (thin black) and after (purple) CDP application, with background (thick black). In all graphs, signal of interest has been assessed in a ROI covering the whole CA1. Bars and points in (a) represents mean ± s.e.m. whereas over imposed lines are single values. Statistical significance has been assessed with two-tailed paired t-test between baseline condition and drug application, while two-tailed unpaired t-test has been used between drug application and respective background (b – e). Scale bars are 25 milliseconds on X-axis and 0.05% $\Delta F*F^{-1}$ on Y-axis. * = $p<0.05$, ** = $p<0.01$, *** = $p<0.001$, **** = $p<0.0001$, ns = not significant.

Figure 3:

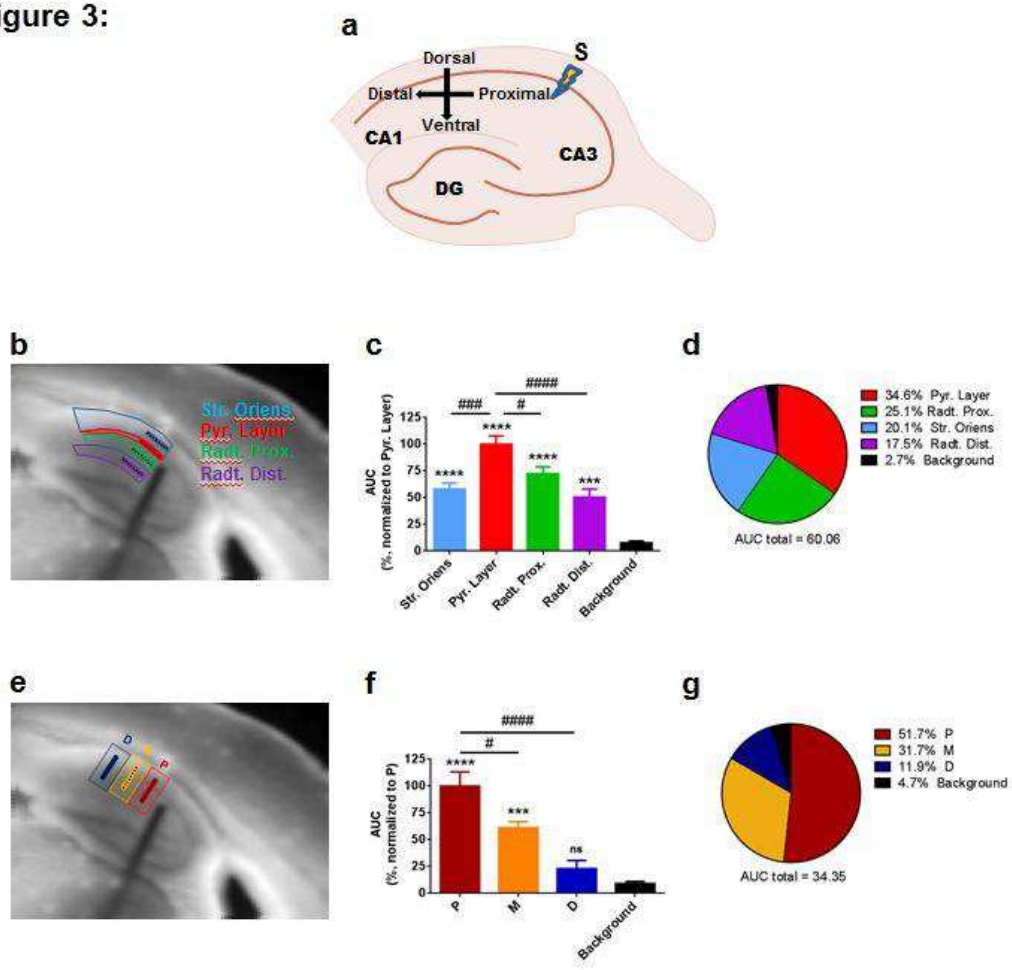

Figure 3. Spatial distribution of VSDI-recorded fIPSPs throughout CA1 region.

(a) Cartoon representing the orientation of the different sub-regions studied in the CA1 (S, stimulation electrode). **(b)** Scheme showing spatial organization of the 8 pixels long ROI lines inside the dorso-ventral axis of CA1 (reference CA1 sub regions are delimited by the colored contour). **(c)** Quantification through AUC of hyperpolarization from the ROI lines shows detectable signal in all the dorso-ventral regions of CA1, which is mainly localized in the pyramidal layer (one-way ANOVA followed by Tukey post-hoc test; asterisks are differences vs. “Background”, while hashes are differences vs. “Pyramidal layer”). **(d)** Pie

chart summarizing the distribution of the signal from the lines along the dorso-ventral part of CA1 showing a predominant presence in the pyramidal layer (percentage of each region respect to the total AUC). **(e)** Scheme showing spatial organization of the 8 pixels long ROI lines inside the proximo-distal axis of CA1 (reference proximo-distal ROIs are delimited by the colored contour); “P” = proximal, “M” = medial, “D” = distal; distances from stimulation electrode are ~106, ~318 and ~531 µm for regions P, M and D respectively. **(f)** Quantification through AUC of hyperpolarization from the ROI lines shows detectable signal at the proximity of the stimulation electrode (lines in regions “P” and “M”) while signal from lines in region “D” is not different from background (one-way ANOVA followed by Tukey post-hoc test; asterisks are differences vs. “Background”, while hashes are differences vs. “P”). **(g)** Pie chart summarizing how the signal from the ROI lines along the proximo-distal part of CA1 is concentrated in the proximity of the stimulation electrode (percentage of each region respect to the total AUC). n = 10 slices from 10 mice. Data are mean ± s.e.m. # = $p<0.05$, ### and *** = $p<0.001$, #### and **** = $p<0.0001$, ns = not significant.

Figure 4:

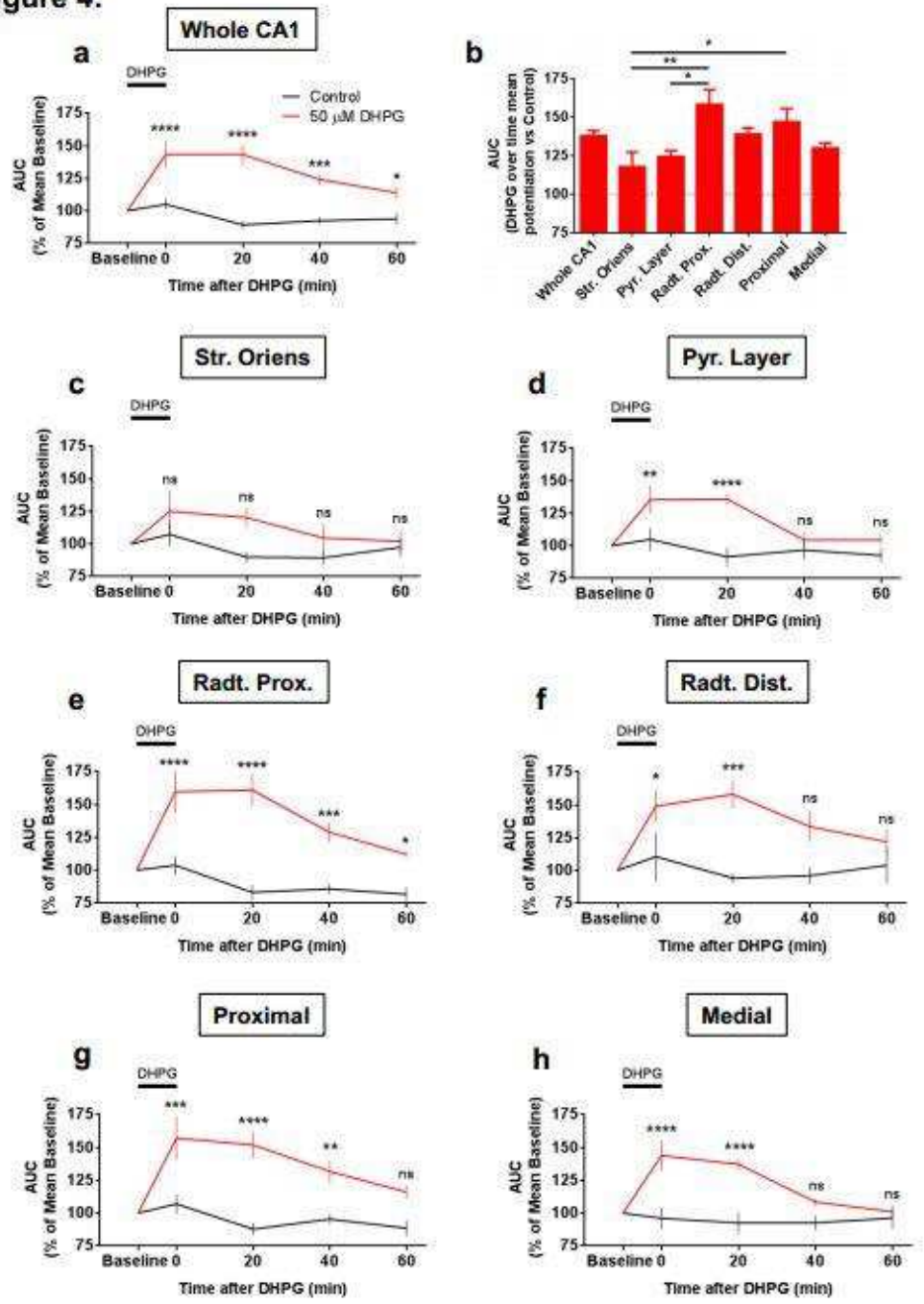
Whole CA1
a
DHPG
Control
50 μM DHPG
AUC (% of Mean Baseline)
Baseline 0
20
40
60
Time after DHPG (min)
b
AUC (DHPG over time mean potentiation vs Control)
Whole CA1
Str. Oriens
Pyr. Layer
Radt. Prox.
Radt. Dist.
Proximal
Medial
Str. Oriens
c
Pyr. Layer
d
Radt. Prox.
e
Radt. Dist.
f
Proximal
g
Medial
h
ns

Figure 4. Long-lasting increase of VSDI-recorded fIPSPs after group I mGluRs activation. Brief application of the selective group I mGluRs agonist (S)-3,5-Dihydroxyphenylglycine (DHPG) for 10 minutes induces long-lasting enhancement of fIPSPs during washout of the drug in the whole CA1 **(a)** and in its different sub-regions **(c-h)**. **(b)** Graph showing mean over time percentage potentiation of DHPG vs control in whole CA1 and in its different sub-fields; one-way ANOVA followed by Tukey post-hoc test. n = (slices, mice): DHPG group = (7, 5), Control group = (7, 4). Data are mean ± s.e.m. Statistical analysis in (a) and (c-h) is two-way ANOVA followed by Bonferroni post-hoc test. * = $p<0.05$, ** = $p<0.01$, *** = $p<0.001$, **** = $p<0.0001$, ns = not significant.

Figure 5:

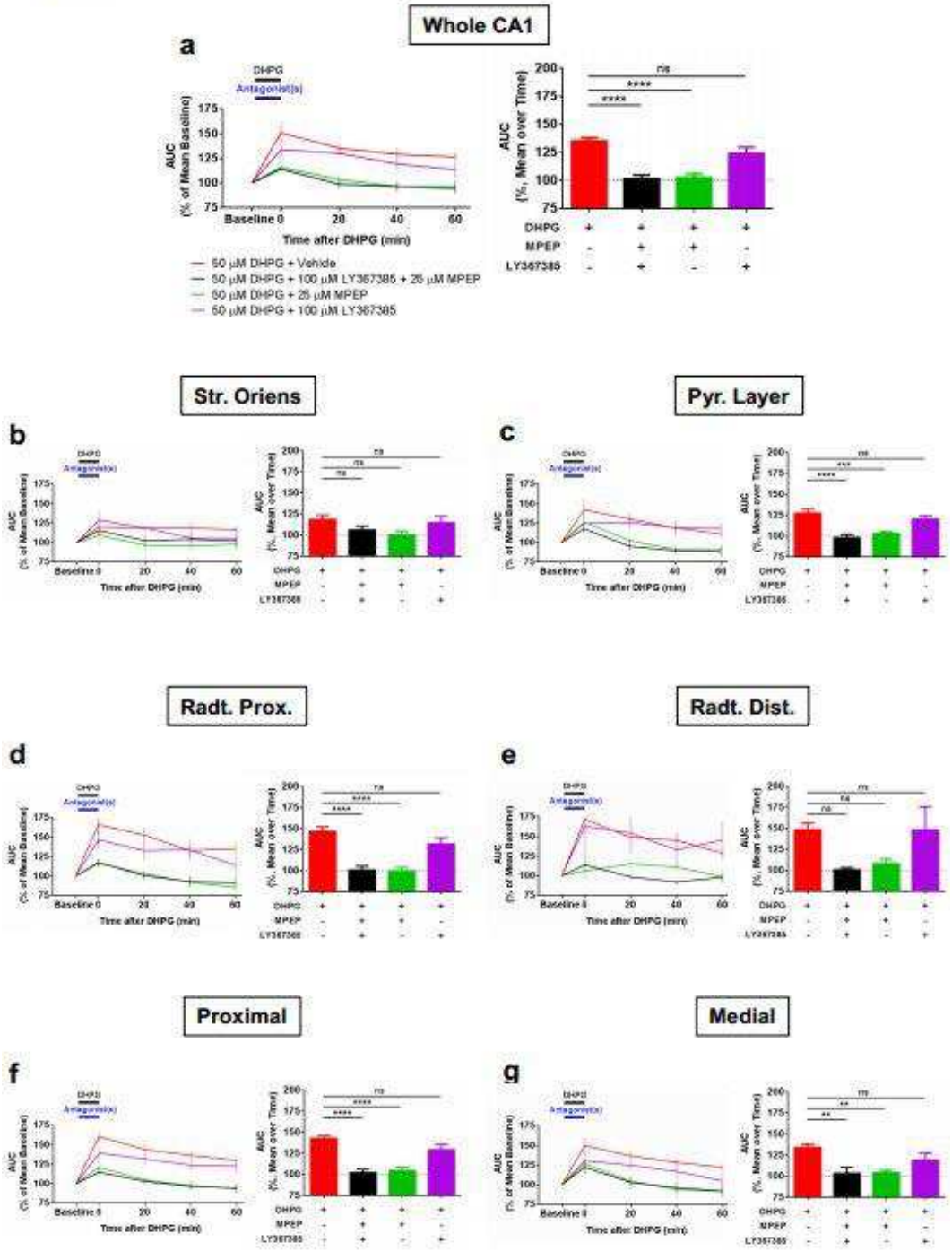
Whole CA1
a
DHPG
Antagonist(s)
AUC (% of Mean Baseline)
Baseline 0
20
40
60
Time after DHPG (min)
50 µM DHPG + Vehicle
50 µM DHPG + 100 µM LY367385 + 25 µM MPEP
50 µM DHPG + 25 µM MPEP
50 µM DHPG + 100 µM LY367385
AUC (%, Mean over Time)
ns
****
****
DHPG
MPEP
LY367385
Str. Oriens
b
Pyr. Layer
c
Radt. Prox.
d
Radt. Dist.
e
Proximal
f
Medial
g

Figure 5. Long-lasting increase of fIPSPs after DHPG application is mediated by mGluR5 activation. Slices were incubated with DHPG in presence of antagonists of group I mGluRs (LY367385 for mGluR1, MPEP for mGluR5 or both) which were kept until the end of DHPG application. In each figure, left panel shows time course, while right panel shows mean over time for each condition and each region. One-way ANOVA followed by Dunnet post-hoc test has been used to assess differences between groups in right panel graphs. ANOVA in *radiatum* distal (e) is: $F(3, 23) = 3.006$, $p=0.0511$. n = (slices, mice): Vehicle group = (7, 7), LY367385 + MPEP group = (7, 7), MPEP group = (6, 5), LY367385 group = (7, 5). Data are mean ± s.e.m. ** = $p<0.01$, *** = $p<0.001$, **** = $p<0.0001$, ns = not significant.

Figure 6:

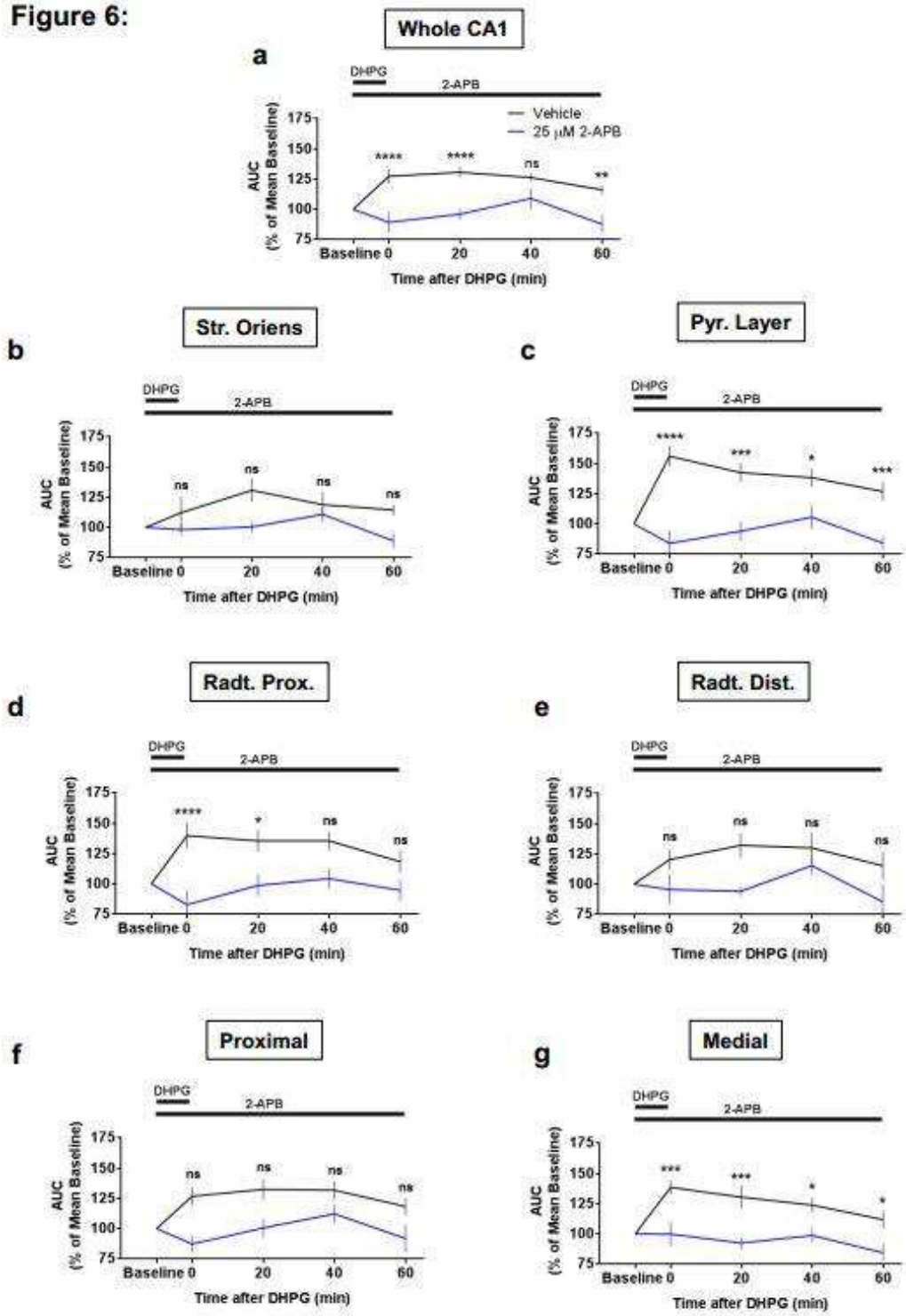
Whole CA1
a
DHPG
2-APB
Vehicle
25 μM 2-APB
AUC
(% of Mean Baseline)
Baseline 0
20
40
60
Time after DHPG (min)
Str. Oriens
b
Pyr. Layer
c
Radt. Prox.
d
Radt. Dist.
e
Proximal
f
Medial
g
ns
*
**
***
****

Figure 6. Long-lasting increase of fIPSPs after DHPG application is mediated by IP_3 receptors activation. In continuous presence of the cell-permeable IP_3 receptor blocker 2-APB, DHPG fails to increase fIPSPs in all CA1 (a) and specifically in its different sub-regions (b-g). In Figure e and f there is no significant "time x treatment" interaction, while only "treatment" effect is present; Treatment: F (1, 45) = 12.73, p=0.0009 for (e) and F (1, 45) = 26.11, p<0.0001 for (f). Statistical analysis is two-way ANOVA followed by Bonferroni post-hoc test. n = (slices, mice): 2-APB group = (5, 5), Vehicle group = (6, 5). Data are mean ± s.e.m. * = p<0.05, ** = p<0.01, *** = p<0.001, **** = p<0.0001, ns = not significant.

Supplementary Figure 1:

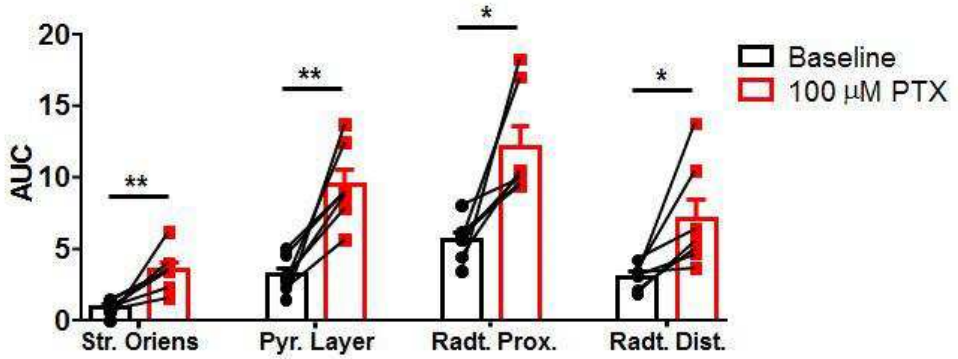

Supplementary Figure 1. Impact of blockade of GABAergic transmission on VSD-recorded depolarization in specific CA1 sub-regions. Application of the $GABA_A$ receptor antagonist Picrotoxin (PTX, 100 µM) significantly increase VSD-recorded depolarization in all the CA1 sub-regions. n = 7 slices from 5 mice. Significance has been assessed with two-tailed paired *t*-test. Data in bars are mean ± s.e.m. whereas over imposed lines are single values. * = p<0.05, ** = p<0.01, ns = not significant.

Supplementary Figure 2:

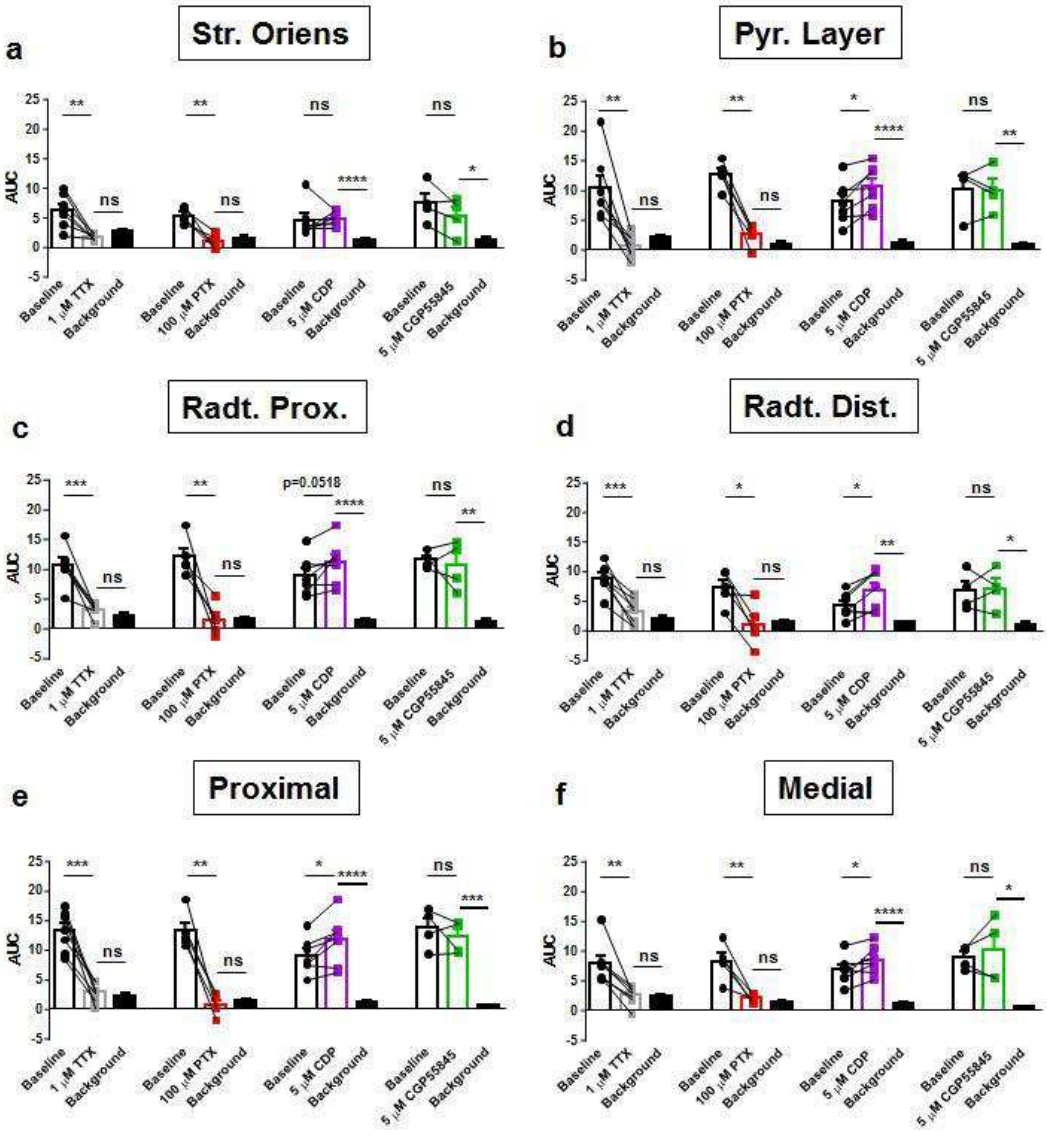

Supplementary Figure 2. Region-specific pharmacological characterization of VSD-recorded fIPSPs in CA1 region. Tetrodotoxin (TTX, 1 µM) = 7 slices from 5 mice; Picrotoxin (PTX, 100 µM) 5 slices from 3 mice ; Chlordiazepoxide (CDP, 5 µM) = 7 slices from 4 mice; CGP55845 (5 µM) = 4 slices from 2 mice. Data in bars are mean ± s.e.m. whereas over imposed lines are single values. Significance has been assessed with two-tailed paired *t*-test between baseline condition and drug application, while two-tailed unpaired *t*-test has been used between drug application and respective Background. * = p<0.05, ** = p<0.01, *** = p<0.001, **** = p<0.0001, ns = not significant.

CHAPTER IV

GENERAL DISCUSSION AND CONCLUSION

The importance of studying neuronal networks is due to the fact that they represent the structural interface between single cell's activity and behavior (Parker, 2006, 2010) and their deeper understanding is instrumental for "closing the explanatory gap" between the firing of single neurons and the behavior that ultimately results from their activity (Parker, 2006). The powerful computational capability of the brain relies on the proper balance between excitatory and inhibitory networks (Isaacson and Scanziani, 2011; Kullmann, 2011), with glutamate that carries the information across brain regions and GABA that acts as a regulator, impeding excessive and asynchronous glutamatergic transmission.

However, while are already available techniques for recording excitatory networks (Buzsaki, 2004; Buzsaki et al., 2012), the possibility to record large-scale GABAergic activity is very limited to date, since has been reported only using one or very few electrodes (Arai et al., 1995; Bazelot et al., 2010; Lambert et al., 1991), therefore unable to provide sufficient spatial information. The last decades were characterized by an enormous improvement of the technology to record neuronal activity, in which photons replaced electrons (Peterka et al., 2011), with the result of an easier access to the neurons due to the lack of recording electrodes. One of the most representative techniques which reports neuronal activity by means of light is voltage sensitive dye imaging (VSDI), which does so through the use of a dye that emits fluorescence proportionally to changes in membrane potential (Chemla and Chavane, 2010; Loew, 2010; Loew et al., 1992; Loew et al., 1985; Peterka et al., 2011; Tominaga, 2013).

Through the use of VSDI and advanced mathematical analysis of the VSDI data, I aimed at studying more in detail the excitatory network in the CA1 area of hippocampus. With the collaboration of a team of mathematicians, we developed an algorithm which is a new method to estimate an optical flow and is based on an old mathematical problem

originally conceived by the French mathematician Gaspard Monge at the end of the 18th century (Monge, 1781) and implemented later by the Russian mathematician Leonid Kantorovich (Kantorovich, 1942). This problem consists in finding a plan to transport a certain quantity of mass from a starting configuration to a final one, minimizing a given functional cost. In our case, the output of this algorithm is a vectorial field in which each vector represents the least distance covered by neuronal depolarization every 2.2 milliseconds, which is the time resolution of the VSDI recordings used in this study. Importantly, these vectors provide two keys quantitative information: distance (quantified by the number of pixels covered during the spreading of neuronal depolarization) and the overall direction of spreading inside each region of interest (represented by the convergence/divergence).

After we successfully validated the algorithm with surrogate data in order to test its accuracy, we analyzed two sets of experiments in which we manipulated CA1 excitatory network activity either by increasing stimulation intensity from 10 to 30 Volts or by blocking GABAergic transmission with the $GABA_A$ receptor antagonist picrotoxin. We found the following:

- both manipulations **significantly increased neuronal depolarization** (represented by increased fluorescence emission, $\Delta F*F^{-1}$) in the overall CA1 and specifically in its sublayers. One different result between the two experiments is that by blocking GABAergic inhibition, excitatory activity is only prolonged and is not significantly affected during the very early steps of signal propagation (~10 milliseconds), suggesting how interneurons are recruited mainly to prevent excessive and prolonged excitatory activity.
- both manipulations **significantly decreased the velocity of depolarization** signal (quantified by the ratio of distance over time) only at the middle-late phase of the

propagation. This finding may be surprising and counterintuitive, but may be explained by the persistence of the network in a more depolarized state compared to control conditions, either after increased stimulation intensity (30 Volts) or after blockade of $GABA_A$ receptors.

- Only **blocking GABAergic inhibition we significantly influenced the overall direction** of spreading of the VSDI signal, making it more focused and less divergent compared to control. This demonstrates how interneurons actively participate in the routing of excitatory signals along the CA1 network.

Regarding inhibitory networks, I characterized for the first time with VSDI evoked $GABA_A$ receptor mediated *field* inhibitory postsynaptic potentials (fIPSP) which spanned in the whole CA1 and in all its sublayers, demonstrating the possibility to use VSDI as a tool for the direct investigation of inhibitory events at network level and not only at single cell resolution. In particular, I show how fIPSP are mainly occurring in the pyramidal layer and not more far than ~500 μm from the stimulating electrode, consistent with the fact that the majority of GABAergic synapses are in the perisomatic region of pyramidal cells in the CA1 (Bezaire and Soltesz, 2013; Megias et al., 2001) and that stimulation activates local populations of interneurons, respectively. Very interestingly, when I applied for a brief period of time (10 minutes) the group I mGluR receptors agonist DHPG, was induced a phenomenon of GABAergic plasticity characterized by a long lasting increase of synaptic strength, whose duration and amplitude depended on the different layers of the CA1, being more long-lasting (60 minutes) and higher in the *stratum radiatum* proximal to the pyramidal layer. Complementary experiments demonstrated that mGluR5 is the receptor mediating this plasticity, by subsequent intracellular activation of IP_3 receptors. Phenomena of long term plasticity of GABAergic synapses are already known

in the hippocampus (Castillo et al., 2011), but is the first time that is reported a mGluR5-dependent long lasting potentiation of GABAergic inhibition, with the addition of being layer-specific concerning duration and magnitude. Further experiments are needed in order to better characterize the mGluR5-dependent long-lasting increase of network GABAergic inhibition in the CA1. For instance, what is the functional impact of this phenomenon on the overall excitatory transmission in the hippocampus? A possible explanation is that in case of intensive excitatory activity, spillover of glutamate in the synaptic cleft may activates the perisynaptic mGluR5 receptors with the subsequent compensatory increase of GABAergic activity. Other open questions include: how exactly mGluR5 potentiates GABAergic transmission? Is it because of increased release of GABA (presynaptic effect) or is because of increased $GABA_A$ receptor conductance and/or increased receptor availability (postsynaptic effect)? Is it modulated in case of pathological conditions which involve mGluR5 signaling such as epilepsy and fragile X syndrome (Alexander and Godwin, 2006; Bear et al., 2004)? If so, how?

Overall, these data provide new insights on mechanisms through which excitatory and inhibitory transmissions tightly cooperate in the CA1 region. The data from the mathematical investigation of excitatory networks further highlight in particular how inhibition by $GABA_A$ receptors is important in the normal spreading of glutamatergic activity but move this concept on a higher neuroarchitectural level such as the network level, instead of a single/few cells. Moreover, the algorithm we developed could potentially be used to analyze data from every optical imaging technique and given their broad use in all the domain of research in health and disease states may significantly enlarge current knowledge. The data from network inhibition indeed demonstrated the possibility to use VSDI with unprecedented large spatial resolution for the investigation of GABAergic transmission and plasticity phenomena, in contrast to electrode-based

recordings. In addition, these data shed new light on the neuromodulatory role of glutamatergic transmission onto GABAergic signaling.

CHAPTER V

GENERAL LIST OF REFERENCES

(1932). Edgar Adrian - Nobel Lecture: The Activity of the Nerve Fibres (<http://www.nobelprize.org/nobel_prizes/medicine/laureates/1932/adrian-lecture.html>).

(2010). A Decade after The Decade of the Brain (http://www.dana.org/Cerebrum/2010/A_Decade_after_The_Decade_of_the_Brain__Compilation/#Hodes).

Alexander, G.M., and Godwin, D.W. (2006). Metabotropic glutamate receptors as a strategic target for the treatment of epilepsy. Epilepsy research *71*, 1-22.

Amaral D., L.P. (2007). Hippocampal Neuroanatomy. In The Hippocampus book (Oxford University press), pp. 37-114.

Andersen P., M.R., Amaral D., Bliss T., O'Keefe J. (2007). The Hippocampal Formation. In The Hippocampus book (Oxford University press), pp. 3-8.

Andrade, R., Malenka, R.C., and Nicoll, R.A. (1986). A G protein couples serotonin and GABAB receptors to the same channels in hippocampus. Science *234*, 1261-1265.

Anwyl, R. (1991). Modulation of vertebrate neuronal calcium channels by transmitters. Brain research Brain research reviews *16*, 265-281.

Anwyl, R. (1999). Metabotropic glutamate receptors: electrophysiological properties and role in plasticity. Brain research Brain research reviews *29*, 83-120.

Arai, A., Silberg, J., and Lynch, G. (1995). Differences in the refractory properties of two distinct inhibitory circuitries in field CA1 of the hippocampus. Brain research *704*, 298-306.

Ascher, P., and Nowak, L. (1988). The role of divalent cations in the N-methyl-D-aspartate responses of mouse central neurones in culture. The Journal of physiology *399*, 247-266.

Azevedo, F.A., Carvalho, L.R., Grinberg, L.T., Farfel, J.M., Ferretti, R.E., Leite, R.E., Jacob Filho, W., Lent, R., and Herculano-Houzel, S. (2009). Equal numbers of neuronal and nonneuronal cells make the human brain an isometrically scaled-up primate brain. The Journal of comparative neurology *513*, 532-541.

Bannister, N.J., and Larkman, A.U. (1995). Dendritic morphology of CA1 pyramidal neurones from the rat hippocampus: I. Branching patterns. The Journal of comparative neurology *360*, 150-160.

Baranano, D.E., Ferris, C.D., and Snyder, S.H. (2001). Atypical neural messengers. Trends in neurosciences *24*, 99-106.

Barnard, E.A., Skolnick, P., Olsen, R.W., Mohler, H., Sieghart, W., Biggio, G., Braestrup, C., Bateson, A.N., and Langer, S.Z. (1998). International Union of Pharmacology. XV. Subtypes of gamma-aminobutyric acidA receptors: classification on the basis of subunit structure and receptor function. Pharmacological reviews *50*, 291-313.

Baude, A., Nusser, Z., Roberts, J.D., Mulvihill, E., McIlhinney, R.A., and Somogyi, P. (1993). The metabotropic glutamate receptor (mGluR1 alpha) is concentrated at

perisynaptic membrane of neuronal subpopulations as detected by immunogold reaction. Neuron *11*, 771-787.

Bazelot, M., Dinocourt, C., Cohen, I., and Miles, R. (2010). Unitary inhibitory field potentials in the CA3 region of rat hippocampus. The Journal of physiology *588*, 2077-2090.

Bear, M.F., Huber, K.M., and Warren, S.T. (2004). The mGluR theory of fragile X mental retardation. Trends in neurosciences *27*, 370-377.

Ben-Ari, Y., Cherubini, E., Corradetti, R., and Gaiarsa, J.L. (1989). Giant synaptic potentials in immature rat CA3 hippocampal neurones. The Journal of physiology *416*, 303-325.

Ben-Ari, Y., and Cossart, R. (2000). Kainate, a double agent that generates seizures: two decades of progress. Trends in neurosciences *23*, 580-587.

Ben-Ari, Y., Khazipov, R., Leinekugel, X., Caillard, O., and Gaiarsa, J.L. (1997). GABAA, NMDA and AMPA receptors: a developmentally regulated 'menage a trois'. Trends in neurosciences *20*, 523-529.

Bezaire, M.J., and Soltesz, I. (2013). Quantitative assessment of CA1 local circuits: knowledge base for interneuron-pyramidal cell connectivity. Hippocampus *23*, 751-785.

Biscoe, T.J., and Straughan, D.W. (1966). Micro-electrophoretic studies of neurones in the cat hippocampus. The Journal of physiology *183*, 341-359.

Bowie, D., and Mayer, M.L. (1995). Inward rectification of both AMPA and kainate subtype glutamate receptors generated by polyamine-mediated ion channel block. Neuron *15*, 453-462.

Buhl, E.a.W., M. (2007). Local Circuits. In The Hippocampus book (The Oxford University press), pp. 297 - 319.

Buzsaki, G. (2004). Large-scale recording of neuronal ensembles. Nature neuroscience *7*, 446-451.

Buzsaki, G., Anastassiou, C.A., and Koch, C. (2012). The origin of extracellular fields and currents--EEG, ECoG, LFP and spikes. Nature reviews Neuroscience *13*, 407-420.

Canepari, M., Willadt, S., Zecevic, D., and Vogt, K.E. (2010). Imaging inhibitory synaptic potentials using voltage sensitive dyes. Biophysical journal *98*, 2032-2040.

Caplan, A. (2002). The brain revolution and ethics. The Scientist *16*, 12-14.

Capogna, M., Gahwiler, B.H., and Thompson, S.M. (1996). Presynaptic inhibition of calcium-dependent and -independent release elicited with ionomycin, gadolinium, and alpha-latrotoxin in the hippocampus. Journal of neurophysiology *75*, 2017-2028.

Castillo, P.E., Chiu, C.Q., and Carroll, R.C. (2011). Long-term plasticity at inhibitory synapses. Current opinion in neurobiology *21*, 328-338.

Castillo, P.E., Malenka, R.C., and Nicoll, R.A. (1997). Kainate receptors mediate a slow postsynaptic current in hippocampal CA3 neurons. Nature *388*, 182-186.

Chamberland, S., and Topolnik, L. (2012). Inhibitory control of hippocampal inhibitory neurons. Frontiers in neuroscience *6*, 165.

Chang, Y., Wang, R., Barot, S., and Weiss, D.S. (1996). Stoichiometry of a recombinant GABAA receptor. The Journal of neuroscience : the official journal of the Society for Neuroscience *16*, 5415-5424.

Chemla, S., and Chavane, F. (2010). Voltage-sensitive dye imaging: Technique review and models. Journal of physiology, Paris *104*, 40-50.

Chevaleyre, V., and Castillo, P.E. (2003). Heterosynaptic LTD of hippocampal GABAergic synapses: a novel role of endocannabinoids in regulating excitability. Neuron *38*, 461-472.

Chittajallu, R., Vignes, M., Dev, K.K., Barnes, J.M., Collingridge, G.L., and Henley, J.M. (1996). Regulation of glutamate release by presynaptic kainate receptors in the hippocampus. Nature *379*, 78-81.

Cohen, L.B. (2010). Historical Overview and General Methods of Membrane Potential Imaging. In Membrane potential imaging in the nervous system, M. Canepari, & Zecevic, D., ed. (Springer), pp. 1 - 11.

Cohen, L.B., Keynes, R.D., and Hille, B. (1968). Light scattering and birefringence changes during nerve activity. Nature *218*, 438-441.

Cohen, L.B., Salzberg, B.M., Davila, H.V., Ross, W.N., Landowne, D., Waggoner, A.S., and Wang, C.H. (1974). Changes in axon fluorescence during activity: molecular probes of membrane potential. The Journal of membrane biology *19*, 1-36.

Colquhoun, D., Jonas, P., and Sakmann, B. (1992). Action of brief pulses of glutamate on AMPA/kainate receptors in patches from different neurones of rat hippocampal slices. The Journal of physiology *458*, 261-287.

Contractor, A., Swanson, G., and Heinemann, S.F. (2001). Kainate receptors are involved in short- and long-term plasticity at mossy fiber synapses in the hippocampus. Neuron *29*, 209-216.

Cossart, R., Epsztein, J., Tyzio, R., Becq, H., Hirsch, J., Ben-Ari, Y., and Crepel, V. (2002). Quantal release of glutamate generates pure kainate and mixed AMPA/kainate EPSCs in hippocampal neurons. Neuron *35*, 147-159.

Cossart, R., Tyzio, R., Dinocourt, C., Esclapez, M., Hirsch, J.C., Ben-Ari, Y., and Bernard, C. (2001). Presynaptic kainate receptors that enhance the release of GABA on CA1 hippocampal interneurons. Neuron *29*, 497-508.

Davila, H.V., Cohen, L.B., Salzberg, B.M., and Shrivastav, B.B. (1974). Changes in ANS and TNS fluorescence in giant axons from Loligo. The Journal of membrane biology *15*, 29-46.

De Blasi, A., Conn, P.J., Pin, J., and Nicoletti, F. (2001). Molecular determinants of metabotropic glutamate receptor signaling. Trends in pharmacological sciences *22*, 114-120.

Destexhe, A., and Sejnowski, T.J. (1995). G protein activation kinetics and spillover of gamma-aminobutyric acid may account for differences between inhibitory responses in the hippocampus and thalamus. Proceedings of the National Academy of Sciences of the United States of America *92*, 9515-9519.

Dolphin, A.C., Errington, M.L., and Bliss, T.V. (1982). Long-term potentiation of the perforant path in vivo is associated with increased glutamate release. Nature *297*, 496-498.

Dudek, F.E., and Sutula, T.P. (2007). Epileptogenesis in the dentate gyrus: a critical perspective. Progress in brain research *163*, 755-773.

Eberwine, J. (2001). Molecular biology of axons: "a turning point...". Neuron *32*, 959-960.

Emptage, N., Bliss, T.V., and Fine, A. (1999). Single synaptic events evoke NMDA receptor-mediated release of calcium from internal stores in hippocampal dendritic spines. Neuron *22*, 115-124.

Essrich, C., Lorez, M., Benson, J.A., Fritschy, J.M., and Luscher, B. (1998). Postsynaptic clustering of major GABAA receptor subtypes requires the gamma 2 subunit and gephyrin. Nature neuroscience *1*, 563-571.

Fagni, L., Chavis, P., Ango, F., and Bockaert, J. (2000). Complex interactions between mGluRs, intracellular Ca2+ stores and ion channels in neurons. Trends in neurosciences *23*, 80-88.

Farrar, S.J., Whiting, P.J., Bonnert, T.P., and McKernan, R.M. (1999). Stoichiometry of a ligand-gated ion channel determined by fluorescence energy transfer. The Journal of biological chemistry *274*, 10100-10104.

Ferraguti, F., and Shigemoto, R. (2006). Metabotropic glutamate receptors. Cell and tissue research *326*, 483-504.

Fishell, G., and Rudy, B. (2011). Mechanisms of inhibition within the telencephalon: "where the wild things are". Annual review of neuroscience *34*, 535-567.

Fluhler, E., Burnham, V.G., and Loew, L.M. (1985). Spectra, membrane binding, and potentiometric responses of new charge shift probes. Biochemistry *24*, 5749-5755.

Fotuhi, M., Standaert, D.G., Testa, C.M., Penney, J.B., Jr., and Young, A.B. (1994). Differential expression of metabotropic glutamate receptors in the hippocampus and entorhinal cortex of the rat. Brain research Molecular brain research *21*, 283-292.

Freund, T.F., and Buzsaki, G. (1996). Interneurons of the hippocampus. Hippocampus *6*, 347-470.

Freund, T.F., and Katona, I. (2007). Perisomatic inhibition. Neuron *56*, 33-42.

Fritschy, J.M., Meskenaite, V., Weinmann, O., Honer, M., Benke, D., and Mohler, H. (1999). GABAB-receptor splice variants GB1a and GB1b in rat brain: developmental regulation, cellular distribution and extrasynaptic localization. The European journal of neuroscience *11*, 761-768.

Fromherz, P., Hubener, G., Kuhn, B., and Hinner, M.J. (2008). ANNINE-6plus, a voltage-sensitive dye with good solubility, strong membrane binding and high sensitivity. European biophysics journal : EBJ *37*, 509-514.

Fuentealba, P., Begum, R., Capogna, M., Jinno, S., Marton, L.F., Csicsvari, J., Thomson, A., Somogyi, P., and Klausberger, T. (2008). Ivy cells: a population of nitric-oxide-producing, slow-spiking GABAergic neurons and their involvement in hippocampal network activity. Neuron *57*, 917-929.

Garcia, E.P., Mehta, S., Blair, L.A., Wells, D.G., Shang, J., Fukushima, T., Fallon, J.R., Garner, C.C., and Marshall, J. (1998). SAP90 binds and clusters kainate receptors causing incomplete desensitization. Neuron *21*, 727-739.

Geiger, J.R., Melcher, T., Koh, D.S., Sakmann, B., Seeburg, P.H., Jonas, P., and Monyer, H. (1995). Relative abundance of subunit mRNAs determines gating and Ca2+ permeability of AMPA receptors in principal neurons and interneurons in rat CNS. Neuron *15*, 193-204.

Gladding, C.M., Fitzjohn, S.M., and Molnar, E. (2009). Metabotropic glutamate receptor-mediated long-term depression: molecular mechanisms. Pharmacological reviews *61*, 395-412.

Greenberg, B.D. (2002). Update on deep brain stimulation. The journal of ECT *18*, 193-196.

Grinvald, A., and Hildesheim, R. (2004). VSDI: a new era in functional imaging of cortical dynamics. Nature reviews Neuroscience *5*, 874-885.

Heuss, C., Scanziani, M., Gahwiler, B.H., and Gerber, U. (1999). G-protein-independent signaling mediated by metabotropic glutamate receptors. Nature neuroscience *2*, 1070-1077.

Hill, D.K. (1950). The effect of stimulation on the opacity of a crustacean nerve trunk and its relation to fibre diameter. The Journal of physiology *111*, 283-303.

Hill, D.K., and Keynes, R.D. (1949). Opacity changes in stimulated nerve. The Journal of physiology *108*, 278-281.

Horgan, J. (1999). The undiscovered mind. (London: Widenfeld and Nicholson).

Howard, A., Tamas, G., and Soltesz, I. (2005). Lighting the chandelier: new vistas for axo-axonic cells. Trends in neurosciences *28*, 310-316.

Iollo, A.L., D. (2011). A lagrangian scheme for the solution of the optimal mass transfer problem. Journal of Computational Physics *230*, 3430–3442.

Isaacson, J.S., and Scanziani, M. (2011). How inhibition shapes cortical activity. Neuron *72*, 231-243.

Ishizuka, N., Cowan, W.M., and Amaral, D.G. (1995). A quantitative analysis of the dendritic organization of pyramidal cells in the rat hippocampus. The Journal of comparative neurology *362*, 17-45.

Johnson, J.W., and Ascher, P. (1987). Glycine potentiates the NMDA response in cultured mouse brain neurons. Nature *325*, 529-531.

Jones, K.A., Borowsky, B., Tamm, J.A., Craig, D.A., Durkin, M.M., Dai, M., Yao, W.J., Johnson, M., Gunwaldsen, C., Huang, L.Y.*, et al.* (1998). GABA(B) receptors function as a heteromeric assembly of the subunits GABA(B)R1 and GABA(B)R2. Nature *396*, 674-679.

Kaila, K. (1994). Ionic basis of GABAA receptor channel function in the nervous system. Progress in neurobiology *42*, 489-537.

Kamboj, S.K., Swanson, G.T., and Cull-Candy, S.G. (1995). Intracellular spermine confers rectification on rat calcium-permeable AMPA and kainate receptors. The Journal of physiology *486 (Pt 2)*, 297-303.

Kantorovich, L.V. (1942). On the transfer of masses. Doklady Akademii Nauk SSSR *37*, 227–229.

Kerner, J.A., Standaert, D.G., Penney, J.B., Jr., Young, A.B., and Landwehrmeyer, G.B. (1997). Expression of group one metabotropic glutamate receptor subunit mRNAs in neurochemically identified neurons in the rat neostriatum, neocortex, and hippocampus. Brain research Molecular brain research *48*, 259-269.

Klausberger, T. (2009). GABAergic interneurons targeting dendrites of pyramidal cells in the CA1 area of the hippocampus. The European journal of neuroscience *30*, 947-957.

Klausberger, T., and Somogyi, P. (2008). Neuronal diversity and temporal dynamics: the unity of hippocampal circuit operations. Science *321*, 53-57.

Kleckner, N.W., and Dingledine, R. (1988). Requirement for glycine in activation of NMDA-receptors expressed in Xenopus oocytes. Science *241*, 835-837.

Kullmann, D. (2007). Synaptic Function. In The Hippocampus book (The Oxford University press), pp. 203-241.

Kullmann, D.M. (2001). Presynaptic kainate receptors in the hippocampus: slowly emerging from obscurity. Neuron *32*, 561-564.

Kullmann, D.M. (2011). Interneuron networks in the hippocampus. Current opinion in neurobiology *21*, 709-716.

Kuner, R., Kohr, G., Grunewald, S., Eisenhardt, G., Bach, A., and Kornau, H.C. (1999). Role of heteromer formation in GABAB receptor function. Science *283*, 74-77.

Lambert, N.A., Borroni, A.M., Grover, L.M., and Teyler, T.J. (1991). Hyperpolarizing and depolarizing GABAA receptor-mediated dendritic inhibition in area CA1 of the rat hippocampus. Journal of neurophysiology *66*, 1538-1548.

Laube, B., Hirai, H., Sturgess, M., Betz, H., and Kuhse, J. (1997). Molecular determinants of agonist discrimination by NMDA receptor subunits: analysis of the glutamate binding site on the NR2B subunit. Neuron *18*, 493-503.

Lauri, S.E., Bortolotto, Z.A., Bleakman, D., Ornstein, P.L., Lodge, D., Isaac, J.T., and Collingridge, G.L. (2001). A critical role of a facilitatory presynaptic kainate receptor in mossy fiber LTP. Neuron *32*, 697-709.

Lerma, J., Morales, M., Vicente, M.A., and Herreras, O. (1997). Glutamate receptors of the kainate type and synaptic transmission. Trends in neurosciences *20*, 9-12.

Lerma, J., Paternain, A.V., Rodriguez-Moreno, A., and Lopez-Garcia, J.C. (2001). Molecular physiology of kainate receptors. Physiological reviews *81*, 971-998.

Lester, R.A., Clements, J.D., Westbrook, G.L., and Jahr, C.E. (1990). Channel kinetics determine the time course of NMDA receptor-mediated synaptic currents. Nature *346*, 565-567.

Li, X.G., Somogyi, P., Tepper, J.M., and Buzsaki, G. (1992). Axonal and dendritic arborization of an intracellularly labeled chandelier cell in the CA1 region of rat hippocampus. Experimental brain research *90*, 519-525.

Loew, L.M. (2010). Design and Use of Organic Voltage Sensitive Dyes. In Membrane Potential Imaging of Nervous System, M.Z. Canepari, D., ed. (Springer), pp. 13 - 23.

Loew, L.M., Cohen, L.B., Dix, J., Fluhler, E.N., Montana, V., Salama, G., and Wu, J.Y. (1992). A naphthyl analog of the aminostyryl pyridinium class of potentiometric membrane dyes shows consistent sensitivity in a variety of tissue, cell, and model membrane preparations. The Journal of membrane biology *130*, 1-10.

Loew, L.M., Cohen, L.B., Salzberg, B.M., Obaid, A.L., and Bezanilla, F. (1985). Charge-shift probes of membrane potential. Characterization of aminostyrylpyridinium dyes on the squid giant axon. Biophysical journal *47*, 71-77.

Lujan, R., Nusser, Z., Roberts, J.D., Shigemoto, R., and Somogyi, P. (1996). Perisynaptic location of metabotropic glutamate receptors mGluR1 and mGluR5 on dendrites and dendritic spines in the rat hippocampus. The European journal of neuroscience *8*, 1488-1500.

Mannaioni, G., Marino, M.J., Valenti, O., Traynelis, S.F., and Conn, P.J. (2001). Metabotropic glutamate receptors 1 and 5 differentially regulate CA1 pyramidal cell function. The Journal of neuroscience : the official journal of the Society for Neuroscience *21*, 5925-5934.

Mayer, M.L., Westbrook, G.L., and Guthrie, P.B. (1984). Voltage-dependent block by Mg2+ of NMDA responses in spinal cord neurones. Nature *309*, 261-263.

McBain, C.J., and Mayer, M.L. (1994). N-methyl-D-aspartic acid receptor structure and function. Physiological reviews *74*, 723-760.

McIntyre, C.C., Savasta, M., Kerkerian-Le Goff, L., and Vitek, J.L. (2004). Uncovering the mechanism(s) of action of deep brain stimulation: activation, inhibition, or

both. Clinical neurophysiology : official journal of the International Federation of Clinical Neurophysiology *115*, 1239-1248.

Megias, M., Emri, Z., Freund, T.F., and Gulyas, A.I. (2001). Total number and distribution of inhibitory and excitatory synapses on hippocampal CA1 pyramidal cells. Neuroscience *102*, 527-540.

Mehta, A.K., and Ticku, M.K. (1999). An update on GABAA receptors. Brain research Brain research reviews *29*, 196-217.

Mintz, I.M., and Bean, B.P. (1993). GABAB receptor inhibition of P-type Ca2+ channels in central neurons. Neuron *10*, 889-898.

Misgeld, U., Bijak, M., and Jarolimek, W. (1995). A physiological role for GABAB receptors and the effects of baclofen in the mammalian central nervous system. Progress in neurobiology *46*, 423-462.

Monge, G. (1781). Memoire sur la theorie des deblais et des remblais, H.d.l.A.d.S.d. Paris, ed.

Mosbacher, J., Schoepfer, R., Monyer, H., Burnashev, N., Seeburg, P.H., and Ruppersberg, J.P. (1994). A molecular determinant for submillisecond desensitization in glutamate receptors. Science *266*, 1059-1062.

Nasonov, D.N.a.S.s., I.P. (1957). Changes in the cytoplasm of myelinated nerve fibers during excitation. Fiziol Zh SSSR, 664–672.

Neves, G., Cooke, S.F., and Bliss, T.V. (2008). Synaptic plasticity, memory and the hippocampus: a neural network approach to causality. Nature reviews Neuroscience *9*, 65-75.

Nowak, L., Bregestovski, P., Ascher, P., Herbet, A., and Prochiantz, A. (1984). Magnesium gates glutamate-activated channels in mouse central neurones. Nature *307*, 462-465.

Nusser, Z., and Mody, I. (2002). Selective modulation of tonic and phasic inhibitions in dentate gyrus granule cells. Journal of neurophysiology *87*, 2624-2628.

Ohishi, H., Akazawa, C., Shigemoto, R., Nakanishi, S., and Mizuno, N. (1995). Distributions of the mRNAs for L-2-amino-4-phosphonobutyrate-sensitive metabotropic glutamate receptors, mGluR4 and mGluR7, in the rat brain. The Journal of comparative neurology *360*, 555-570.

Ohishi, H., Shigemoto, R., Nakanishi, S., and Mizuno, N. (1993). Distribution of the mRNA for a metabotropic glutamate receptor (mGluR3) in the rat brain: an in situ hybridization study. The Journal of comparative neurology *335*, 252-266.

Osten, P., Wisden, W., Sprengel, O. (2007). Molecular Mechanisms of Synaptic Function in the Hippocampus: Neurotransmitter Exocytosis and Glutamatergic, GABAergic and Cholinergic Transmission. In The Hippocampus book (The Oxford University press), pp. 243-316.

Overstreet, L.S., and Westbrook, G.L. (2001). Paradoxical reduction of synaptic inhibition by vigabatrin. Journal of neurophysiology *86*, 596-603.

Parker, D. (2006). Complexities and uncertainties of neuronal network function. Philosophical transactions of the Royal Society of London Series B, Biological sciences *361*, 81-99.

Parker, D. (2010). Neuronal network analyses: premises, promises and uncertainties. Philosophical transactions of the Royal Society of London Series B, Biological sciences *365*, 2315-2328.

Patenaude, C., Chapman, C.A., Bertrand, S., Congar, P., and Lacaille, J.C. (2003). GABAB receptor- and metabotropic glutamate receptor-dependent cooperative long-term potentiation of rat hippocampal GABAA synaptic transmission. The Journal of physiology *553*, 155-167.

Peterka, D.S., Takahashi, H., and Yuste, R. (2011). Imaging voltage in neurons. Neuron *69*, 9-21.

Pin, J.P., and Duvoisin, R. (1995). The metabotropic glutamate receptors: structure and functions. Neuropharmacology *34*, 1-26.

Pyapali, G.K., Sik, A., Penttonen, M., Buzsaki, G., and Turner, D.A. (1998). Dendritic properties of hippocampal CA1 pyramidal neurons in the rat: intracellular staining in vivo and in vitro. The Journal of comparative neurology *391*, 335-352.

Rivera, C., Voipio, J., Payne, J.A., Ruusuvuori, E., Lahtinen, H., Lamsa, K., Pirvola, U., Saarma, M., and Kaila, K. (1999). The K+/Cl- co-transporter KCC2 renders GABA hyperpolarizing during neuronal maturation. Nature *397*, 251-255.

Rodriguez-Moreno, A., Herreras, O., and Lerma, J. (1997). Kainate receptors presynaptically downregulate GABAergic inhibition in the rat hippocampus. Neuron *19*, 893-901.

Rodriguez-Moreno, A., and Lerma, J. (1998). Kainate receptor modulation of GABA release involves a metabotropic function. Neuron *20*, 1211-1218.

Rose, S.P. (2002). 'Smart drugs': do they work? Are they ethical? Will they be legal? Nature reviews Neuroscience *3*, 975-979.

Ross, W.N., Salzberg, B.M., Cohen, L.B., Grinvald, A., Davila, H.V., Waggoner, A.S., and Wang, C.H. (1977). Changes in absorption, fluorescence, dichroism, and Birefringence in stained giant axons: : optical measurement of membrane potential. The Journal of membrane biology *33*, 141-183.

Salzberg, B.M., and Bezanilla, F. (1983). An optical determination of the series resistance in Loligo. The Journal of general physiology *82*, 807-817.

Scanziani, M. (2000). GABA spillover activates postsynaptic GABA(B) receptors to control rhythmic hippocampal activity. Neuron *25*, 673-681.

Scanziani, M., Salin, P.A., Vogt, K.E., Malenka, R.C., and Nicoll, R.A. (1997). Use-dependent increases in glutamate concentration activate presynaptic metabotropic glutamate receptors. Nature *385*, 630-634.

Schell, M.J., Molliver, M.E., and Snyder, S.H. (1995). D-serine, an endogenous synaptic modulator: localization to astrocytes and glutamate-stimulated release.

Proceedings of the National Academy of Sciences of the United States of America *92*, 3948-3952.

Schloss, P., and Henn, F.A. (2004). New insights into the mechanisms of antidepressant therapy. Pharmacology & therapeutics *102*, 47-60.

Schoepp, D.D. (2002). Metabotropic glutamate receptors. Pharmacology, biochemistry, and behavior *73*, 285-286.

Schummers, J., Yu, H., and Sur, M. (2008). Tuned responses of astrocytes and their influence on hemodynamic signals in the visual cortex. Science *320*, 1638-1643.

Semyanov, A., and Kullmann, D.M. (2000). Modulation of GABAergic signaling among interneurons by metabotropic glutamate receptors. Neuron *25*, 663-672.

Semyanov, A., and Kullmann, D.M. (2001). Kainate receptor-dependent axonal depolarization and action potential initiation in interneurons. Nature neuroscience *4*, 718-723.

Shigemoto, R., Kinoshita, A., Wada, E., Nomura, S., Ohishi, H., Takada, M., Flor, P.J., Neki, A., Abe, T., Nakanishi, S.*, et al.* (1997). Differential presynaptic localization of metabotropic glutamate receptor subtypes in the rat hippocampus. The Journal of neuroscience : the official journal of the Society for Neuroscience *17*, 7503-7522.

Sik, A., Penttonen, M., Ylinen, A., and Buzsaki, G. (1995). Hippocampal CA1 interneurons: an in vivo intracellular labeling study. The Journal of neuroscience : the official journal of the Society for Neuroscience *15*, 6651-6665.

Sommer, B., Kohler, M., Sprengel, R., and Seeburg, P.H. (1991). RNA editing in brain controls a determinant of ion flow in glutamate-gated channels. Cell *67*, 11-19.

Spruston N., M.C. (2007). Structural and Functional Properties of Hippocampal Neurons. In The Hippocampus book (Oxford University press), pp. 133 - 201.

Storm-Mathisen, J., and Iversen, L.L. (1979). Uptake of [3H]Glutamic acid in excitatory nerve endings: light and electronmicroscopic observations in the hippocampal formation of the rat. Neuroscience *4*, 1237-1253.

Tasaki, I., Watanabe, A., Sandlin, R., and Carnay, L. (1968). Changes in fluorescence, turbidity, and birefringence associated with nerve excitation. Proceedings of the National Academy of Sciences of the United States of America *61*, 883-888.

Tominaga, T., Kajiwara, R. and Tominaga, Y. (2013). VSD Imaging Method of Ex Vivo Brain Preparation. Journal of Neuroscience and Neuroengineering *2*, 211 - 219.

Trommald, M., Jensen, V., and Andersen, P. (1995). Analysis of dendritic spines in rat CA1 pyramidal cells intracellularly filled with a fluorescent dye. The Journal of comparative neurology *353*, 260-274.

Turrigiano, G. (2011). Too many cooks? Intrinsic and synaptic homeostatic mechanisms in cortical circuit refinement. Annual review of neuroscience *34*, 89-103.

van Hooft, J.A., Giuffrida, R., Blatow, M., and Monyer, H. (2000). Differential expression of group I metabotropic glutamate receptors in functionally distinct

hippocampal interneurons. The Journal of neuroscience : the official journal of the Society for Neuroscience *20*, 3544-3551.

van Vreeswijk, C., and Sompolinsky, H. (1996). Chaos in neuronal networks with balanced excitatory and inhibitory activity. Science *274*, 1724-1726.

Vereninov, A.A., Nikolsky, N.N., Rosenthal, D.L. (1962). Neutral red sorption by the giant axon of Sepia at excitation. Tsitologiya 666–668.

Vignes, M., Clarke, V.R., Parry, M.J., Bleakman, D., Lodge, D., Ornstein, P.L., and Collingridge, G.L. (1998). The GluR5 subtype of kainate receptor regulates excitatory synaptic transmission in areas CA1 and CA3 of the rat hippocampus. Neuropharmacology *37*, 1269-1277.

Villani, C. (2009). Optimal Transport, Old and New (Springer Verlag).

Walker, M.C., Galley, P.T., Errington, M.L., Shorvon, S.D., and Jefferys, J.G. (1995). Ascorbate and glutamate release in the rat hippocampus after perforant path stimulation: a "dialysis electrode" study. Journal of neurochemistry *65*, 725-731.

Warren, D.H.a.S., E.R. (1985). Electronic Spatial Sensing for the Blind: Contributions from Perception (Springer).

Wenthold, R.J., Petralia, R.S., Blahos, J., II, and Niedzielski, A.S. (1996). Evidence for multiple AMPA receptor complexes in hippocampal CA1/CA2 neurons. The Journal of neuroscience : the official journal of the Society for Neuroscience *16*, 1982-1989.

Whiting, P.J., Bonnert, T.P., McKernan, R.M., Farrar, S., Le Bourdelles, B., Heavens, R.P., Smith, D.W., Hewson, L., Rigby, M.R., Sirinathsinghji, D.J.*, et al.* (1999). Molecular and functional diversity of the expanding GABA-A receptor gene family. Annals of the New York Academy of Sciences *868*, 645-653.

Wigstrom, H., and Gustafsson, B. (1986). Postsynaptic control of hippocampal long-term potentiation. Journal de physiologie *81*, 228-236.

Yeckel, M.F., Kapur, A., and Johnston, D. (1999). Multiple forms of LTP in hippocampal CA3 neurons use a common postsynaptic mechanism. Nature neuroscience *2*, 625-633.

Yokoi, M., Kobayashi, K., Manabe, T., Takahashi, T., Sakaguchi, I., Katsuura, G., Shigemoto, R., Ohishi, H., Nomura, S., Nakamura, K.*, et al.* (1996). Impairment of hippocampal mossy fiber LTD in mice lacking mGluR2. Science *273*, 645-647.

Yuste, R. (2015). From the neuron doctrine to neural networks. Nature reviews Neuroscience *16*, 487-497.